UiT
THE ARCTIC
UNIVERSITY
OF NORWAY

FACULTY OF SCIENCE AND TECHNOLOGY

Shallow fluid seepage systems in the Hammerfest Basin and adjacent Fault complex

Master's Thesis in Energy, Climate and Environment

Yohannes Tesfay

December 2014

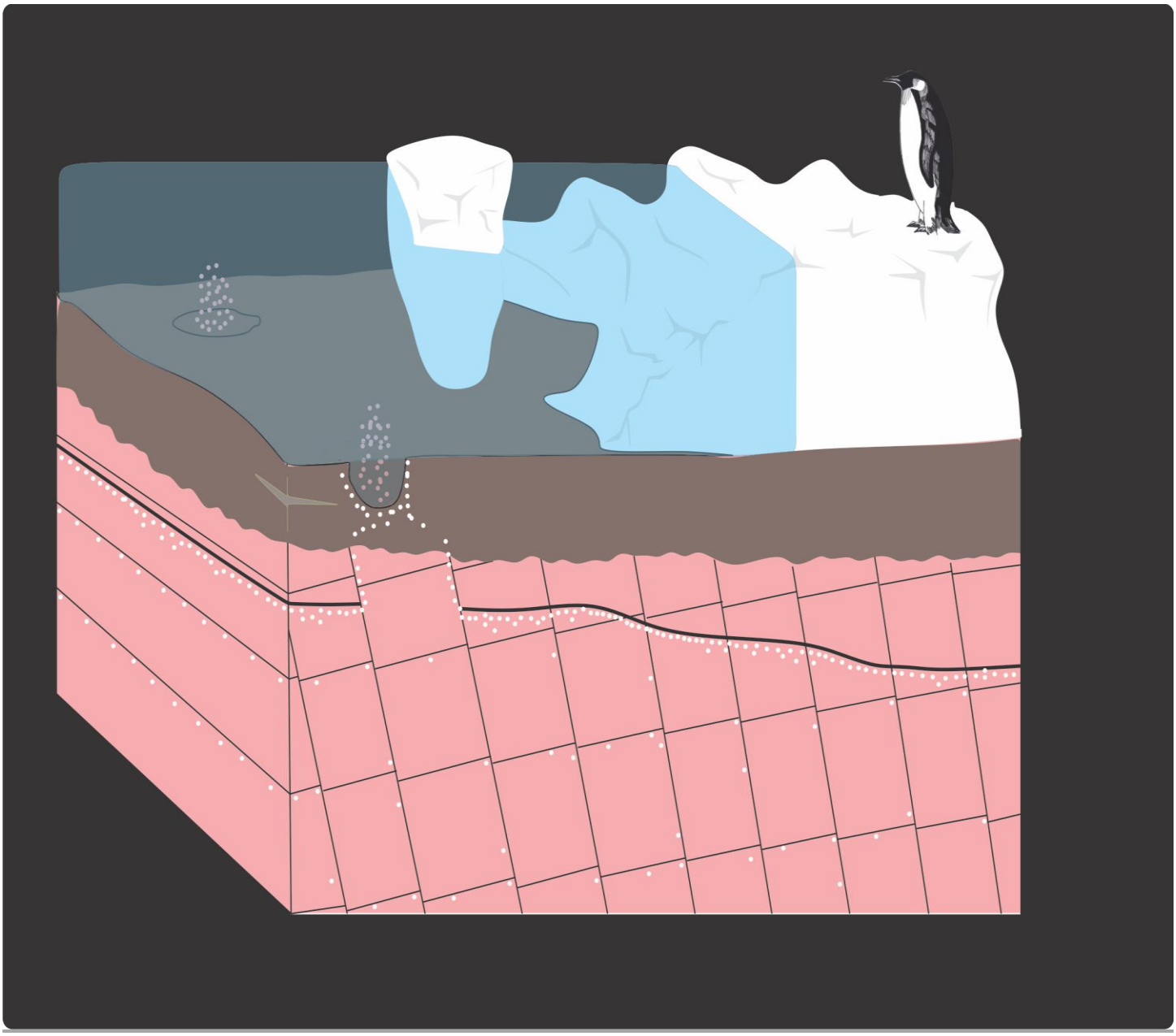

UNIVERSITY OF TROMSØ

EKM-3901

Master's Thesis Energy, Climate And Environment

Shallow fluid seepage systems in the Hammerfest Basin and adjacent Fault complex

Yohannes Tesfay

December, 2014

Abstract

This study was carried out using three high resolution 3D P-cable seismic datasets to explore shallow gas distribution and possible fluid migration pathways in the Snøhvit field and Ringvassøy-Loppa Fault Complex. The Snøhvit field situated in the center of the Hammerfest Basin is oil and gas field discovered in 1994. Ringvassøy-Loppa Fault complex marks the border between the Hammerfest and Tromsø Basin.

The seismic data cover seabed pockmarks and gas chimney in the Snøhvit field, and a buried pockmark area in the Ringvassøy-Loppa Fault Complex. These features were examined in this these. Bedding planes of early Triassic Clinoforms are understood to have been used as fluid flow pathways by fluids ascending from deeper strata and they terminate under glacial deposits that act as permeability barrier. Enhanced reflections aligned perpendicularly to the dip of the clinoforms are common at the base of the glacial unit. The investigation of pockmarks reveled a close relationship between ice free conditions and fluid flux.

Keywords: Pockmarks, fluid flow, Snøhvit field, shallow gas, RLFC

Acknowledgement

I want to use this opportunity to show my gratitude to my supervisor Ass. Prof. Dr. Stefan Bünz sharing his knowledge and experience in guiding me through this process.

I have been fortunate to share an office with Petter Lundekvam who has been very supportive during my time working on my master's thesis. This study has benefited hugely from Isaac and his artistry. Roberts has been a great part of lighting my days up. Special thanks to all of you. Your help has been deeply appreciated.

I also want to show appreciation to my family and friend who has shown great interest in how I was doing, making sure I was well fed, rested and had my weekly workouts.

Last but not least I want to thank Lamri for having been there for me every single day.

Yohannes Tesfay
December 2014

Contents

Chapter 1:

Subsurface fluids and Migration Pathways

1.1 objectives

The objective of this thesis is to map the distribution of structures related to fluid flow such as pockmarks and shallow gas accumulations in the Hammerfest Basin and on the adjacent Ringvassøy-Loppa Fault Complex in order to get a better understanding of the fluid flow system. Additional attention is given to the relationship between the paleo-environment and the fluid flow features. The appearance and distribution of pockmarks has also received a closer look.

1.2 Origin of hydrocarbons and subsurface fluids

Some of the solar radiation reaching earth is converted into glucose by plants in a process known as photosynthesis. Glucose can be converted to more complex compounds such as proteins, lipids and lignin by living organisms. These organic matters are usually oxidized to complete the cycle. A tiny fraction of this organic matter is preserved in anoxic conditions. The preservation of organic matter in seas and oceans depends on organic production rates, sedimentation rates and water column stratification. Anoxic bottoms that are needed for preservation of organic matter are often found in lakes (thermally induced water column stratification), barred basins (salinity induced stratification), upwelling dominated continental shelves (oxygen deficiency between 200m – 1500m depth) and anoxic ocean basin. In continental environment the preservation of organic matter happens largely in swamp deposits. (Selley, 1998; Bjørnlykke, 2001).

Most of the organic matter that falls through the water column is consumed by the benthic ecosystem. The organic matter that makes it through the water column enriches the organic content of the bottom sediment (Judd and Hovland, 2007). Sedimentary rocks with at least 2% TOC (total organic carbon) which is deposited in steadily subsiding sedimentary basin gets exposed to increasingly higher pressure and temperature regimes as it gets buried deeper. In this process organic rich sediments undergo three phases. Digenesis is the first phase where the organic matter losses much of its oxygen content due to biological and abiological decay in near normal temperature and pressure conditions. This phase produces Kerogen, insoluble amorphous organic remains. The next phase is known as catagenesis. This takes place in higher

temperature and pressure condition leading to the release of first oil and then gas by thermal cracking of kerogen. The last phase occurs near metamorphic temperature and pressures. At this stage only methane is produced. (Selley, 1998; Bjørnlykke, 2001; Veeken, 2007)

In addition to the thermal decomposition of organic matter to hydrocarbons, there is microbial genesis of methane. In an anoxic environment, microbial methane can be produced by methane producing anaerobic species. These species operate within anaerobic environments with sufficient organic matter supply (0,5% TOC) and they are mostly found in the temperature range between 4 – 55 ^{o}C. These species produce methane by reduction of CO_2 which is result of fermentation reactions of organic matter as in equation 1 (Hovland and Judd, 2007).

Equation 1--- $CO_2 + 4H_2 \rightarrow CH_4 + 2H_2O$

Petroleum fluids are often accompanied with water (from muddy sediments, released from compacting muds, ground water and so on), gases from hydrothermal activity, and mantel derived fluids beneath the surface. (Hovland and Judd, 2007)

1.3 Trapping of Fluids in the subsurface:

Hydrocarbons are often found in porous and permeable rocks, which are different to source rocks they emanate from. There are evidences suggesting that hydrocarbons in reservoirs have migrated to the reservoir rocks after their formation. The migration of hydrocarbons from the source rock to the reservoirs is subdivided in to two ways, primary and secondary migration. Primary migration happens as hydrocarbons escape from the source rock. One way this can happen is as the pore pressure in the source rock increase as kerogen is transformed to hydrocarbons. This increase in pore pressure can cause fracturing of the source rock which can then be used as migration pathway by the newly generated fluids (Selley, 1998; Bjørnlykke, 2001; veeken, 2007).

The secondary migration of hydrocarbons happens after the fluids have escaped the source rock and to the reservoir. Buoyancy force forces oil droplets through the carrier bed as long as the pore throat diameter is larger than the oil droplets. Oil will rise further up if it has higher displacement pressure than the capillary pressure. This will continue until the pore throats are so small that the oil droplets no longer can get squeezed through. At this point the fluids start to accumulate unless there is another escape route. If a seal mechanism as described above is formed it is known as capillary seal. If nothing hinders the flow of the fluids then the fluids can

migrate all the way to the surface (Selley, 1998; Bjørnlykke; 2001; Veeken, 2007). The further migration of hydrocarbons from the reservoir is known as Tertiary migration (Hovland and Judd, 2007).

Hydrocarbon accumulation must be assisted by some trapping mechanisms. These different trapping mechanisms are roughly classified into five major groups (Structural traps, stratigraphic traps, diapiric traps, hydrodynamic traps and combinational traps). Structural traps are formed by post depositional tectonic activity and are further subdivided into anticlinal and fault and fault related traps. Stratigraphic traps result from depositional morphology or digenesis. Diapiric traps are made as lower density mud or salt is moved through strata to form diapiers. Hydrodynamic traps are caused by the physical conditions that are formed as fluids (water) move in the subsurface. (Selley, 1998)

The presence of traps slows down the migration of hydrocarbons, but does not stop it. There are several ways the integrity of a trap may get compromised. Cartwright et al define seal bypass systems (SBS) as "large-scale (seismically resolvable) geological features embedded within sealing sequences that promote cross-strata fluid migration and allow fluids to bypass the pore network." SBS can allow Cross-strata fluid migration episodically or semi-permanently. (Cartwright et al, 2007)

1.4 Physical controlling mechanisms:

The flow of hydrocarbons from reservoirs through the cap rock in consolidated sediments occurs usually as Darcy flow, fracture flow and diffusion (Løseth et al, 2009). The main forcing mechanisms for subsurface fluid flow are excess pore fluid pressure and buoyancy. Whenever the pore fluid pressure is greater than the hydrostatic pressure (eq. x) there is overpressure within the sediments. Overpressure is caused by pore fluids not being able to flow out of pore space during burial. This usually happens as a result of tectonic compression and/or sedimentation rates exceeding the rate of compaction which in turn decreases the permeability before the fluids are squeezed out of the pore space. (Hovland and Judd, 2007).

The buoyancy force is set up by a density contrast between two bodies. Layers with low density overlain by denser material are buoyant. This buoyancy force is expressed by the following equation. . (Judd and Hovland, 2007).

Equation 2 $$BFp = (\rho p - \rho os) * g * hp$$

BF_p- buoyancy force of the parent material, ρ_p- density of parent material, ρ_{os}- density of overlaying sediments, g- gravitational acceleration and h_p- thickness of the parent material.

Buoyancy it the most dominant force in driving gas bubbles to the surface. The buoyancy of the gas in some cases aids the upward migration of oil. . (Judd and Hovland, 2007).

Darcy's law can be used to explain the flow of hydrocarbons in the subsurface. It states the flow rate of a fluid through a medium is proportional to the permeability of the material and the pressure drop, and it is inversely proportional to the viscosity of the fluid. It is mathematically stated as follows;

Equation 3 $$Q = \frac{kA(P2-P1)}{L\mu}$$

Q – discharge [m^3/s], K- permeability of the medium[m^2], A- cross section area[m^2], P2-P1- pressure drop [Pa], L- the length in which the pressure drop takes place[m] and μ- viscosity of the fluid[Pa.s]

Darcy's law states that the amount of fluid flowing through a rock depends on the permeability of the rock, pore-water pressure differences at the two ends of the flow and the viscosity of the fluid. The pressure difference that drives the flow arises from the increase of pore fluid pressure due to burial depth. This pore fluid pressure may exceed the hydrostatic pressure. If the host rock has sufficient hydraulic conductivity, fluid will start to flow to even out the raise in pore pressure. In some cases pore pressure may raise a lot higher than the hydrostatic pressure. This may lead to fracturing in the host rock and focused fluid flow. (Berndt, 2005)

Hydrostatic pressure is the pressure at a given depth in a static fluid. This pressure is the sum of the weight of the overlaying fluid on a unit area and the pressure applied on the surface of the fluid. Fluids in hydrostatic equilibrium i.e. at rest or flow velocity at each point is constant over time, exists as the force of gravity balances the pressure gradient force.

Equation 4 $$Phydro = \rho gh + Ps$$

Phydro- Hydrostatic pressure[bar] at depth h[m], ρ – density of the fluid[g/cm^3], g – gravitational constant and Ps –pressure at the surface of the fluid.

In order for a fluid to flow through a carrier bed, it needs to overcome the capillary pressure. The fluid then follows the path of least resistance. The capillary pressure in fine grained sediments is seldom exceeded by the viscous forces of the fluid. The fluid usually uses the path that connects the largest pore throats. As a consequence fluid flows tend to get focused. The capillary pressure is defined mathematically by the equation below. (Judd and Hovland, 2007)

Equation 5 $$Pcap = \frac{2T}{Rc}$$

Pcap – capillary pressure, T – surface tension, Rc - radius of curvature of the meniscus radius of curvature of the meniscus at the bubble boundary

The vertical stress (δ_v) imposed on sediments is a function of the depth and the density of the overlaying sediments. The vertical stress is only acted upon the solid components of the sediments. The pore fluid pressure works against this vertical stress. The "effective stress (δ')" takes into account the effect of the pore fluid pressure. As the sediments get buried deeper, the effective stress is increased and pore fluid squeezed out. This allows the compaction of sediments adding tensile strength to the lithified rock. In the absence of any preexisting migration pathways such as faults and fractures, the buoyant fluid forces its way up whenever this tensile strength of the lithified sediments or shear strength of the unlithified sediments are overcome by the buoyancy force. Gas has been observed forcing a pathway through clay as the gas pressure marginally exceeded the shear pressure. Once an upward movement is prompted, the feedback process illustrated in figure 1.1 leads to further continuation of the upward movement. (Judd and Hovland, 2007)

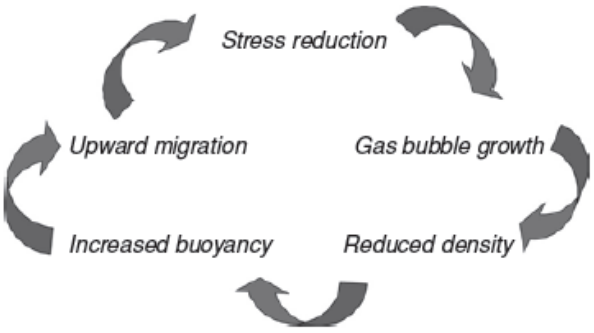

Figure 1.1: *Illustration of a feedback process that enhances upward migration. Once a fluid starts to migrate upwards the stress is reduced and gas bubbles start to grow. This leads to reduction in density which in turn increases buoyancy. The increase in buoyancy then further aids the upward migration. (Judd and Hovland, 2007)*

Diffusion occurs over large parts of traps with low flow rates (Løseth et al, 2009). This flow mechanism is driven by concentration difference of chemicals in the pore fluid. Diffusion leads to the flow of fluids from higher to lower concentrations and this causes the dispersion rather than concentration. (Judd and Hovland, 2007) Portions of the fluid can be transport independent from the fluid itself (Berndt, 2005).

1.5 External factors controlling subsurface fluid flow

There are several external factors that trigger fluid leakage by directly or indirectly causing increase in the pore fluid pressure. Earthquakes are often linked to fluid migration. Wet, water saturated sediments tend to get compacted as a result of an earthquake. If the pore fluids are not allowed to escape, the increase in the pore fluid pressure causes some of the sediment grains to flow along with the fluid (liquefaction). (Judd and Hovland, 2007)

Another external factor that may aid the pore fluid migration is unloading of mass over an overpressure area. The removal of mass leads to decrease in vertical stress, hence lesser pore fluid pressure is needed to fracture the host rock. Once a fluid migration pathway is created the feedback process in figure 1.1 further enhances the fluid flow towards the surface. (Judd and Hovland, 2007)

Additional load such as ice sheets can cause over pressure if the fluids trapped in the sediments are not able to escape. This happens particularly in fine grained and low permeability rocks. Overpressure builds up in such environments as the vertical stress is increased because of the added load and the trapped fluid which inhibits compaction. The outcome of this process is density inversion. If buoyancy force is raised sufficiently, it leads to mud diaparism. (Judd and Hovland, 2007)

Hot magma in the sub-surface boils fluids increasing the volume and pressure of the fluids. The increase in pore pressure can lead to fracturing of the host rock. The explosive nature of the fluid ascend can lead to fluidization and formation of erosive, conical depressions in the seabed. These fluid flow pathways created by the hydrothermal fluid can be reused as flow pathways later as the magma cools. (Judd and Hovland, 2007)

Sediments affected by permafrost have very low permeability (close to zero). The low permeability in the frozen sediments leads to the development of overpressure beneath. If the overpressure beneath is raised enough it can force fluid flow pathways to the seabed. Ice and

gas hydrates have similar sealing effect as permafrost. Iceberg scour marks have often been observed in the vicinity of fluid flow features. The permeability near the seabed sediments gets increased as the iceberg keel ploughs the seabed sediments creating small scale faults and fractures. These small scale faults and fractures can be used as migration path. (Judd and Hovland, 2007)

1.6 Subsurface Fluid flow pathways

In cases where seal bypass systems (SBS) are present in the traps, the roles of the capillary pressure, hydraulic conductivity and wettability to predict seal capacity are reduced, because of the SBS ability to drain fluids. Three main groups of SBS are recognized; Fault bypass, intrusive bypass and pipe bypass. (Cartwright et al, 2007)

Fault bypass are related to seismically resolvable faults, and have the potential to aid fluid migration over long vertical distances as faults can cross hundreds of meters of stratigraphic section. (Cartwright et al, 2007) Leakage of fluids through faults is usually associated with weak points in the fault zone. Fault intersections are one of the weak points in a fault zone that are thought to be one of the most important fluid pathways. The effective stress within fault intersections is reduced due to minor faults and fractures that exist within. The reduction within the fault intersections leads to higher fluid flux. In addition to that, faults are play greater role as fluid conduits in deeper areas where the sediments are more consolidated and lithified (Ligtenberg, 2005) However, faults have been observed prohibiting fluid flow and acting as a sealing agent. Fault bypass can be further subdivided into trap defining (defines the trap integrity) and supratrap (embedded within the seal). Most fault bypasses are thought to have act SBS at the formation stages and sealed later. The presence of large pockmarks or craters, mud mounds, hydrate mounds and temperature anomalies on top of a fault indicate fluid flux from the fault plane. (Cartwright et al, 2007) Polygonal faults are small extensional faults that together form a polygonal network. They were first discovered in the North Sea, but have later been observed on many passive continental margins. They are often confined to single stratigraphic intervals often with very low permeability. Escape of pore fluid causing bulk shrinkage during early burial on highly porous and fine grained sediments is thought to be the origin of this these polygonal faults. (Cartwright and Huuse, 2005) They play a great role in enhancing permeability heterogeneity in otherwise low permeable sediments as their fault planes transmit fluids. Polygonal faults have been observed within sealing sequences without

compromising the seal integrity. This suggests that fluid passage through the polygonal faults are not always sufficient enough to compromise seal integrity.(Cartwright et al, 2007)

Intrusive bypass compromise the seal integrity in three different ways. First type occurs as the intrusion event itself is responsible for the breach of the trap. This takes place when mud volcanoes intrude the seal. The second type is related to high permeable material occupies an area previously occupied by impermeable host rock. Sandstone intrusion is typical of this type. Fluid flow takes place through the highly permeable material. The third type materializes as the intrusion leads to fracturing of the surrounding rocks enhancing permeability, thus fluid migration. This often happens with salt diapirs and igneous intrusions. (Cartwright et al, 2007)

Pipe bypass are observed having circular shape in the planar view and are vertically or sub-vertically extended. Internal fracturing enhances the permeability of the pipes which makes then good fluid conduits. They often seem to have their root planted in crustal structures with positive topography. Cartwright et al suggests classification of pipes in to four classes; dissolution pipes (dissolution of rocks causing the formation of subsurface cavities), hydrothermal pipes (hydrothermal fluid leading to metamorphism), blowout pipes (fracturing due to over pressure in fine grained sediments) and seepage pipes (occur in sand or silt dominated sediments to prohibit the development of over pressure). (cartwright et al, 2007)

In the presence of sedimentary layers with sufficient porosity and permeability, the buildup of overpressure is prohibited since excess fluids can easily be transported from the higher pressure area to a lower pressure area. Porous and permeable rocks can be used as fluid flow pathways as they can overcome the capillary pressure. (Bjørlykke 2001)

1.7 Features developed by flowing subsurface fluids

Physical alteration and replacement of primary structures of sediments in the seabed can be created by migrating fluids entering the water column. (Løseth et al, 2009) The nature of the migrating fluid varies from just fluids escaping to sediments flowing with no significant fluid content. Marks left by migrating fluid depend among others on the nature of the fluid flowing. (Judd and Hovland, 2007)

Pockmarks are shallow sub-circular erosional depression formed on soft, fine grained seabed sediments as fluids seeps into the water column (Løseth et al, 2009). Pockmarks are found in every sea, ocean and some lakes in the world and are normally tens of meters across and few

meters deep. Different types of pockmarks exist, including unit pockmarks, elongated pockmarks, eyed pockmarks and pockmark strings. They are produced as the pressure due to gas accumulation near the seabed causes doming of the sediments near seabed. The tension created by the doming produces small fractures that can be used as migration routes to the seabed. Pockmarks are generated as gas ascends towards the seabed, the pressure drops and the gas expands. The expansion leads to violent bursts escaping gas. The gas along with the sediments trapped within rise into the water column as sediment plum. The fine grained parts of the sediment plume are transported in suspension while the coarser one are deposited in the surrounding. The pockmark formation is illustrated in the figure below. The pockmark size and density is a function of the thickness, strength and permeability of the sediments near the seabed. Once pockmarks that are generated, they can be re-used as fluid migration pathways repeatedly. (Judd and Hovland, 2007)

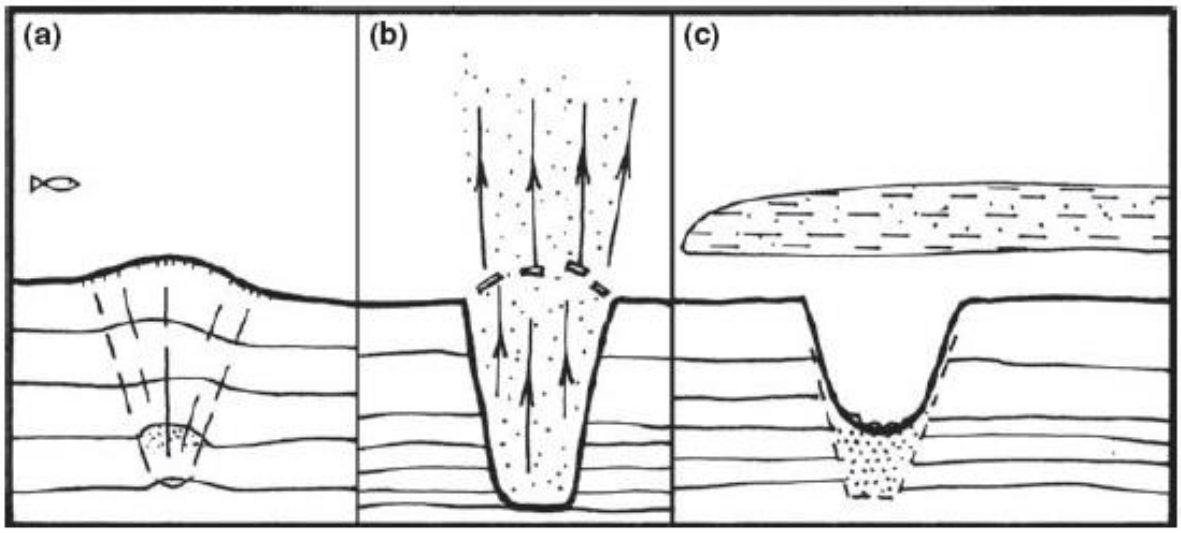

Figure 1.2: Model of pockmark formation. (a) Overpressure creates doming and fracturing of the near seabed sediments. (b) Sediment plume rises to the water column. (c) Some of the sediments are transported in suspension, while the coarser grains are deposited in and around the pockmark. (Judd and Hovland, 2007)

Mud volcanoes are conical hills with a summit crater. A venting liquid mud along with mixture of gas, liquids and trapped sediment produce these features. They have been observed on various areas in the world some underwater and others on land. Most mud volcanoes are spotted on areas that have undergone rapid sedimentation in subsiding basins, deltas and deep water fans, and sediments accumulated in accretionary wedges. Trapped pore fluid cannot escape the pores as the shear stress is increased and that causes overpressure. Development of the

overpressure inhibits the compaction of sediments which in turn causes density inversion. The density inversion can gives rise to a buoyancy force that can trigger diapiric movement. Additional buoyancy maybe provided by the expansion of gas when the fluid migrates upwards as illustrated in figure 1.1. The feedback system shown in figure can aid the fluid movement all the way to the surface creating a mud volcano. They vary in size from a few cm to more than a km in height and tens to hundreds of meters in diameter. Viscosity, density, volume and grain size of the fluid mix, and emission frequency determine the size of the mud volcanoes. There are three types of mud volcanoes; Lokbotan type which is short lived and explosive, Chikishlyar type which is developed under gentle and continuous conditions and Schugine type which is an intermediate type. And intrusive mud volcanoes are commonly known as mud diapirs. (Judd and Hovland, 2007)

Sand intrusions and extrusions are similar to volcanic sills and dykes in appearance. They generally appear in tectonically active mud dominated areas with high sedimentation rate. Tectonic stress increases the pore pressure in unconsolidated sandy sediments. The elevated pore fluid pressure drives the fluidized sand into lower pressure environment as the seal fails. (Judd and Hovland, 2007) These sand bodies are highly porous and permeable and tend to enhance permeability heterogeneity of the otherwise impermeable and fine gained sediments in the surrounding. The high porosity and permeability in the sand bodies makes them suitable as fluid flow pathways. (Hurst et al, 2004)

There are several minor features associated with fluid migration. Shallow and broad *seabed domes* are found above gas accumulations near the seabed sediments. Seabed domes are about a meter high and few hundred meters across. *Collapse depressions* are observed in the vicinity of rapidly deposited, soft, organic rich sediments. They are form as liquefied seabed sediments collapse. These features are elongated, bowl shaped depressions with hummocky floors, and are normally around 3m deep and 50-100 m across. *Sedimentary diatremes* are vertical features piercing through sedimentary rocks produced by explosive eruption initiated by sediment fluidization. These diatremes are indicative of focused fluid flow. *Freak sandwaves* are considered to form by the removal of sediment by the escape of gas at the seabed. The gas seeps hinder the resettlement of the grains at their preferred position. They are therefore steeper than normal sand waves in the surrounding. (Judd and Hovland, 2007)

1.8 Hydrocarbons in seismic data:

Seismic reflections are produced because of different acoustic properties (v, ρ) of the environment above and below a reflector. The acoustic impedance (ai) (Z=v. ρ) of rocks control the reflection coefficient. The difference in acoustic impendence occurs as a result of changes physical properties of rocks. The resulting reflection coefficient (R=Z2-Z1/ Z2+Z1) at a boundary defines the nature of the reflected signal. Higher reflection coefficient gives rise to stronger reflection. R is positive when Z increases as the wave propagates from one layer to another, and R is negative if Z decreases from one layer to another. The reflection amplitude strength is proportional to magnitude of R (Badly, 1985). The vertical seismic section usually displays sedimentary reflections set up by ai differences between different lithological units, unconformities, seismic artefacts such as multiples, and non-sedimentary reflections such as fluid contacts and fault planes (Veeken, 2007).

Presence of petroleum especially gas in the subsurface can be detected in a seismic data since it affects the acoustic properties of the host rock. Free gas in the pore space of rocks reduces the p-wave velocity which in turn diminishes the acoustic impedance of the rock causing the generation of a seismic reflection. Figure 1.3a show that only 4% gas is needed in the pore space to reduce the p-wave velocity dramatically (Andreassen et al, 2007).

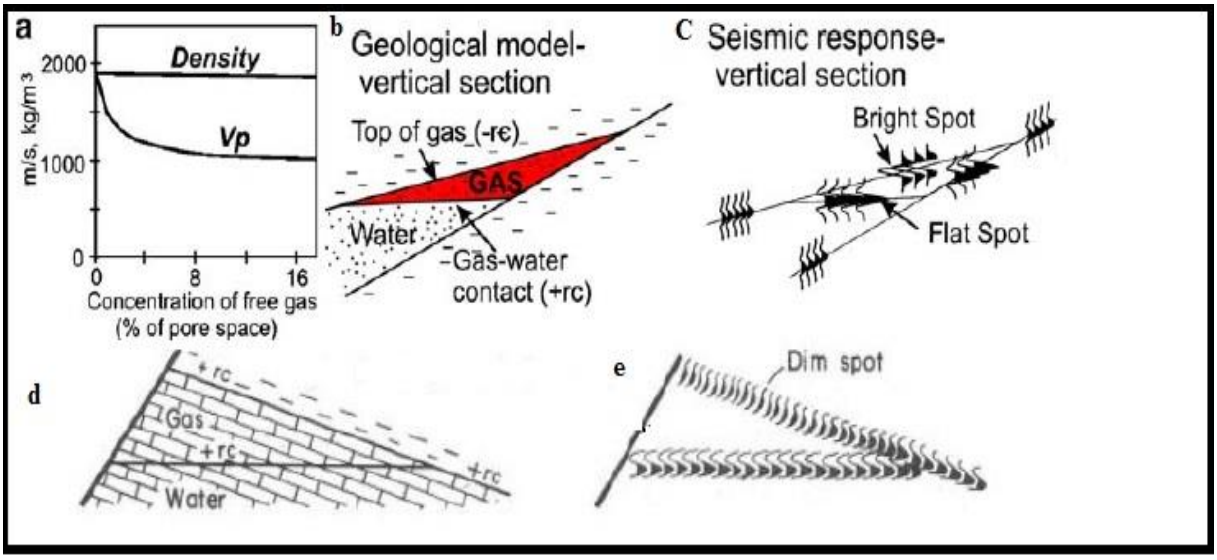

Figure 1.3: a) Diagram showing how density and p-wave velocity vary with increasing concentration of free gas in the pore-space. b) Geological model showing a gas saturated area C) The seismic response b would give. d) Geological model that shows a compacted limestone saturated with gas. e) The seismic response to be expected from d. (Andreassen et al, 2007a)

Under a thick gas reservoir, a gas-water contact or gas oil contact appears as a sub-horizontal event that is discordant with adjacent reflections on a vertical seismic section. This event is known as Flat spot (fig) and has a positive reflection coefficient. (Andreassen et al 2007; Badly, 1985; Veeken, 2007) Oil-water contact is often absent from the vertical seismic section because of the insufficient acoustic impendence contrast there is between oil and water and the limited thickness of the oil column. (Veeken, 2007) Since the marked reduction in p-wave velocity due to the presence of gas is confined to the top 2,5 km, flat spots are often found within this interval.(Badly, 1985) The flat spot may at times appear to be pulled down due to the reduction of p-wave velocity by the overlaying gas baring sediment. (Andreassen et al 2007 ; Badly, 1985)

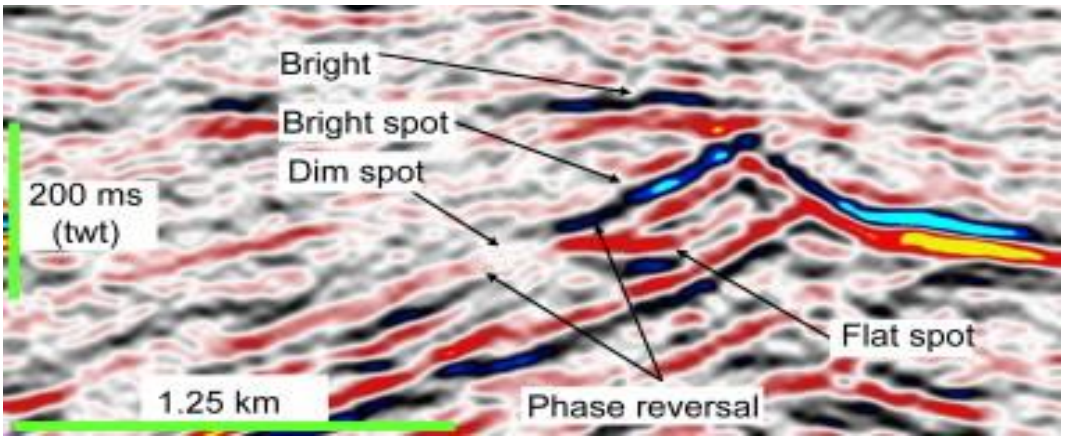

Figure 1.4: A vertical seismic section shows bright spot, dim spot, flat spot and phase reversal. (Løseth et al, 2009)

Changes to the acoustic properties of rock materialize as formation waters of rocks are substituted by hydrocarbons. These changes result in reduction of the acoustic impedance of highly permeable rocks. At shallow levels, this often produces a soft response, and at deeper levels hard responses are expected. The appearance of hydrocarbons in low permeability cap rocks varies from reflection free to high amplitude anomalies in a vertical seismic section. (Løseth et al, 2009)

Anomalously high amplitude reflection known as Bright spot is produced from the top of a gas baring porous layer (figure 1.4). This reflection is caused by a decrease in acoustic impedance resulting in a large negative reflection coefficient (fig – b-c). Bright spots show a polarity reversal compared to the seabed reflection because of the strong negative RC (Andreassen et al 2007; Badly, 1985; Veeken, 2007).

A decrease in amplitude is sometimes observed at the top of a reservoir known as dim spot (figure 1.3). Dim spots indicate the reduction of RC due to change in porefill. They are often

associated with reduction of RC in well compacted sandstone and carbonate reservoirs (figure 1.3 d and e) (Badly, 1985; Veeken, 2007).

The presence of gas in soft and fine grained sediments leads to acoustic energy being absorbed and scattered and this is displayed as chaotic seismic reflections on the vertical seismic section. These features are called acoustic turbidity zones. (Badly, 1985; Hovland and Judd, 2007)

A coherent reflection positioned directly below thick gas-loaded sediments may exhibit a pulldown effect as in figure 1.9. This effect gives the impression that the sediments are sagging. Flat spots sometimes appear to be curved as a result of the pulldown effect. This is due to the acoustic velocity reduction in the gas rich area causing a delay in the seismic signals. Therefore the two-way travel time is prolonged. (Badly, 1985; Hovland and Judd, 2007; Veeken, 2007)

Some diagenetic processes are related to the presence of hydrocarbons in the pore space, they are known as Hydrocarbon-Related Diagenetic Zones (HRDZs). HRDZ are a result of CO_2 which is produced by oxidization of hydrocarbons. That then causes an intense carbonate cementation of otherwise poorly cemented sand stones. The carbonate cements poses higher acoustic velocity than the host rock. This high acoustic velocity in the diagenetic zones produces a positive acoustic impendence contrast which appears as high amplitude anomalies in the vertical seismic section. They are sometimes accompanied by velocity pull up beneath. (Løseth et al, 2009)

Frequency loss is occasionally observed beneath gas-charged sediments. This happens because gas-bearing sediments absorb more seismic energy than water-bearing intervals. Diffractions associated with bright spots are also common features in areas where there is a sufficient lateral acoustic impedance contrast. These features are usually found at the edges of bright spots. (Badly, 1985)

1.9 Hydrocarbon leakage in seismic data

The hydrocarbon leakage processes can lead to permanent changes to the primary structures that were in place in the host rocks. These changes can be of direct consequence of the flow itself as damage to the primary layering and formation of surface structures takes place where the fluids reach surface. Permanent changes to the rock can also be caused to the host rocks which are not direct consequences of the migration. Increased biological activity due to

hydrocarbon migration can cause changes in the host rock. These changes leave their marks on their environment that can be detected in seismic data. (Løseth et al, 2009)

Physical alteration and replacement of primary structures of sediments in the seabed can be created by migrating fluids entering the water column. Pock marks (figure 1.5 & figure 1.9) are such features that can be observed on the vertical seismic section as small depressions on the seabed often underlain by acoustic turbidity, faults, and amplitude anomalies that indicate the presence of gas. They appear as shallow depressions on surface structure maps as shown in the figure below. (Løseth et al, 2009)

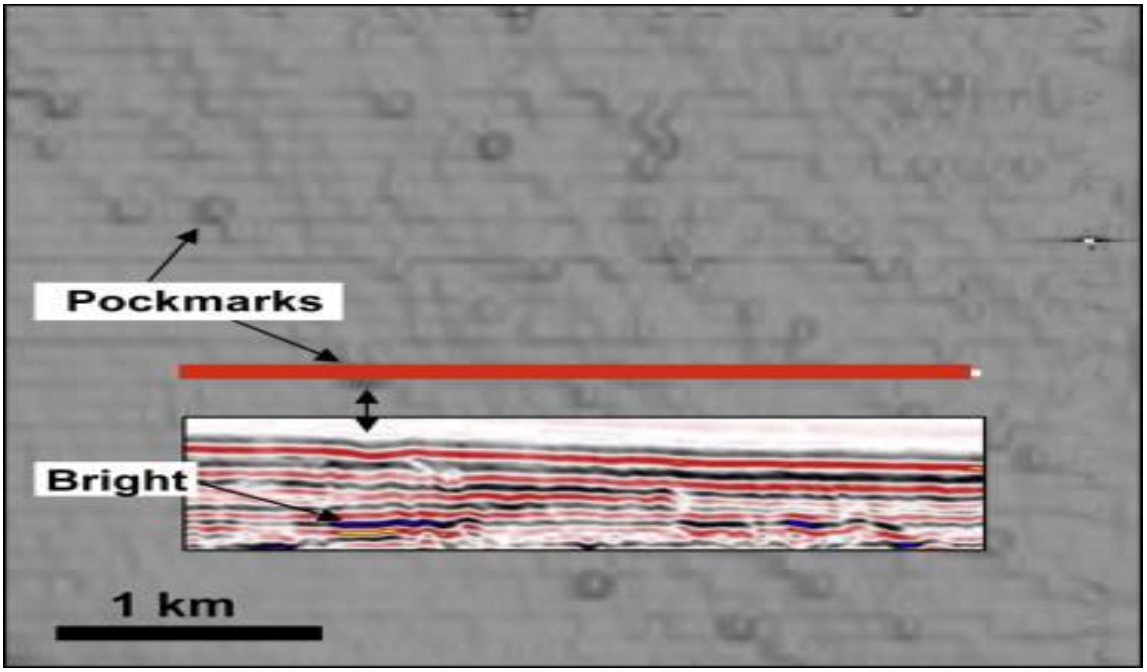

Figure 1.5: Display of circular depression interpreted as pockmarks on a correlation map. The pockmarks displayed as a small depression overlaying a high amplitude anomaly, interpreted as shallow gas accumulation that is feeding the pockmark with gas, on a vertical seismic section. (Løseth et al, 2009)

Craters are larger seabed circular depressions than pockmarks that indicate violent gas blowout. They often have hundreds of meters in diameter and tens of meters in depth. These features often found over faults. The craters along with their collapse zones and pipes are often a result of violent, episodic gas blow out. They come often with a vertical and wide zones characterized by chaotic seismic reflection in the vertical seismic section that is indicative of gas migration. Figure 1.6 shows the appearance of seabed crater along with their collapse zones and the blowout pipes. (Løseth et al, 2009)

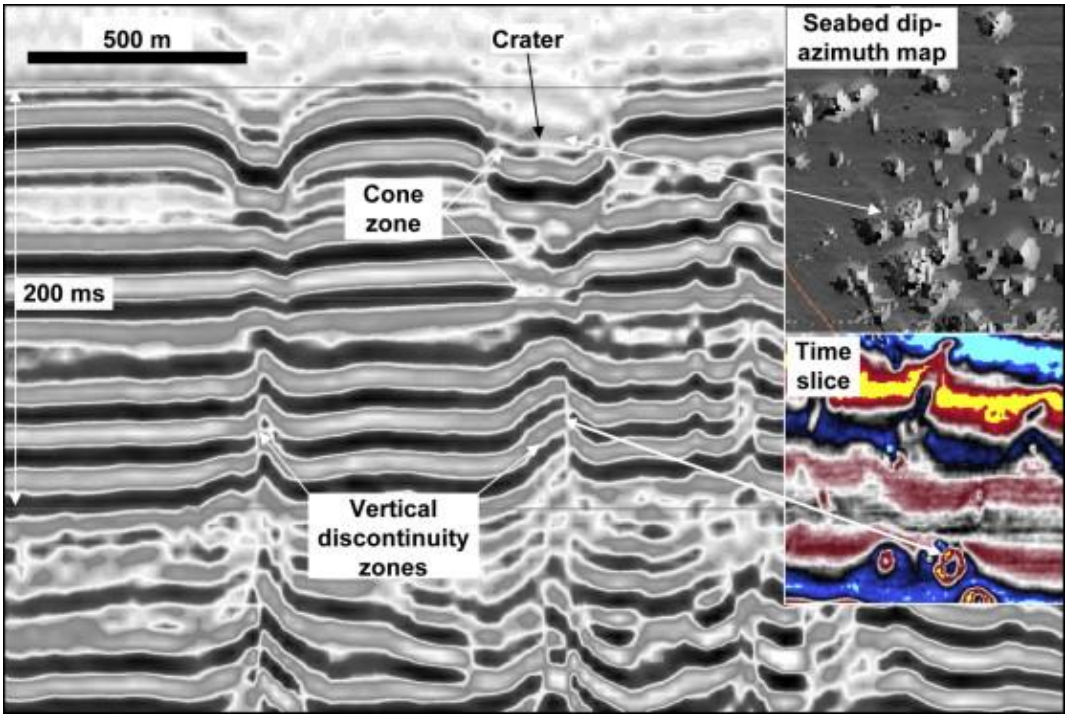

Figure 1.6: A vertical seismic section displays a seabed depression with an underlying con-shaped zone and vertical discontinuity zone. The seabed depression is interpreted as a seabed crater, the con-shaped zone as collapse crater and the vertical discontinuity as a blowout pipe. Dip-azimuth map shows the plane view of the craters and the time slice map the circular nature of the blow out pipes. (Løseth et al, 2009)

On the vertical seismic section, vertical zones with distorted amplitudes and the phases of reflectors are observed as the leakage zone in figure 1.7 illustrates. These anomalies in the seismic section are known as gas chimneys (Arntsen, 2007; Heggland 1997, 1998; Judd and Hovland, 2007; Løseth et al, 2009). The distortion in the reflections are caused by parcels of gas, slightly displaced sediment (Judd and Hovland, 2007) and distribution of the gas in sediments (Arntsen, 2007). These features are often found in fine grained, low permeability sediments such as shales. Gas can enter the impermeable sediments by diffusion, fracture networks (Arntsen, 2007) and failure of capillary seal (Cathles et al, 2010). The fractures can be tectonically induced above salt and clay diapires, and hydraulically fractured above high pressure zones (Løseth et al, 2002). The chimneys often represent past and currently active fluid migration pathways (Heggland,1998). Top and sides of a gas chimney are typically associated with high amplitude anomalies, pull ups and pushdowns (Løseth et al, 2009), gas hydrates (Gay et al, 2006; Parnell and Schwab,2003) and pockmarks (Cathles, 2010; Gay et al, 2006; Judd and Hovland, 2007).

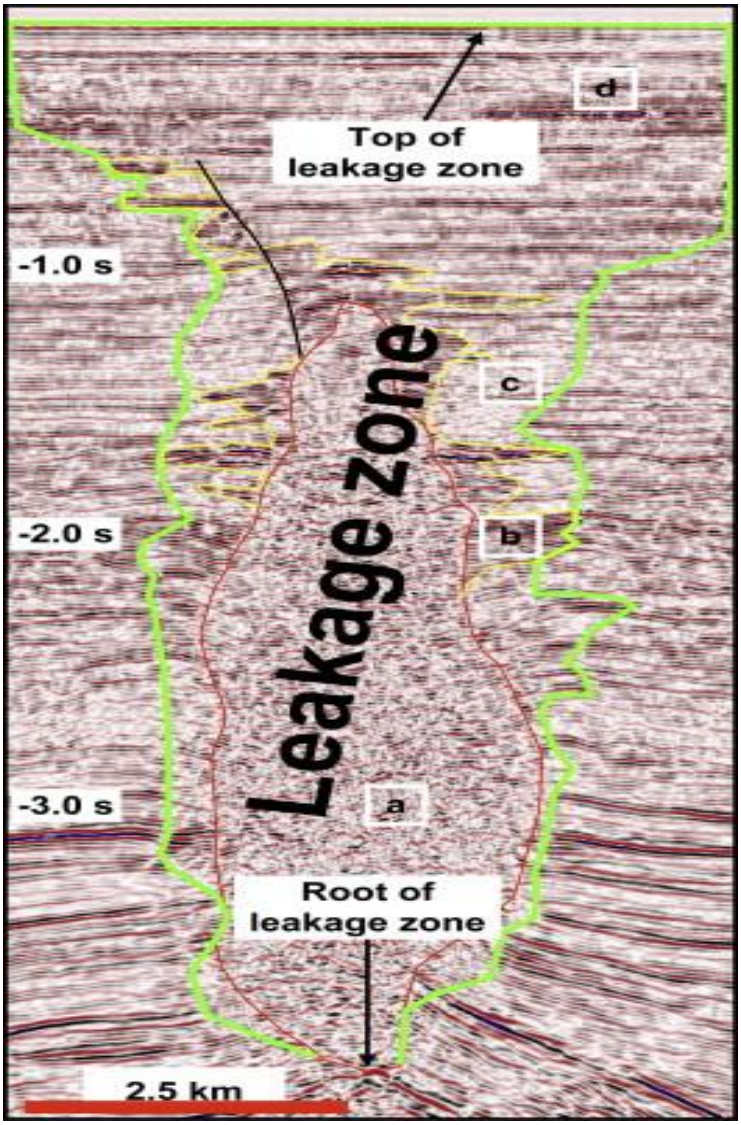

Figure 1.7: A seismic section showing various leakage related anomalies a) A vertical zone of deteriorated seismic signal interpreted as a gas chimney defining the area affected by migrations of hydrocarbons and outlining the leakage zone. b) Gas accumulations are found on the sides of the gas chimney and are displayed as high amplitude anomaly. c) A dim zone which is likely to have originated from gas laden areas is located on the side of the gas chimney. d) Top of the leakage zone marked by bright spots, dim spots and a pockmark. (Løseth et al, 2009)

Faults with throws larger than 10 meters can be observed in the seismic vertical seismic section. Faults may act as cross-stratal migration routes on a semi-permanent basis are often found in the vicinity of gas related anomalies (figure 1,8). The presence of pockmarks, mud volcanoes and gas hydrates just above faults suggests that the faults act or have acted as fluid conduits. (Cartwright et al, 2007) Polygonal faults were recognized using a 3D seismic data. They are identified on the vertical seismic section as a set of small extensional faults forming a complex polygonal shape on a time-slice. (Cartwright and Huuse, 2005; Cartwright et al, 2007)

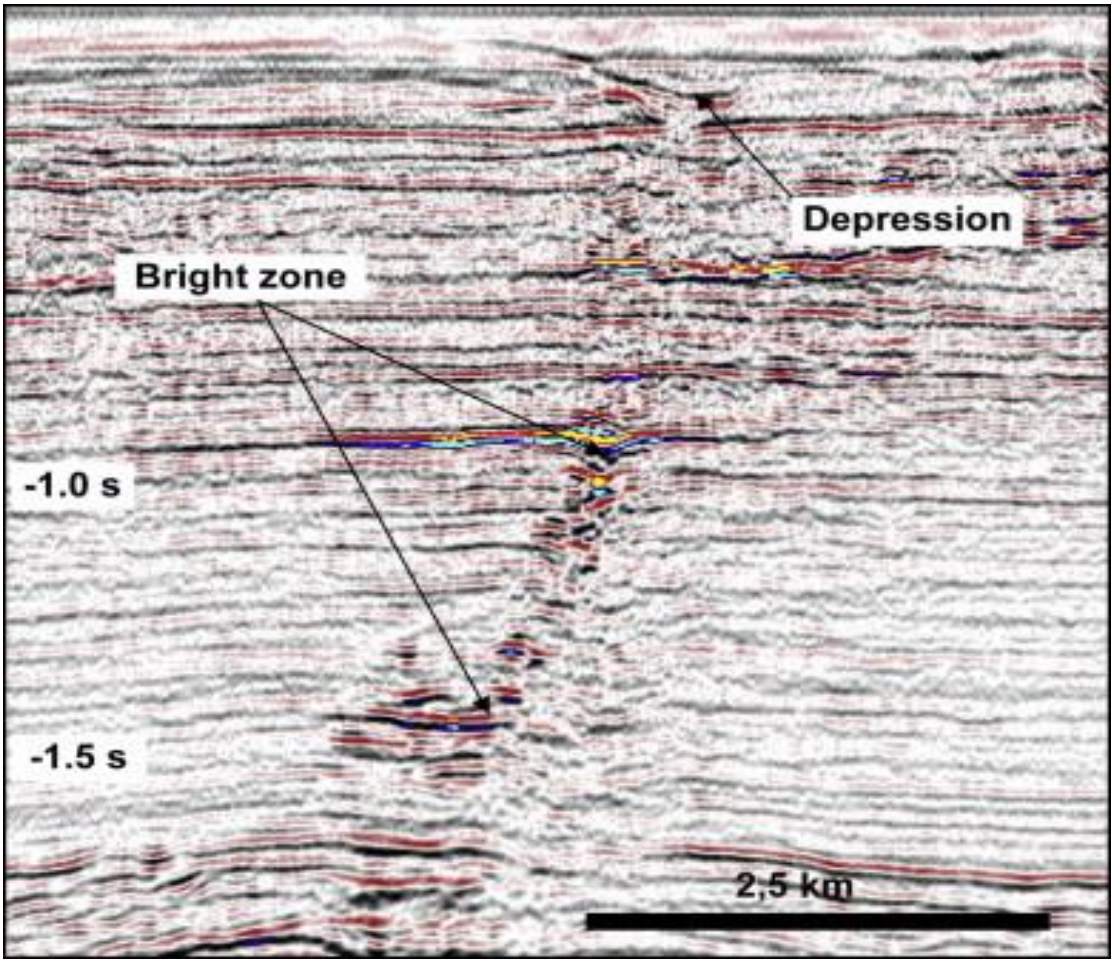

Figure 1.8: A vertical seismic section shows high amplitude anomalies stacked along the hanging wall of a fault. The amplitude anomalies are interpreted to arise from gas using the fault as its pathway. (Løseth et al, 2009)

Pipes are often associated with columnar zones of deteriorated reflections. Their vertical geometry in the vertical seismic section leads often to them being regarded as seismic artefacts. They have a circular to sub circular appearance on slice based or horizon based attribute maps (figure 1,6) and they commonly originate at crestal structures such as fold crests and sand bodies with positive topographies. (Cartwright et al, 2007).

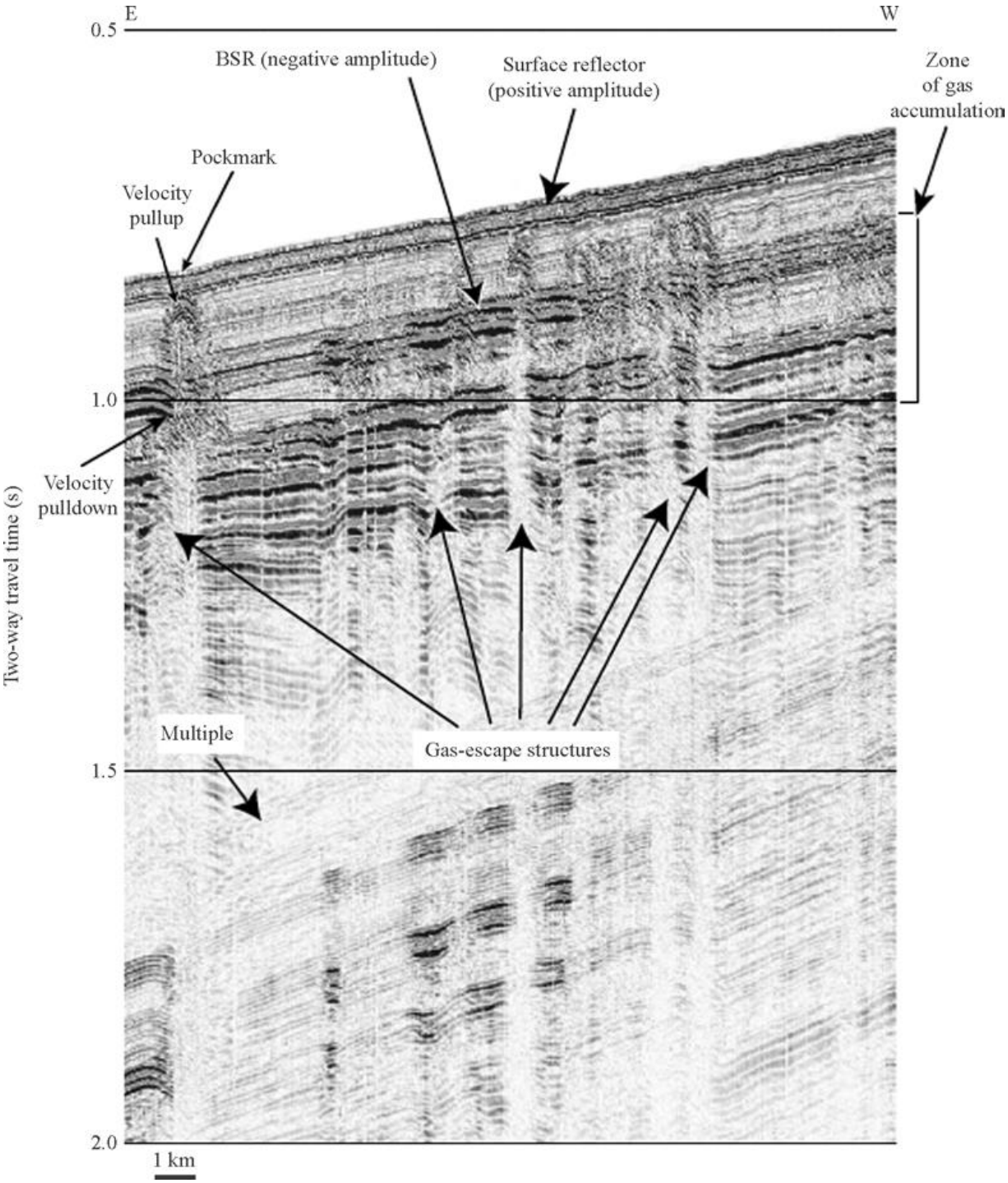

Figure 1.9: A vertical seismic section from the Sea of Okhotsk displaying some gas related anomalies. A bottom simulating reflector (BSR) indicating the bottom of gas hydrate stability zone (GHSZ). Vertical blank zone interpreted as gas-escape structures are found below pockmarks and velocity pullup likely to be due to MDAC. In addition a velocity pull up is observed just above some of the vertical blank zone. (Judd and Hovland, 2007)

Fluid seepage at the seabed can act as nutrient and can boost biological activity on the seabed. Long lasting seepage may lead to buildup of biological masses such as accumulation of shells

forming mounds on the seabed. (Hovland and Judd, 2002) Evidence of biological activity related to seeps are observed on various environments. Methane derived authigenic carbonates (MDAC) associated with pockmarks, shallow gas and gas hydrates have been found in several geological environments. (Judd et al, 2002) Concentrations of methane in the bottom waters correlates well with biological activity and carbonate mounds covering the seabed in a giant pockmark of the lower Congo basin. (Gay et al, 2007) High biological activity due to the seepage of hydrocarbons can be seen on seismic sections as minor build ups and sometimes with high amplitude anomalies on RMS amplitude attribute maps. If they appear to be stack, long term seepage is the likely explanation. (Løseth et al, 2009)

Bright spots and some of the other hydrocarbon indicators on a seismic data can be produced by factors other than the existence of gas in the area. Flat spots can indicate digenetic effects, and bright sports can be set up by carbonates. The appearance of just one of the previously mentioned seismic expressions does not solely indicate the occurrence of gas in the pore space. The likelihood of the effects being generated by fluids increases with the presence and variety of the effects mentioned above. (Badly, 1985)

Chapter 2: Geological evolution:

2.1 Study area

The Barents Sea named after the sixteenth century Arctic explorer Willem Barents is a large epicontinental sea with an average water depth of 300m (Rønnevik et al, 1982) bounded by the Norwegian Sea to the west and the Novoya Zemlya to the east, to the south by Finnmark County and northern Russia, and to the north by Svalbard and Franz Joseph Land (figure 1). Hydrocarbon exploration has been ongoing since the first seismic data was acquired in 1970 and made available for oil companies in 1977 (Linjordet & Olsen, 1992).

The Snøhvit field situated in the Center of the Hammerfest basin was discovered in 1984, with 160 billion standard m^3 gas and 73million standard m^3 oil estimated to be in place (Linjordet and Olsen, 1992). Two of the three available high resolution 3D p-cable seismic cubes for this study are acquired in the Snøhvit field area and the third is acquired in the neighboring Ringvassøy-Loppa Fault Complex (RLFC) (figure 3.2).

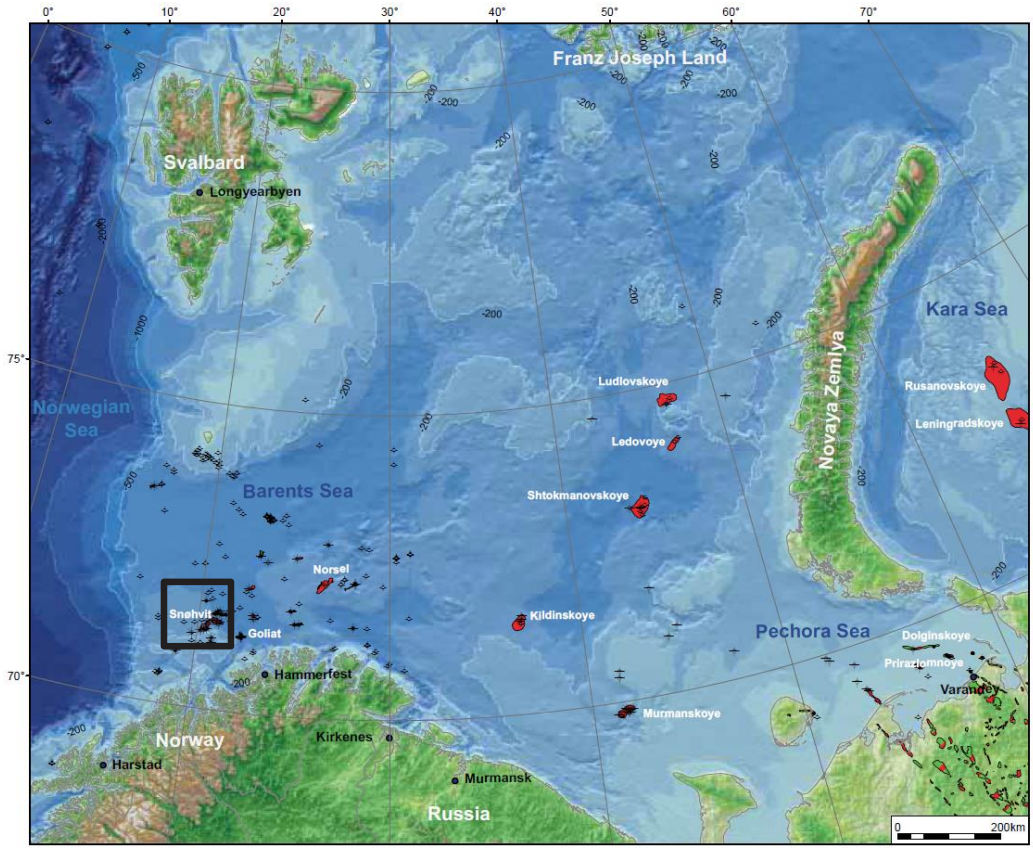

Figure 2.1: *Bathymetry of the Barents Sea and adjacent land area. The black rectangle highlights the location of study area.(Figure from Henriksen et al, 2011)*

2.2 Tectonic Development of the Barents Sea:

Plate movements along with the corresponding changes in the climate and depositional conditions molded the Barents Sea into its current form. The main tectonic events in the Barents Sea geological history are Caledonian and Uralian Orogenies, Cimmerian tectonics, the opening of the Norwegian-Greenland Sea. (Faleide et al, 1993)

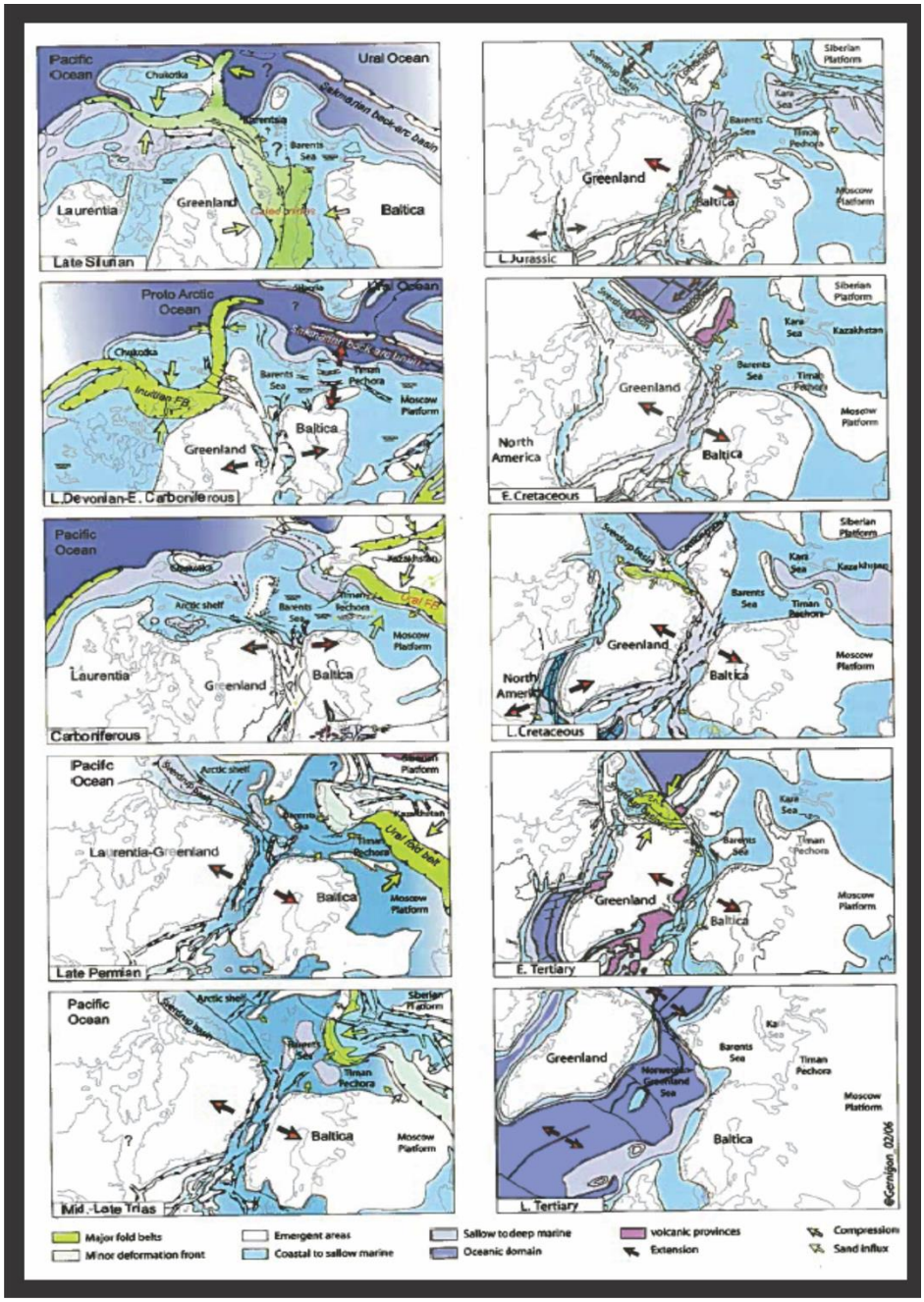

Figure 2.2: *Geological evolutions of the North Atlantic and Arctic regions starting in the late Silurian to late Tertiary (figure from Smelror et al, 2009)*

2.2.1 Palaeozoic:

The basement of the western Barents Sea was primarily affected by and consolidated during the Caledonian Orogeny. The Caledonian Orogeny led to the closure of the Iapetus Ocean and consolidation of Laurentian and Baltica plates into the Laurentian continent. The origin of Caledonian Orogeny can be traced back to a first Finnmarkian (late Cambrian-Early Ordovician) phase and a later Scandian (mid Silurian-early Devonian) phase. This tectonic activity ceased in the early Devonian (approximately 400 Ma). (Dore, 1995, Henriksen et al, 2011) The Caledonian compressional regime changed to left-lateral and strike-slip movement during the late Devonian time. (Faleide et al, 1984)

Uralian Orogeny involved the closure of the Uralian Ocean followed by continental collision of Baltica and west Siberian Cratons which gave rise to the formation of Ural Mountains between the early Carboniferous and Triassic time. Carboniferous-Permian carbonates in the eastern Barents Sea are folded and thrusted as a result of the mountain building process related to the Ural Mountains. (Smelror et al, 2009) The Uralian Orogeny also caused uplift to the eastern parts of The Barents Sea during Devonian to Carboniferous-Permian time which was followed by post-Permian subsidence in basins surrounding Novaya Zemlya. (Henriksen et al, 2011) The Caledonian and Uralian Orogenies dominate the basement structures in the Barents Sea. (Dore, 1995)

Erosion of the hinterland and deposition of red sandstones on the western parts of the Barents Sea followed the Caledonian Orogeny (Smelror et al, 2009), while the post-Caledonian rifting developed some of the early rift basins along weakness zones in the Caledonian basement in the Devonian-early Carboniferous time. (Gudlaugsson et al 1998, Smelror et al, 2009) The Caledonian trends are immensely influential in the tectonic evolution of the Barents Sea as they are activated time after time (Dore, 1991). Fan-shaped arrays of basins in the western Barents Sea developed and are orientated mainly in a north easterly direction in the major rift zones and northerly direction in the western margins. These orientations were inherited from the Scandinavian-Greenland caledonides which followed a north easterly trend, the Svalbard Caledonides-Innuitian foldbelt which followed a northerly trend and the fan-shaped structures displays the combined effect of both. (Dore, 1991, Gudlaugsson et al, 1998) This extensional tectonic phase is related to pre-opening rifting episode in the North Atlantic region. This tectonic phase caused the formation of several sedimentary basins in the Barents Sea such as Hammerfest, Tromsø, Bear Island, Nordkapp basins and continued throughout the mid

Carboniferous. This tectonic phase then changed into regional differential subsidence during the late carboniferous time. (Gudlaugsson et al 1998, Henriksen et al, 2011) The regional subsidence developed to a large regional sag basin that was present over the entire Barents Sea towards the end of the Palaeozoic. This event is understood to be caused by the closure of the Uralian Ocean along the eastern margins of Baltica during the mid-Carboniferous, but the propagation of the collusion reached the eastern Barents Sea at the transition between Carboniferous and Permian time. (Smelror et al, 2009) The south western Barents Sea was continental up until the mid-late Carboniferous time (Gudlaugsson et al 1998), but a transgressional pulse in the carboniferous time forced the northern areas in to marine setting (Faleide et al, 1984). The closure of Uralian Ocean together with the opening of a regional sea way in Early-Late Permian forced a change in depositional regime in the western Barents Sea from warm-water carbonates to cold- and deep-water, fine clastics and silica-rich spiculites. (Smelror et al, 2009) The change in the climate and depositional environment is marked by a regional unconformity in the Barents Sea between the late Carboniferous and early Permian strata. (Henriksen et al, 2011) During the Permian-Early Triassic time another extensional tectonic phase impacted the current western margin of the western parts of the Barents Sea. (Gudlaugsson et al 1998)

2.2.2 Mesozoic:

The Triassic time was a tectonically quite period accompanied with post-rift thermal regional subsidence over most of the western Barents Sea. The occurrence of minor movements on the Bjarmeland and Finnmark platforms and uplift and erosion of the Loppa High due to Permian-Early Triassic extension in the western margin were the exceptions in the otherwise tectonically quite western Barents Sea. (Henriksen et al, 2011, Smelror et al, 2009) The salt deposits in the Nordkapp and Maud Basins were started during the early and late Triassic respectively. (Henriksen et al, 2011) The South and North Barents Basins in the eastern parts of the Barents Sea subsided rapidly during the late Permian and throughout Triassic (Henriksen et al, 2011, Smelror et al, 2009). The eastern, southern and northern area of the Barents Sea were uplifted during the mid-late Triassic time (Smelror et al, 2009).The eastern Barents Sea was affected by early Permian and early Triassic compressional phase of the Uralian Orogeny, which reached the eastern areas of the Barents Sea during the late Triassic-early Jurassic and that led to folding and trusting in the eastern areas particularly in Timean Pechora and Novaya Zemlya. (Henriksen et al, 2011)

The late Triassic – Early Cretaceous Cimmerian tectonic event in the Barents Sea was composed of several discrete rift pulses related to Arctic–North Atlantic rift during the breakup of the mega-continent Pangaea, and it was the main tectonic incident in the Mesozoic time of the Barents Sea region. High angle normal faults with restricted impact to the underlying layers in the southwestern parts of the Barents Sea during the Middle Jurassic marks the onset of the Cimmerian tectonics in the Barents Sea. The western Barents Sea exhibited regional differential subsidence during the mid-late Jurassic. (Faleide et al, 1984) At this period the Barents Sea was rifted through the Hammerfest and Bjørnøya Basins. Up until the mid-Jurassic the Hammerfest basin was along with the Tromsø basin part of a larger epeirogenic depositional regime. Since the mid-Jurassic the Hammerfest basin has been a separate basin and is defined at the reference level. (Linjordet and Olsen, 1992; Faleide et al, 1993) The late Jurassic extensional tectonics has left its mark as far east in the Barents Sea as the areas adjacent to Novaya Zemlya (Dore, 1991). The Cimmerian tectonics ceased for a while during the uppermost Jurassic before it resumed in the transitional time between Jurassic and Cretaceous with a chain of large deep-seated normal faults along preexisting tectonic grains of Caledonian basement. (Faleide et al, 1984) The development of the Bear Island, Tromsø and Harstad Basins as major depocenters in the southwestern Barents Sea took place during the early Cretaceous time (Breivik et al, 1998) A thermal subsidence situated in the Tromsø Basin further affected Harstad, Bear Island and to some extent the Hammerfest Basin during the early Cretaceous phase of the Cimmerian tectonics. Towards the late early-Cretaceous a large scale westwards oriented extensional with sinistral transtensional and a minor north trending dextral strike slip fault complex located in the Bjørnøyrenna fault complex separated the rapidly subsiding western Basins from the stable east. (Faleide et al, 1993) After the conclusion of the Cimmerian tectonics, strong differential subsidence dominated the western Barents Sea with faster subsidence rates to the west of the Ringvassøy-Loppa Fault Complex than to the east, while the Svalbard Platform was uplifted and eroded. This subsidence continued throughout the rest of Cretaceous at a slower pace. (Faleide et al, 1984)

2.2.3 Cenozoic:

The Cenozoic North Atlantic Breakup in the southwestern Barents Sea developed in three distinct phases. An early Eocene phase of continent-continent transform movement prior to crustal break-up was followed by Eocene- earliest Oligocene phase of ocean-continent transform movement took place as the Atlantic spreading ridge spread northwards along the

shear zone and then a passive continental margin was finally developed starting during the earliest Oligocene as figure 2.3 shows. (Faleide et al, 2008; Vågnes, 1997)

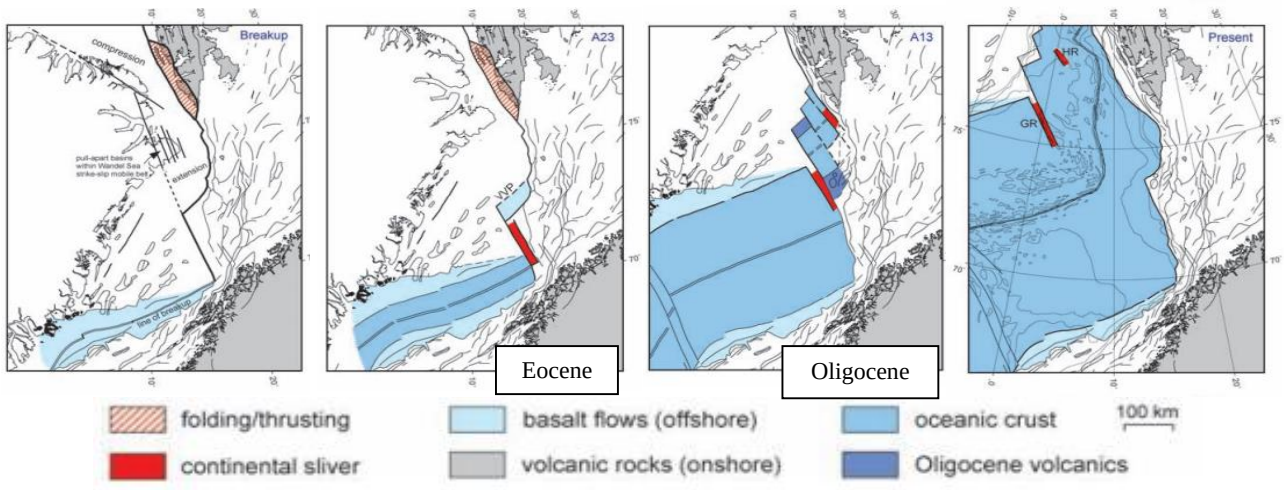

Figure 2.3: *The northwards opening of the Norwegian-Greenland Sea. (Figure from Faleide et al, 2008)*

A leaky transform system with both transtensional and transpressional elements in the early Eocene initiated the early developmental stage of western Barents Sea margin near the Senja Fracture Zone as in(Faleide et al, 1993) fig (above and below) leading to uplift in the eastern and northern parts of the shelf, while the western most basins subsided (Smelror et al, 2009). The southern parts of the Sørvestsnaget and Harstad Basins were uplifted during early Eocene time, whereas the northern parts of the basins were subjected to extensional faulting and deposition of Palaeogene strata. (Faleide et al, 1993) Meanwhile, a compressional component of the early Eocene tectonic phase along the Hornsund Fault Zone induced Fold- and Trust-belt on Svalbard (Smelror, 2009) as illustrated in figure 2.3. The opening of northern Greenland Sea took place in the earliest Oligocene as a result of a shift in the direction of the early Eocene tectonics. The formation of new oceanic crest followed by subsidence, and accumulation of thick sedimentary wedge in the Barents Sea margin has been ongoing since the Oligocene (figure 2.3). (Faleide et al, 1996) The Stappen, Loppa and Vestlemøy Highs exhibited tectonic induced uplifted during the Eocene-Oligocene time and remained as Highs throughout the Cenozoic (Reemst and Cloetingh, 1994).

The late Cenozoic evolution of the western Barents Sea was molded by the interaction between glaciation/deglaciation cycles, variations in sea level and local and regional tectonic activity in the area (Reemst and Cloetingh, 1994). A late Pliocene-Pleistocene uplift and erosion took place in the entire Barents Sea with the maximum effects imposed to the northern platforms and areas around Svalbard, whereas Hammerfest, Nordkapp basins and Loppa high exhibited

lesser amount of uplift (not exceeding 2km) (Smelror et al, 2009). Isostatic readjustments coupled with intraplate compression (could be related to reorganization of spreading rate along the central Atlantic spreading center 2.5 MA and climax in compressional tectonics in northern Alaska and northern Canada 6Ma) induced stress are suggested by Reemst and Cloetingh (1994) to be the main driving forces to the late Paleocene- Quaternary uplift to the area east of the Barents Sea margin and increased subsidence to the west of the Margin as illustrated by Figure 2.4.

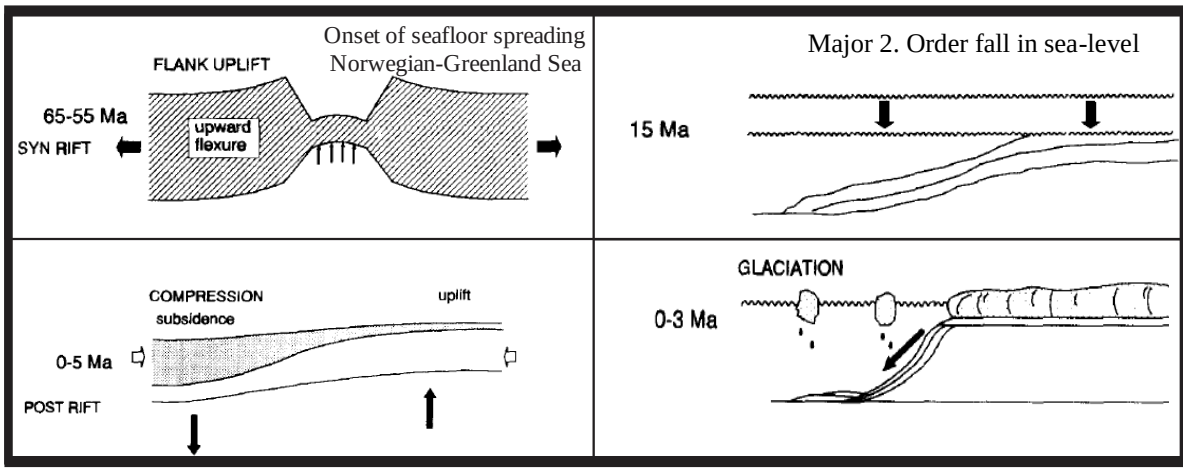

Figure 2.4: A model presents a possible explanation to the major episodes of Cenozoic evolution of the Southwestern Barents Sea. (Modified from Reemst and Cloetingh, 1994)

2.3 Lithostratigraphy and depositional setting:

Figure 2.5 shows the Hammerfest basin lithostratigraphic chart containing a 5000 m thick Mesozoic and Cenozoic strata starting at the Triassic period (Linjordet and Olsen, 1992).

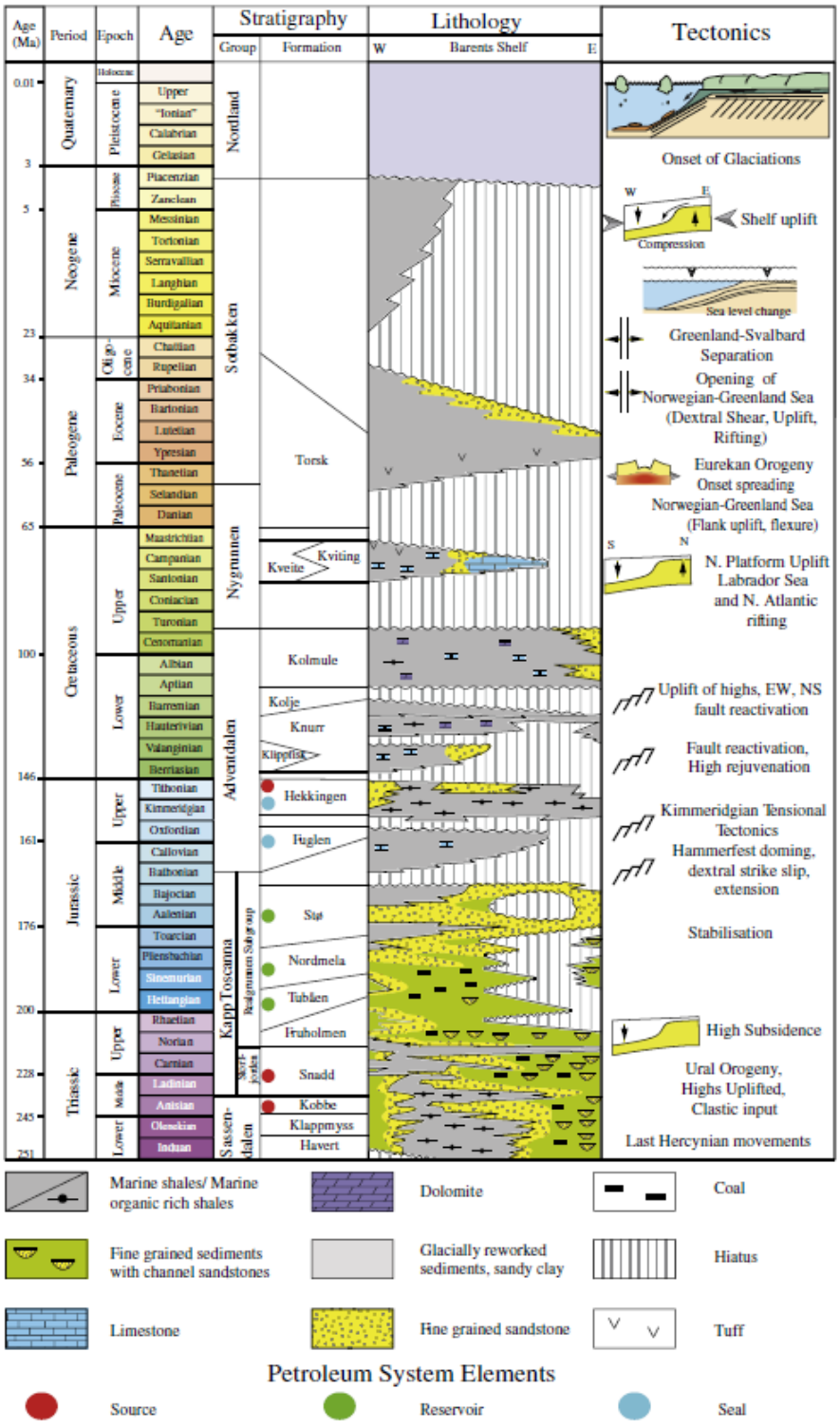

Figure 2.5: *Mesozoic and Cenozoic lithostratigraphic chart of the Hammerfest basin. (Figure from Ostanin et al, 2012)*

2.3.1 Paleozoic:

During the Devonian time rapid erosion of high grade metamorphic Caledonian mountains took place. This led to deposition of continental siliclastic material in the basin in the Barents Sea. These deposits are currently only found in few grabens and subbasins in the western Barents Sea that formed as a result of late Caledonian tectonic movements. The shallow water basin in the eastern part of the Barents Sea was dominated by carbonates throughout early Lochkovian (early Devonian) and the depositional environment changed towards the late Lochkovian which led to the deposition of black shales and development of carbonate platform at the flanks of the basin. Marine shelf and distal, deep marine conditions dominated the eastern Barents Sea during the Late Devonian time which caused the development of prograding delta systems from west to east. (Smelror et al, 2009)

The western parts of Barents Sea were covered by highlands, alluvial and fluvial plains, marsh and eastwards prograding delta systems with sedimentation patterns controlled mainly by basin formation tectonics during the early Carboniferous time. Meanwhile, several types of carbonate shelf conditions prevailed in the eastern parts of the Barents Sea. (Smelror et al, 2009) Humid climate conditions dominated on the carboniferous throughout most of the Barents Sea. Climate changed from humid tropical to sub-tropical and arid climate During Moscovian (early late-Carboniferous) time. The depositional conditions in the Barents Sea during mid-late carboniferous time were mainly controlled by the climate change and the transgression pulse in the Bashkirian time. In this time period most of the Barents Sea, apart from horst-like features to the west, was transgressed. Shallow water carbonates dominated the eastern Barents Sea, while central parts of the western Barents Sea such as the Tromsø and Nordkapp basins consisted of thick succession of evaporites. (Henriksen et al, 2011, Smelror et al, 2009)

The western Barents Sea was separated by structural highs from the eastern areas and was only connected to the sea through narrow straits during the Early Permian. Icehouse climatic conditions dominated this time. The entire Barents Sea was flooded during the high sea-levels. This led to the development of up to 100m thick shallow-water carbonates on the structural highs, while the deeper parts where characterized by braided high-stand carbonates and low-stand anhydrate deposits. During the low sea levels and when the western areas were totally separated from the sea, local karst landscape development and halite deposition in central parts of the basins took place. The eastern areas were dominated by shales and carbonate mudstones deposits. (Henriksen et al, 2011, Smelror et al, 2009) The arid climate of carboniferous and

early-Permian changed to temperate climate in the mid-Permian. The climate change coincided with a Wordian transgression that submerged the Barents Sea underwater. The entire area was under Shallow to deep marine depositional condition as a result of the changes. These events along with the flourishing of sponge species led to silification of the sediments as a transition from carbonate deposits to silicified clasts and muds. The deep-shelf environments to the west were prevailed by swamp colonies, while deposition of shallow marine sand-, silt- and mudstone was common in most of the eastern areas in the mid Permian. (Smelror et al, 2009)

2.3.2 Mesozoic:

The marine connection of the Barents Sea towards the end of Permian and early Triassic was restricted to west, as the south eastern connection was cutoff due to the Uralian orogeny. The western Barents Sea remained under marine conditions during this time period. The Hammerfest, Nordkapp basins and the northern parts of the Finnmark Platform are thought to have been the deepest areas to the west, with the development of submarine fans from the margins to the axis of the basins during the early Triassic. The sediments that constitute the submarine fans originate from the Fennoscandian Shield. The sub-aerially exposed eastern Barents Sea consisted mainly of alluvial and lagoonal sandstones, siltstones and mudstones during the early Triassic. (Smelror et al, 2009) The early Triassic Havert and Klappmyss formations consist mainly of medium to dark grey shales with minor siltstone and sandstone beds (Dalland et al, 1988).

The Barents Sea existed as a central marine shelf with open marine connection into the North Atlantic rift system towards the south west during the mid-Triassic time. Fennoscandian and Uralian sand was deposited in the NE-SW trending paleocoastline, while sand, silt and shales were deposited at the delta front in the southwestern Barents Sea. Mudstone deposited in an anoxic condition with up to 12% organic content is also found in the southwestern Barents Sea in the mid-Triassic strata. (Smelror et al, 2009) The mid-Triassic Kobbe formation overlays Klappmyss formation and is made up of lower shale unit which gradually changes to interbedded shale, siltstone and carbonate cemented sandstone (Dalland et al, 1988). The eastern parts of Barents Sea were under lacustrine and flood plain depositional environment during the Mid-Triassic time. Mid-Triassic grey, plant bearing mudstones, siltstone and sandstones were deposited in an alluvial plain setting in the eastern Barents Sea. (Smelror et al, 2009)

The Upper Triassic time in the Barents Sea was mainly dominated by westwards progradation of the coastal and near-shore depositional environment derived by regional regression in the Arctic area. The coastal plains stretched from Novoya Zemlya and Timian Pechora in the east to the Hammerfest and Fingerdjupet Basins in the west. (Smelror et al, 2009) The Snadd formation overlain by the Fruholmen formation concludes the Triassic strata in the western Barents Sea. The Snadd formation contains shales interbedded with siltstones and sandstones, while the Fruholmen formation is made up of a lower shale unit followed by a sandstone unit and an upper shale unit. (Dalland et al, 1988) Meanwhile floodplain and deltaic mudstone, siltstone and sandstone were deposited in the eastern parts of the Barents Sea (Smelror et al, 2009).

During the late Triassic- early Jurassic, uplift and erosion took place throughout most Barents Sea shelf. This led to the scarcity of sedimentary rocks of this time interval in most of the Barents Sea. However, some areas in western parts of the Barents Sea such as the Hammerfest, Nordkapp and Tromsø basins remained under shallow marine depositional environment, and it was there the rocks of the earliest Jurassic intervals were preserved. The preserved early Jurassic strata consist mainly of estuarine, lagoonal sandstones. Towards the late Early-Jurassic global sea level rice caused the flooding of the Barents Sea. The eastern Barents Sea, separated from the western Barents Sea by the mountain ranges of Novaya Zemlya, was flooded from the Paleo-Pacific, while the western Barents Sea had marine connection towards the southwest. The Toarcian (late Early-Jurassic) strata consist of deltaic and near shore sandstones interbedded with siltstone which was deposited during transgressional pulses. The depositional condition in the southwestern Barents Sea changed from flood-plain setting to shallow marine setting during the early Jurassic. Sandstone, siltstone and minor shale beds constitute later portions of the early Jurassic strata. (Smelror et al, 2009) Tubåen and the Nordmela formations constitute the early Jurassic strata in the Hammerfest Basin (Dalland et al, 1998). Sandstone with minor shale beds deposited in shallow marine to coastal plain depositional environment makeup the Tubåen formation, while the overlying Nordmela formation consist of silty shales and fine grained sandstones (Dalland et al, 1988; Linjordet and Olsen, 1992).

A regressive pulse hit the Barents Sea during the mid-Jurassic triggering erosion of the sub-aerially exposed Barents Sea shelf. Depositional gap is observed over most of the Barents Sea shelf apart from the western most basins such as the Hammerfest and Nordkapp Basins to the west and the South Barents Sea basin to the east. Shallow marine sandstones constitute most of the Bojocian (mid-Jurassic) strata in the Hammerfest and Nordkapp Basins, whereas alternating

shallow shelf clay and sand stemming from several transgressive-regressive cycles dominated the South Barents Basin. (Smelror et al, 2009) The mid Jurassic strata in the Hammerfest Basin consist of moderately to well sorted mature sandstones with minor shale and silt stone units of the Stø Formation (Linjordet and Olsen, 1992; Dalland et al, 1988). The sands were deposited in a prograding coast, while the shale and silt units mark a regional transgressive pulse (Dalland et al, 1988).

After the regressive phase of the mid-Jurassic time, the Barents Sea exhibited yet another transgressional phase resulting in marine shelf depositional condition prevailing most of the area. Water depths up to 200-300 are inferred over large parts of the Barents Sea during the Tithonian (upper Jurassic) time. (Smelror et al, 2009) The late Jurassic sediments are of the Fuglen and Hekkingen formations deposited in an anoxic deep water conditions created by local circulation barriers associated to Kimmerian movements in the Hammerfest Basin (Linjordet and Olsen, 1992; Dalland et al, 1988). The sediments in the Fuglen formation are dominated by dark brown pyritic mudstones and thin limestone units, while the Hekkingen formation consist of brownish-gray to very dark gray shales and claystone with minor units of limestone, dolomite, siltstone and sandstone (Dalland et al, 1988).

Marine connection through the southern parts of the Barents Sea remained open in the earliest Cretaceous, though the extents of the areas of marine sedimentation were reduced. Deposition of continuous, thick units of clay with minor limestone dolomite layers took place in the deeper basin of the southwestern Barents Sea during the early Cretaceous, while the platforms and highs had higher carbonate and lesser clastic content. Near-shore depositional conditions with major silt layers and some sand and clay content existed in the eastern parts of the Barents Sea during the earliest Cretaceous. Marine depositional conditions prevailed in the western and central Barents Sea, while the northeastern areas were up lifted during the late early-Cretaceous. The rapidly subsiding Harstad, Tromsø, and Bear Island Basins in the western margins accumulated shale, siltstone and minor sandstones during the middle Cretaceous. Alternating marine and continental depositional conditions led to deposition of sandstone interbedded with coal bearing silt in the eastern Barents Sea during the Middle Cretaceous. (Smelror et al, 2009) The lower Cretaceous Nordvestbanken Group consists of claystone with minor limestone and dolomite interbeds deposited in marine setting in the Hammerfest Basin (Dalland et al, 1988).

The Late Cretaceous strata are preserved in the subsiding basins towards the western margins of the Barents Sea, whereas to the east these strata are truncated below the Cenozoic

unconformity (Henriksen et al, 2011). Claystone with minor limestone deposited in open marine shelf environment are preserved in the Tromsø, Hammerfest and Sørvestsnaget Basins. (Faleide et al, 1993) The central and eastern parts of the Hammerfest basin encompass calcareous sandstone with interbeds of glauconitic and mudstone interbeds of the upper Cretaceous Kviting Formation, while Greenish to grayish shales and claystones of the Kveite Formation are present in the Tromsø basin, Ringvassøya-Loppa fault complex and continues into the Hammerfest Basin (Dalland et al, 1988).

2.3.3 Cenozoic:

The Barents Sea underwent several episodes of uplift and erosion during the Cenozoic time which led to variation in the thickness and completeness the Cenozoic succession across the continental shelf and margin. In the marginal area such as the Sørvestsnaget Basin and Vestbakken volcano province a more or less complete Cenozoic strata are preserved. (Henriksen et al, 2011) Whereas in the Finnmark and Bjarmeland platforms the quaternary sediments directly overly the cretaceous strata (Smelror et al, 2009).

The transition from Mesozoic to Cenozoic is marked by a major hiatus in most of the Barents Sea (Faleide et al, 1984). Following this Hiatus Mid/Late Paleocene bathyal mudstones were deposited in transgressed intracratonic basins. These sediments are preserved in the Hammerfest, Tromsø, Bear Island and Nordkapp Basins. The Eocene opening of the Norwegian-Greenland Sea south of the Senja Fracture Zone created a new depocenter along the newly created margin. The northward opening of the Norwegian-Greenland Sea made the continental margin the main depocenter of the area since the middle Eocene with sediment supply from the continental shelf, slop and the highs. Thick Eocene to recent sediments are accumulated along the continental margin. Starting the Mid Miocene the continental shelf, shelfbreak and slope areas of the Barents Sea were eroded induced by fall in sea level. The erosion of the Barents Sea shelf intensified enhanced by reduction of vegetation cover in the area. Up until the Mid-Pliocene the fluvial processes were the main erosion mechanism in the area. (Vorren et al, 1991)

A cooling of the climate took place towards the late Pliocene which led to glaciation of high altitude areas and coastline. This phase lasted from 3.5 to 2.4Ma. Glaciation expanded from the coastal area and ice sheets covered the parts of the Barents Sea between 2.4 - 1.0 Ma. This was then followed by at least five to six episodes of shelf edge glaciation of the Barents Sea during the latest 800 Ky. (Kneis et al 2009; Smelror et al, 2009) Fluvial and glaci-fluvial

processes eroded an average of 420 m of sediment from the shelf area between 3 and 0.8 Ma and an additional 400m of sediments of the shelf were eroded during the last 800Ky in the Barents Sea (Vorren et al, 1991). Troughs such as the Bear Island trough act as channels for the glacial derived erosion and fans build up at the end of the troughs as debris flow lobes due to deposition of vast amount of sediments on the continental shelfbreak and slope. These fans are known as trough mouth fans (TMF) and are thought to develop further when the grounded ice sheets reach the shelfbreak. During periods of minor glaciations, glacio-marine conditions dominated the shelf break, while the interglacial lead to sediment scarcity at the continental margins. (Vorren et al, 1988; Vorren & Laberg, 1997) The glacigenic sediments are separated from the underlying Tertiary sediments by an unconformity commonly referred to as the Upper Regional Unconformity (URU) molded due to long periods of uplift and erosion in the Barents Sea (Vorren et al, 1991). The thickness of the quaternary glacigenic sediments varies greatly throughout the Barents Sea. The continental margins are covered by 900-1000m quaternary glacigenic, whereas the shelf areas are buried under 300- 0m of glacial sediments. These quaternary sediments consist predominantly of muddy diamictons. Following several cycles of glaciations, the southeastern and western Barents Sea has exhibited conditions similar to the present one for the last 10ky. (Vorren et al, 1988)

Bathyal depositional environment dominated the Hammerfest Basin following the Paleocene transgressions. This led to deposition of sediments sourced at Loppa High from suspension in low energy environment during the Mid/late Paleocene – Early Eocene in the Hammerfest Basin. (Knutsen and Vorren, 1991; Vorren et al, 1991) Claystones with minor silt- and lime-stones deposits make up the Torsk formation in the Hammerfest basin (Dalland et al, 1988). An angular unconformity URU separates the underlying dipping Torsk formation from the glacial deposits. (Vorren et al, 1991) The younger parts of the glacial Nordland group makes up the glacial unit in the Hammerfest Basin (Dalland et al, 1998). The Nordland Group is made 100 to 250 m thick soft Claystone and sands and clay grades into sandstones in the Hammerfest Basin (Linjordet and Olsen, 1992; Dalland et al, 1988).

Chapter 3: Data and Method

3.1 P-Cable Data:

The seismic datasets used in this study are P-cable 3D high resolution seismic surveys. The P-cable system is cost-effective systems best suited for acquiring small and shallow datasets with high resolution to be utilized in geo-scientific research, core-log seismic integration and drilling safety (Planke et al, 2013). The acquisition system is made up of two paravanes extending a cross cable perpendicular to the sailing direction of the vessel with 25 to 50 densely employed streamers towed to the cross cable (Eriksen et al, 2014) providing the acquisition of several seismic lines simultaneously(Planke et al, 2013). The streamers are typically between 25 and 50 m long, and the shot and receivers are also placed close to each other. The combination of the density of the streamers and source receiver configuration provides high resolution data, while the length of the streamers limits the depth of the data (sub-bottom depth usually comparable to the water depth). (Planke et al, 2014; Eriksen et al, 2014)

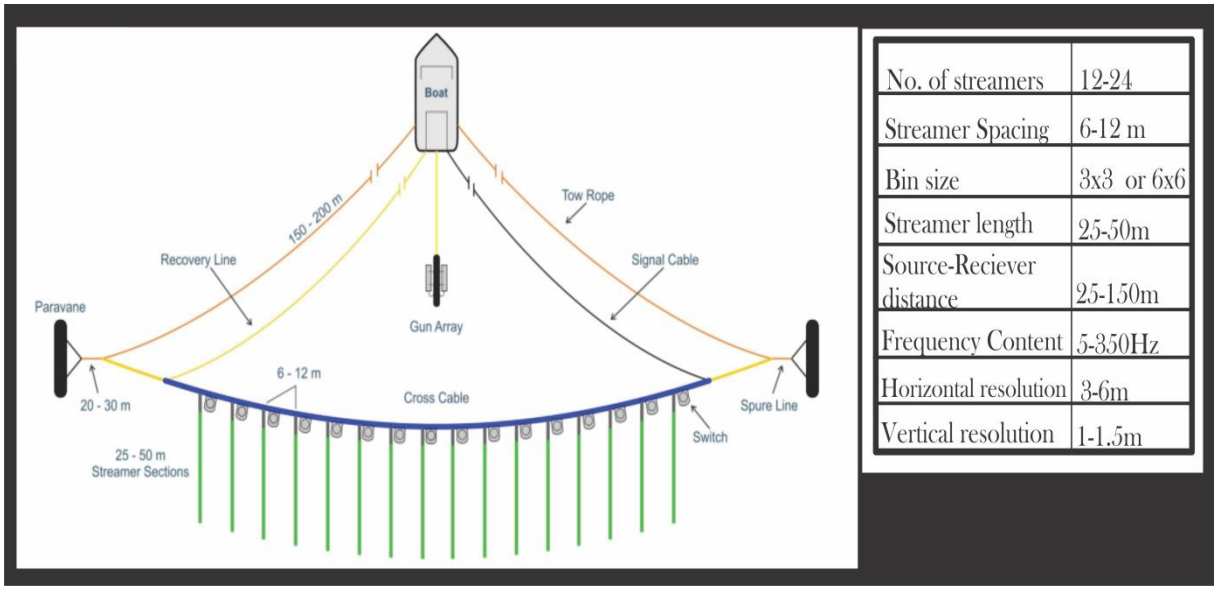

No. of streamers	12-24
Streamer Spacing	6-12 m
Bin size	3x3 or 6x6
Streamer length	25-50m
Source-Reciever distance	25-150m
Frequency Content	5-350Hz
Horizontal resolution	3-6m
Vertical resolution	1-1.5m

Fig 3.1: illustration of a simplified P-Cable 3D acquisition configuration with the typical system specifications on the table to the right. (Figure from Eriksen et al (2014))

3.2 3D Seismic Cubes

In this study, 3D seismic data has been used to identify fluid migration pathways and shallow gas distribution in the study area. Three high resolution 3D P-Cable seismic cubes acquired at the Hammerfest basin and the adjacent Ringvassøy-Loppa Fault Complex has been provided by University of Tromsø, The Arctic University of Norway for this study. Snøhvit 1 3D P-Cable cube spans over 14 Km^2 (1,8km X 7,9km) over a pockmarks dominated area in the Snøhvit field, in the Hammerfest Basin. Snøhvit 2 cube is acquired over of a shallow acoustic masked area in the northern parts of the Snøhvit field and covers 11.8 km^2 (6,9km X 1,7km) area. The third dataset, Area 1 covers 16 km^2 (2,5km X 6,5 km) over buried pockmark rich area in the Ringvassøy-Loppa Fault complex, northwest of the Hammerfest Basin. The vertical penetration depth of these seismic cubes is up to -850ms TWT below sea surface (corresponds roughly to the water depth).

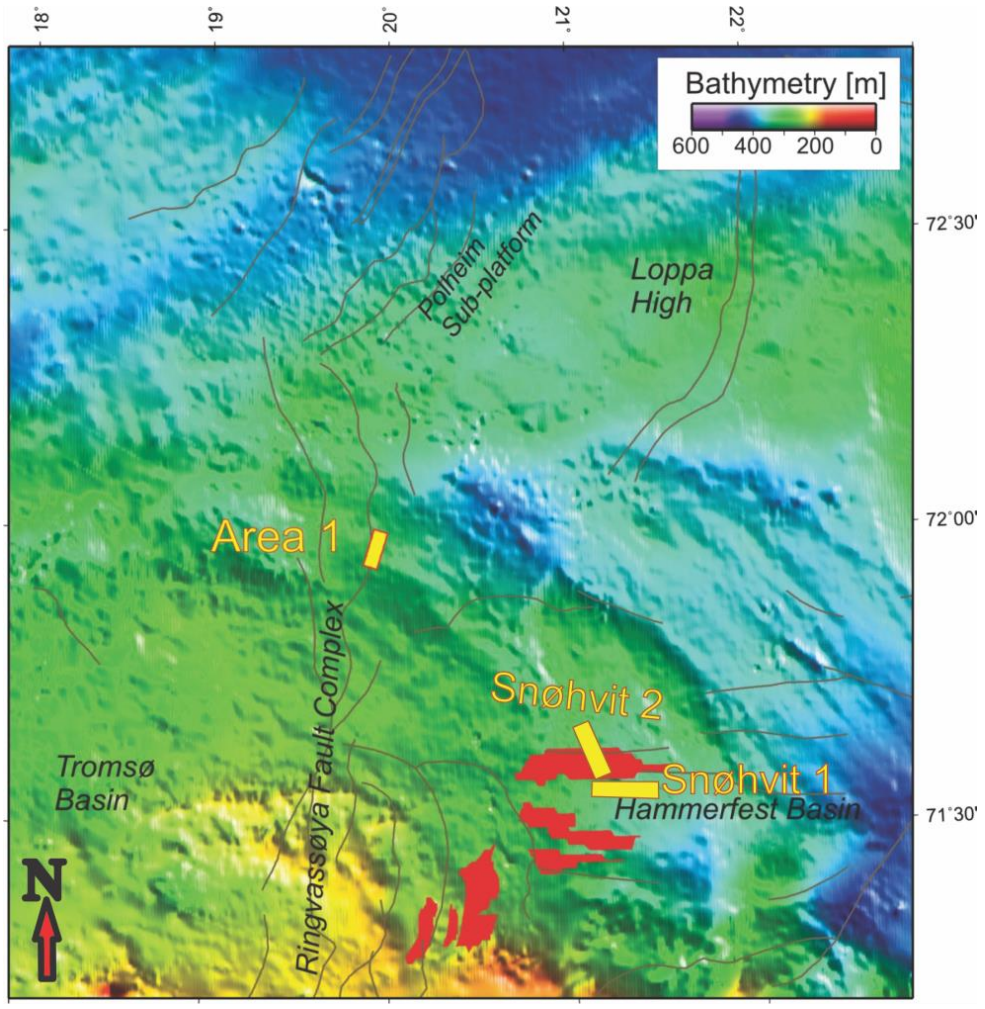

Fig 3.2: Location of the high resolution 3D P-cable datasets highlighted by yellow rectangles

3.3 Seismic resolution:

Seismic reflections are setup by the acoustic impedance contrast between adjacent rock units, but their resolution and detection capabilities depend on factors such as signal to noise ratio, interval velocity of the rocks, frequency and bandwidth of the recorded data and space between rock units. Seismic resolution refers to the smallest distance between reflectors to be specifically recognized on the recorded data, whereas the detectability deals with the minimum size at which a single feature can be detected by a slight interference in the recorded data. (eg. Veeken, 2007)

3.3.1 Vertical resolution:

The least vertical spacing between two layer boundaries with sufficient acoustic impedance contrast to set up a seismic reflection that is clearly distinguished on the recorded data is known as the vertical resolution of the seismic data. The vertical resolution of a seismic data depends on the frequency and bandwidth of the acoustic signal and the interval velocity of rocks. If the distance between the layers is less than the vertical resolution, overlapping of the seismic traces leads to positive (enhancing) or negative (canceling) interference. The vertical resolution of the data deteriorates with increasing depth due to loss of higher frequencies and increase of interval velocities with depth (enlarging the wave length). (Veeken, 2007)

The vertical resolution is defined as one fourth of the dominant wave length, while layer boundaries spaced as close as one thirtieth of the wavelengths are detectable in the seismic data (Badly, 1985).

$$V_r = \frac{\lambda}{4} = \frac{v}{4f} \qquad \text{Eq. 3.1}$$

Where Vr- Vertical Resolution (m), λ - Dominant wave length (m), v - interval velocity (m/s), f - signal frequency (Hz)

3.3.2 Horizontal resolution:

The horizontal resolution defines the minimum lateral distance required between reflectors to be identified as separate feature and is controlled by factors such as trace spacing (the common midpoint spacing), migration and Fresnel zone radius. The signals received at the hydrophones are not reflected of a single point on the reflector, but of an area cover by the wave front and neighboring points on the reflector enclosed within one fourth of the dominant wavelength. This area is referred to as the Fresnel zone and controls the horizontal resolution of unmigrated data. (Veeken, 2007) The radius of the Fresnel zone is defined by equation 3.2.

$$r_F = \frac{v}{2}\sqrt{\frac{t}{f}} \qquad \text{Eq. 3.2}$$

Where r_F- radius of the Fresnel zone(m), v-interval velocity(s), t-Twice travel time(s) and f- dominant frequency(Hz)

As with the vertical resolution, the horizontal resolution worsens with increase in depth as a result of increase in the interval velocity and loss of the high frequency signal. On the other hand the migration process of unmigrated data boosts the lateral resolution. (Veeken, 2007) Increase in the in-line sampling density collapses the Fresnel zone in the in-line direction of the migrated data. The horizontal resolution is further enhanced by 3D migration and increase in cross-line spacing leading to the collapse of the Fresnel zone. The lateral resolution of a migrated 3D seismic data is comparable to the bin spacing. (Cartwright and Huuse, 2005)

3.4 Petrel as Interpretation & Visualization Software platform:

Petrel E&P software platform 2013 was used as the interpretation and visualization software for the seismic data in this study. Petrel 2013 software provided means of horizon interpretations, volume and surface attribute generation that aided the work in the study of shallow gas distribution and identification of possible fluid migration pathways. In addition, various types of surface and volume based calculation and operations were carried out using the Petrel 2013 E&P software platform. Unfortunately the hardware of the workstation didn't allow for Geobody interpretation and Volume rendering. Images obtained through petrel were further processed using CorelDraw X5.

3.4.1 Horizon interpretation:

Horizon interpretation can be performed on any vertical seismic section and the 2D and 3D windows using the petrel platform. Several tracking options are available on the platform to interpret the Horizons on the vertical seismic section and on the 2D and 3D windows. Tracking parameters need to be set in order to perform autotracking. Peaks, troughs or zero-crossings of a reflector can be chosen as the signal feature to be tracked. In addition seed confidence (the minimum value that can be tracked as a percentage of the seed point) and value range (minimum and maximum amplitudes to be tracked) are some of the parameters that are defined to autotrack a reflector in 2D or 3D direction. Manual and guided autotracking options are also available to interpret a horizon. (Schlumberger. 2011) A combination of seeded 2D autotracking and manual tracking are the methods utilized in interpreting the horizons in the vertical seismic sections, while paintbrush autotracking (tracking out wards from the seed points) is used to fill the gaps between the interpreted lines in generating the horizons and their associated attribute maps used in this thesis.

3.4.2 Volume Attribute cubes:

Volume attribute cube are obtained from seismic cubes or a combination of seismic cubes and other attribute cubes. They enhance the interpretation and visualization of features greatly. (Schlumberger. 2011) The following attribute cubes have been used to aid the interpretation of fluid migration pathways and features related to them.

3D Edge Enhancement

The 3D edge enhancement volume attribute is obtained by running a dip guided 3D contrast filter (petrel, 2013). This attribute cube enhances the detection of faults.

Dominant frequency

The dominant frequency attribute cube is computed by finding the hypotenuse of instantaneous bandwidth and instantaneous frequency and is useful in detecting low frequency shadows. (Schlumberger. 2011)

Envelop

Envelop attribute cube also known as reflection strength is calculated using the instantaneous energy of the signal without taking the instantaneous phase into account. This attribute cube is helpful in detecting gas accumulation features such as bright spots. (Schlumberger. 2011)

RMS (Root Mean Square) amplitude

The RMS amplitude attribute cube calculates the root mean square of the traces over a limited TWT interval. It enhances high amplitude anomalies independent of their polarity. (Schlumberger. 2011) This attribute is mostly utilized in this thesis.

Structural smoothing

The structural smoothing attribute cube enhances the continuity of reflections by smoothing the input cube, and is great in reducing the signal to noise ratio of the input data. (Schlumberger. 2011)

Trace AGC (Amplitude Gain Control)

Trace AGC amplitude cube enhances the weak reflections in the seismic data, and is helpful when interpreting low amplitude reflection areas. (Schlumberger. 2011)

Variance (Edge method)

The Variance attribute cube is great in identifying discontinuity in the data and is great in detecting features such as channels. (Schlumberger. 2011)

3.4.3 Surface Attribute maps:

Surface attribute maps can be generated using the volume attribute cubes, the surface structures and using two distinct surfaces (Schlumberger, 2011).

Extract Value:

Extract value is helpful in obtaining values from attribute cubes using a horizon. The values of the attribute cube on the horizon are extracted. (Schlumberger, 2011)

RMS Amplitude:

RMS Amplitude attribute maps are made by obtaining the root mean square of the amplitude enclosed within two horizons or within a defined window around a single horizon (Schlumberger, 2011).

Thickness Map:

The thickness between two horizons in millisecond can be computed by defining the base and reference horizons. (Schlumberger, 2011)

Chapter 4: Results

4.1 Seismo-stratigraphy:

The vertical seismic sections show a marked unconformity separates the top most successions from the underlying dipping reflectors. Based on Vorren et al (1991) the top most unit is interpreted as late Pliocene-Pleistocene glacial deposits of the Nordland group and the unconformity as URU. The glacial successions show the largest thickness at Ringvassøy-Loppa Fault complex (RLFC). The thickness increases southwestwards where it is 140ms twt thick, while the thinnest covers towards the east display half the thickness. There is a reflector, intra-glacial reflector dividing the glacial sediments in to two units in the RLFC. This is absent in the Snøhvit datasets. The glacial sediments are of similar size in the Snøhvit area with a thickness ranging from 85 to 40ms twt. Underneath the URU several sets of dipping clinoforms appear. These clinoforms are based on Vorren et al (1991), Knutsen & Vorren (1991), Linjordet & Olsen (1992) and Dalland et al (1988) interpreted as part of the mid/late Paleocene – Eocene Torsk formation. The glacial sediments consist mainly of soft and sandy claystones, and the sand content increases upwards. The dipping Torsk formation is dominated by silty and sandy Claystones. (Dalland et al, 1988; Linjordet and Olsen, 1992).

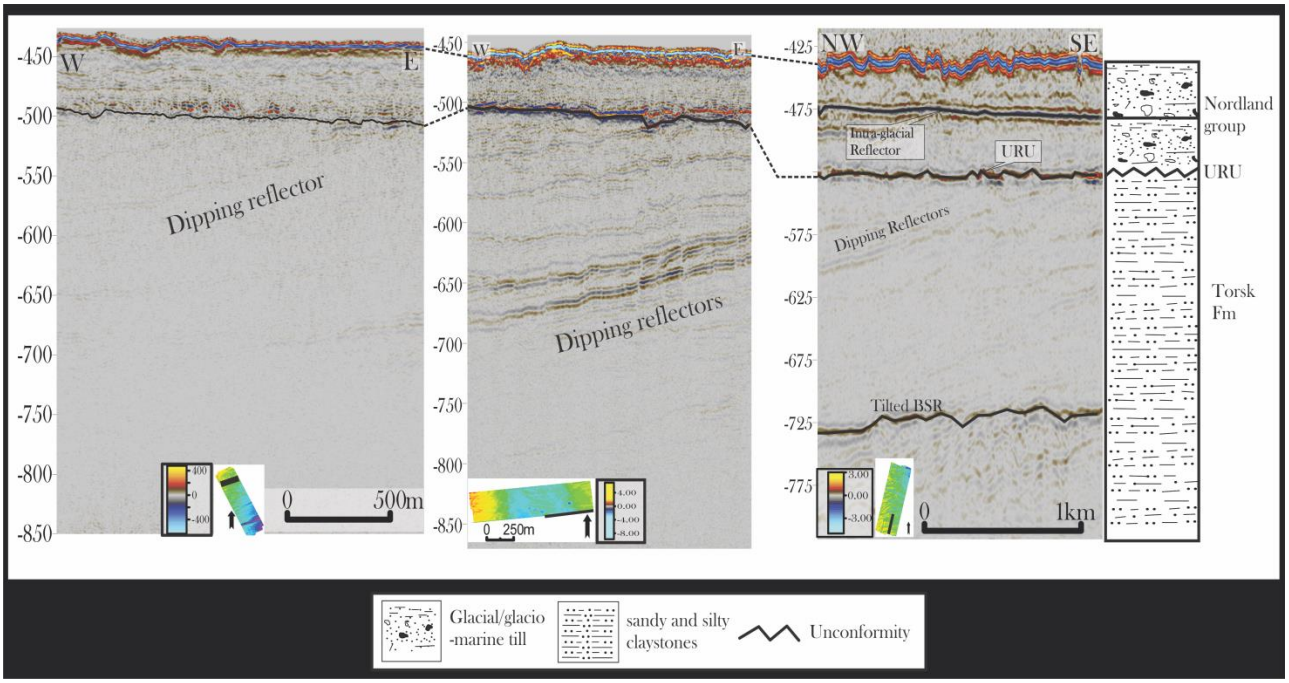

Figure 4.1: *Seismo-stratigraphic correlation of the datasets in the study area.*

4.2 Curvilinear features:

The interpreted seabed horizons of the three data sets in the study area are presented in figure 4.2. The water depth in the interpreted seabed surface in the study area is calculated to ranges from 316 to 360 m by using 1500m/s as the speed of sound waves propagating in the water column. Arching elongated linear depressions appear to have been engraved on the interpreted seafloor of the study area. The preferred orientation of the morphological features is NE-SW with some furrows cross cutting each other in random directions. The curved furrows vary in length from about 100m to more than 3 kms within the data sates available. The variation in width ranges from 40m to 180m. The furrows appear as u- and v-shaped features in the vertical seismic section (Figure 4.3), and they are typically between 4-10 meters deep.

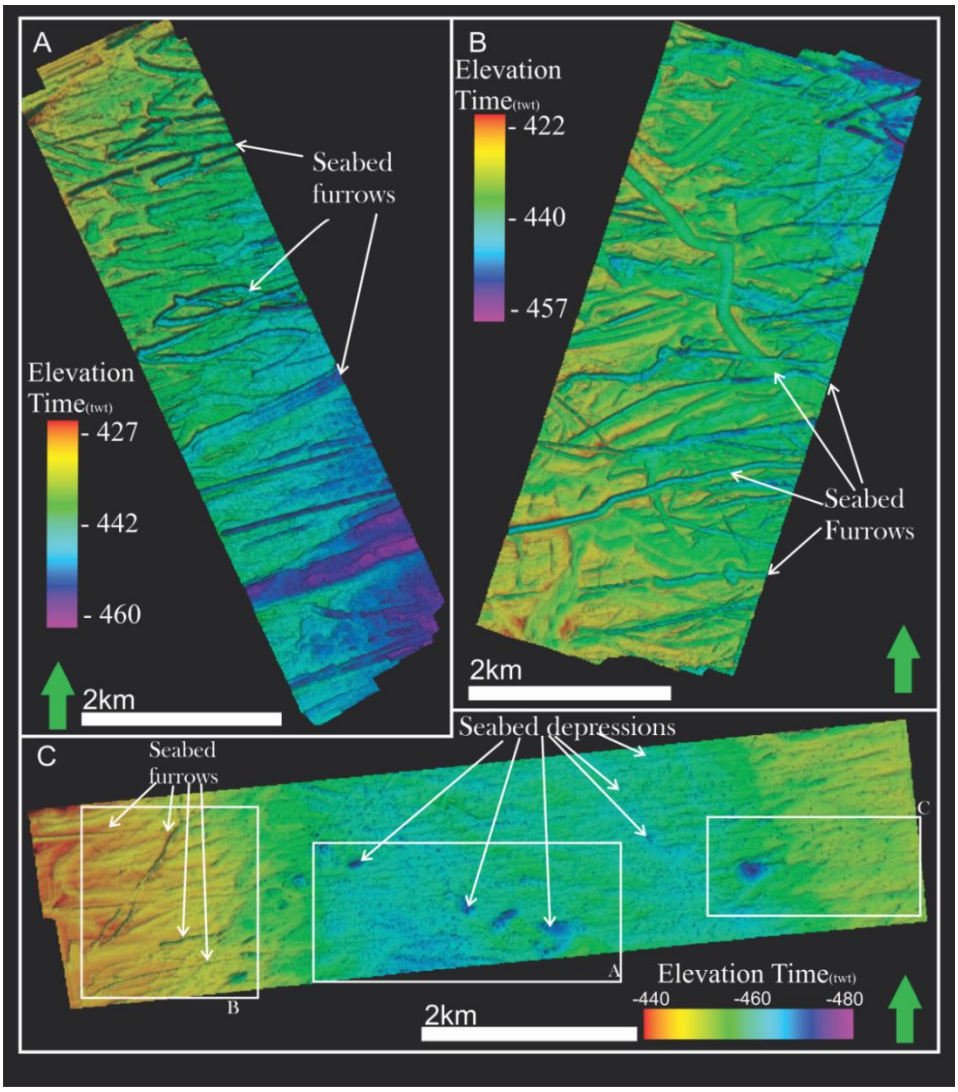

Figure 4.2. Seabed time structural maps A) Snøhvit 2 is dominated by iceberg ploughmarks B) iceberg ploughmarks dominate the seabed geomorphology of Area 1 C) ploughmarks and pockmarks on the Snøhvit 1 seabed. (vertical scale is 5x exaggerated)

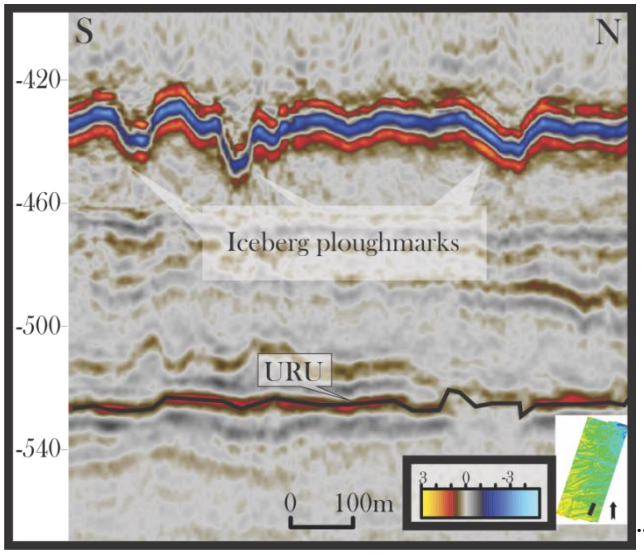

Figure 4.3: *cross section of Iceberg plough marks shown from a vertical seismic section.*

Linear to curvilinear seabed scour structures are known to occur mainly in glaciated continental margins (Vorren, 2005) carved by wind and current driven (Andreassen et al, 2008) keels of detached icebergs vertically penetrating and horizontally displacing the seabed sediments (Woodworth-Lynas et al, 1991). Similar features are commonly found in the bank areas of the southwestern Barents Sea (eg. Andreassen et al, 2008; Rafaelsen et al, 2002). The Arching elongated linear depressions observed in the study area resemble the iceberg plough marks described by Andreassen et al (2008) in shape and size. The latest geological evolution of the area is dominated by glacial and interglacial cycles (Andreassen et al, 2008; Kneis et al 2009; Vorren et al, 1991) thus allows the formation of such features in the study area. They are therefor interpreted as iceberg plough marks.

Iceberg plough marks are encountered in deeper horizons and within the glacial unit in the study area. The buried chaotic linear and curvilinear scour marks are randomly oriented and distributed. Buried ploughmarks have been encountered on paleo-surfaces within the quaternary sediments in the North Sea (Dowdeswell & Ottesen, 2013; Haavik & Landrø, 2014), the Norwegian Sea (Plaza-Faverola et al, 2011) and the Barents Sea (Rafaelsen et al, 2002). There are iceberg plough marks like features which mimic the seabed iceberg plough marks on the intra-glacial horizons of Area 1 (Figure 4.6). They appear directly beneath the deepest area of the seabed plough marks in the vertical seismic section. The appearance of these features is likely due to the delay of the seismic signal resulting from longer traveling distance in the water column, i.e. lower signal velocity.

4.3 Circular and semi-circular depressions:

Snøhvit 1

The interpreted seafloor horizon of the Snøhvit 1 data set is dominated by numerous small circular and some larger semi-circular depressions (figure 4.2C & 4.4). The seabed circular depression density ranges from 46 to just under 200 small circular depressions/km^2, with average of 120 depressions /km^2 (Figure 4.4). In addition to the small circular depressions there are 8 semi-circular depressions with diameters larger than 100m. In some cases the smaller depressions are aligned within the iceberg plough marks or display a configuration which is typical of the plan shape of iceberg plough marks, and in other cases the smaller depressions are enclosed by the larger depressions as illustrated by figure 4.2C and figure 4.5A&B. The diameters of the smaller depressions are predominantly between 20 and 40 meters and up to 3m deep. The larger seabed depressions are up to 500 m wide and up to 10m deep. Stacked bright amplitude anomalies are seen directly beneath the large depressions on the vertical seismic section, while most of the small depressions are located on the upper terminations of very narrow vertical transparent zones (figure 4.5D, E, F). The stacked bright amplitudes anomalies underlying the large depressions are slightly narrower than the depressions near the seabed and decrease in width with distance from the seabed. The thickness of these stacked bright amplitude ranges between 9 and 14ms twt.

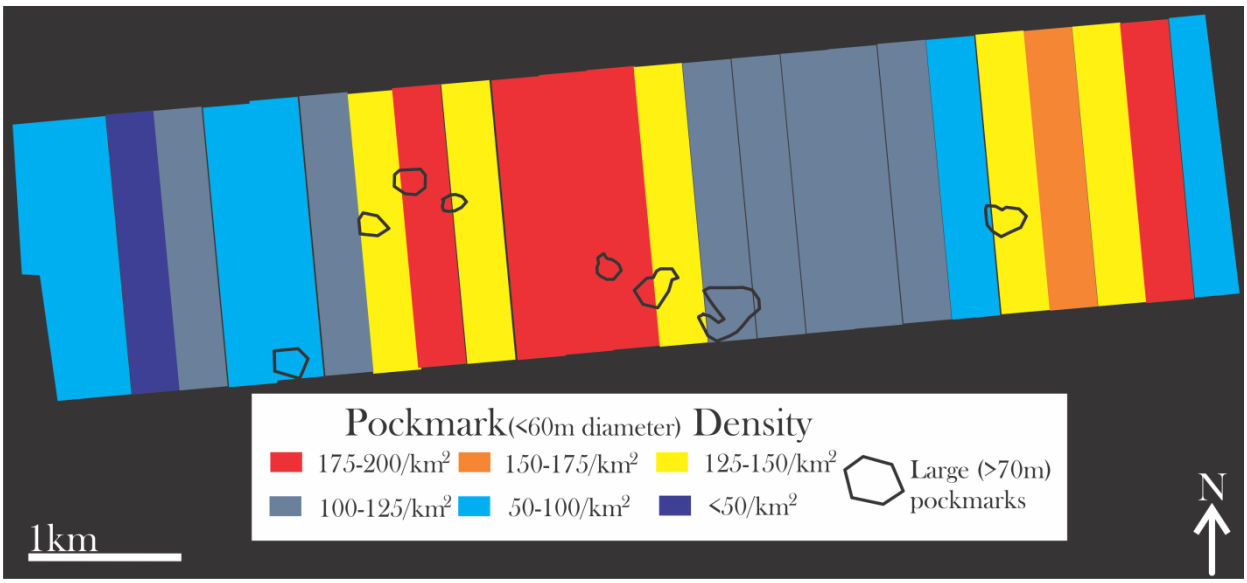

Figure 4.4: *Pockmark density distribution on the Snøhvit 1 seabed horizon.*

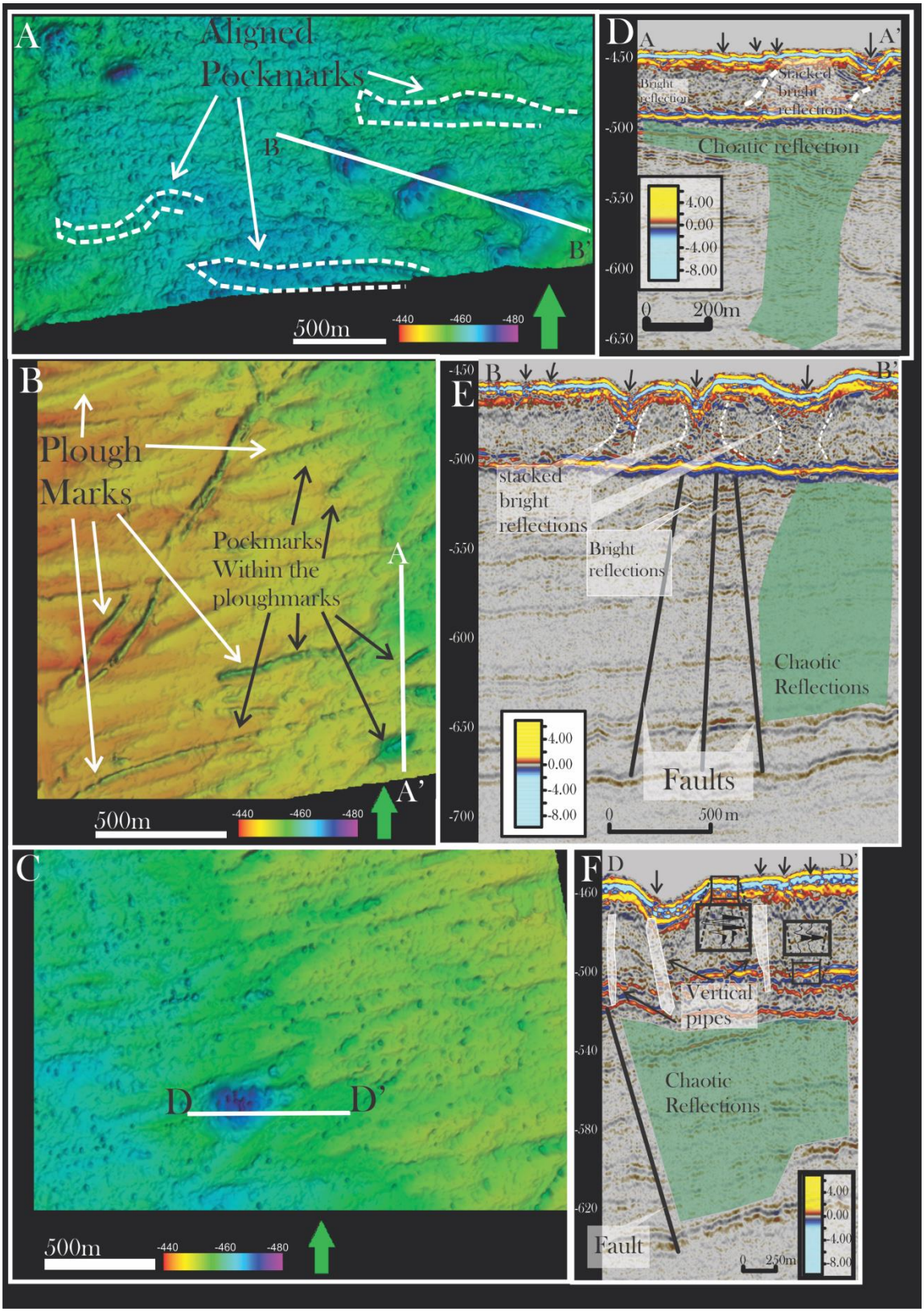

Figure 4.5: A) *up to 500 m wide pockmarks surrounded by randomly placed small pockmarks and some aligned pockmarks. B) Iceberg plough marks and small pockmarks within the pockmarks. C) Uniformly distributed pockmarks surrounding larger pockmarks which have small pockmarks within. The vertical scale in A, B & C is 5x exaggerated. D) Vertical seismic section displaying the cross sectional view of the pockmarks within the iceberg plough marks and the features beneath. E&F) Vertical seismic section displaying the cross sectional view of the large pockmarks and the small pockmarks enclosed in the large ones and the underlying reflectors.*

Circular and semi-circular depressions ranging in diameters from 1 m to several hundreds of meters and up to 45 m depth, are often associated with acoustic turbidity, enhanced reflections, columnar zone of disturbance have been encountered across the world and are interpreted as Pockmarks (Judd and Hovland, 2007). They are created as vertically migrating fluid seeping through the seabed (Hovland, 1981; Solheim and Elverhøi, 1985) leaving its marks on soft sediments on the seafloor (Hovland, 1981; Chand et al, 2012). Pockmarks with comparable with the depression in the study area have been identified on the western flank of Loppa High (Pau et al, 2014), an array of pockmarks aligned along pockmarks on the Loppa High (Chand et al 2012), the Hammerfest Basin (Ostanin et al, 2013) and near the Goliat field in the Barents Sea (Chand et al, 2009). The circular depressions in the study are interpreted to be pockmarks since they are associated with underlying Direct Hydrocarbon Indicators (DHI figure 4.5 D, E&F) such as enhanced reflections, and their similarities with the pockmarks in the surrounding area.

A string of small circular pockmarks aligned mostly along plough mark trails and some isolated circular depressions are evident on the URU horizon of the Snøhvit 1 dataset (figure 4.6). These pockmarks are comparable in size with the ones on the seabed, but are spread more sparsely than on the seabed. The density of the buried pockmarks increase westwards on the URU horizons where the buried iceberg ploughmarks are predominantly located. The diameters of the buried depressions range between 20 and 40 m and are about 4 meters deep (assuming 1700 m/s as the speed of seismic signal in the glacial sediments).

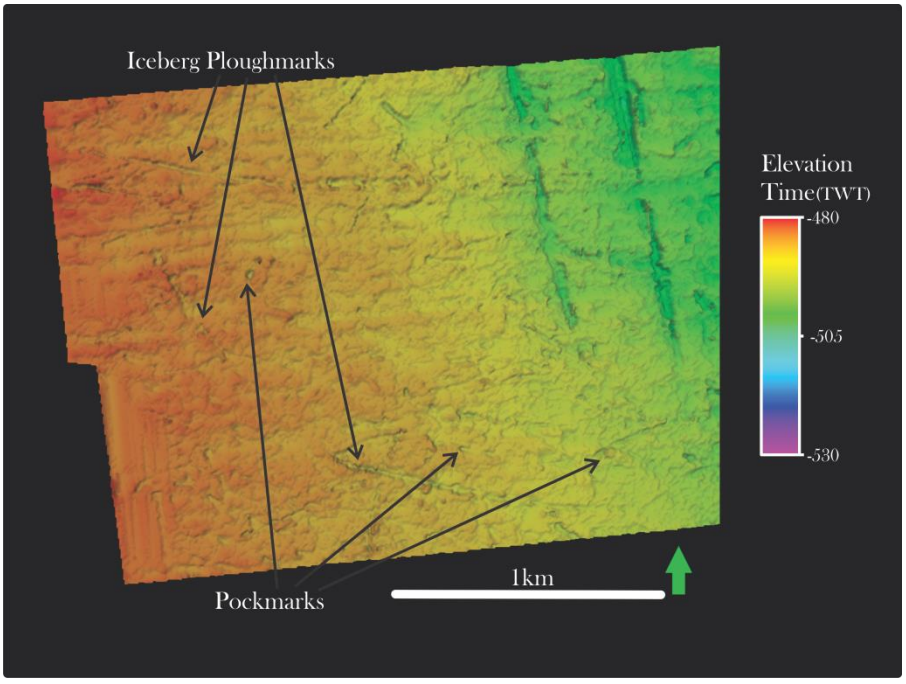

Figure 4.6: *Structural map of western parts of the URU horizon displays pockmarks and ploughmarks*

Area 1

The seabed horizon of the area 1 seismic cube is dominated by iceberg ploughmarks, which makes the process of identifying pockmarks challenging. However, some very small arrays of pockmarks were found on the seabed. The pockmarks identified had diameters ranging from 15 to 40 meters and around 3 meters deep (Figure 4.7). The alignment of the seabed pockmarks has resemblance with the plan shape of iceberg ploughmarks. Buried pockmarks are located under the seabed pockmarks in some instances, and in other cases Bright spots are found beneath the seabed pockmarks. Narrow zones of vertical discontinuities dominate the glacial deposits, a lot of the time leading towards the pockmarks.

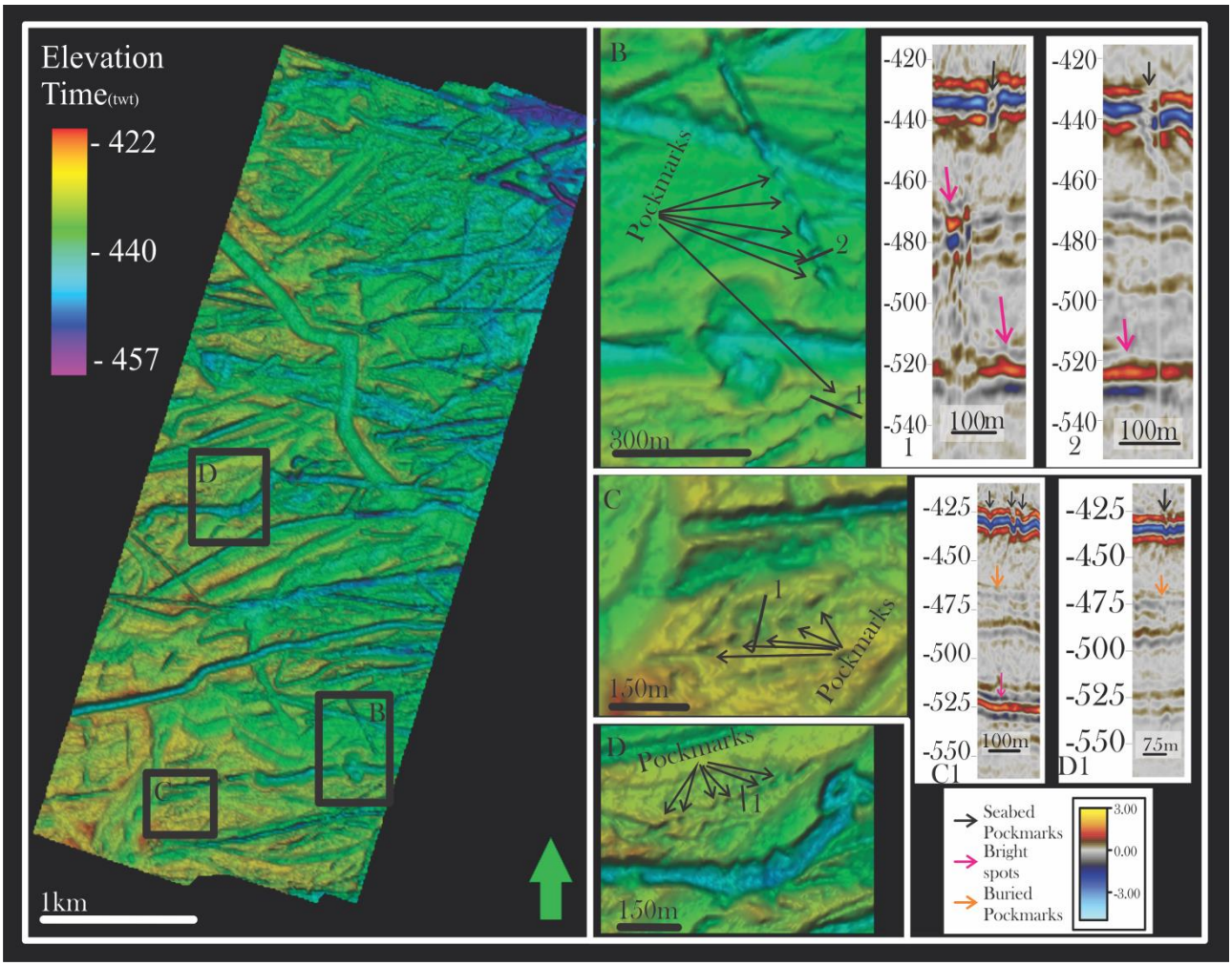

Figure 4.7: *Seabed structural map with positions of B, C &D. B) an array of small seabed pockmarks. B1) Bright spots underlying seabed pockmark B2) Seabed pockmark with a clear vertical pipe underneath C) A group of pockmarks embedded on the seabed. C1) buried pockmark and bright spot below a seabed pockmark D) aligned seabed pockmarks D1) pockmark on top of a buried pockmark.*

Several pockmarks are found on the intra-glacial surface of the Area 1 data set (Figure 4.8). The density of the pockmarks on the intra-glacial surface is 13 pockmarks/km^2, more at densely than on the seabed. These pockmarks have for the most part diameters between 10-50m and up to 4m deep. They are distributed randomly on the intra-glacial horizon. Many of the buried depressions are associated with high amplitude anomalies, narrow pipes (narrow vertical zones of reflection discontinuity), local dimming of reflections and faults (Figure 4.6). Some of the pockmarks on the intra-glacial horizons are connected to the seabed horizons with narrow pipes.

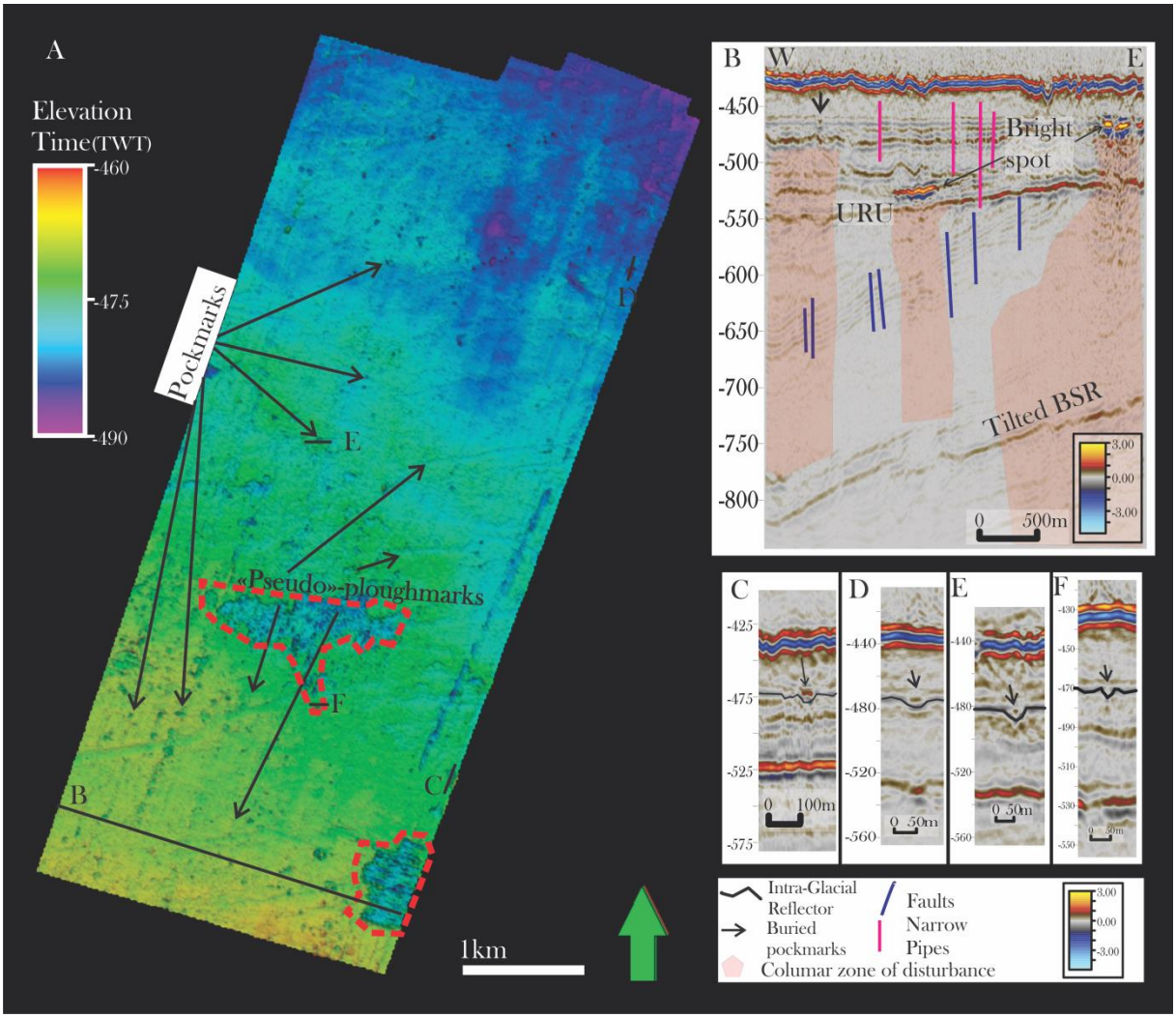

Figure 4.8: A*) 200 pockmarks are spread over the intra-glacial horizon. There are some iceberg ploughmarks like features on the horizon termed "pseudo" ploughmarks. (Vertical scale 5x exaggerated) B) Vertical seismic section shows the distribution of Pipes (vertical zones of discontinuity), BSR, Pockmarks and bright spots in relation to each other. C, E) randomly chosen pockmarks located just above a bright spot. Narrow pipes connecting the pockmark with the bright spot and the seabed. D) Pockmark surrounded by dimming reflections F) Narrow pipes present around the pockmark connecting it to the underlying URU reflector.*

Snøhvit 2

The pockmarks in the seabed horizon of the Snøhvit 2 dataset differ from the pockmarks earlier described in their configurations. These pockmarks are predominantly unit pockmarks, and are distributed on the seabed randomly (figure 4.9). These seabed pockmarks are slightly larger than the pockmarks in Snøhvit1 and Area 1. Their diameters range between 50 and 70, while their depth is primarily between 3m to 7m (figure 4.9). The vertical seismic sections show bright spots just 20ms below the pockmarks. The bright spots are cut by vertical zones of discontinuity in some cases connecting them to the pockmarks (Figure 4.9 A1,B1,C1 & D1).

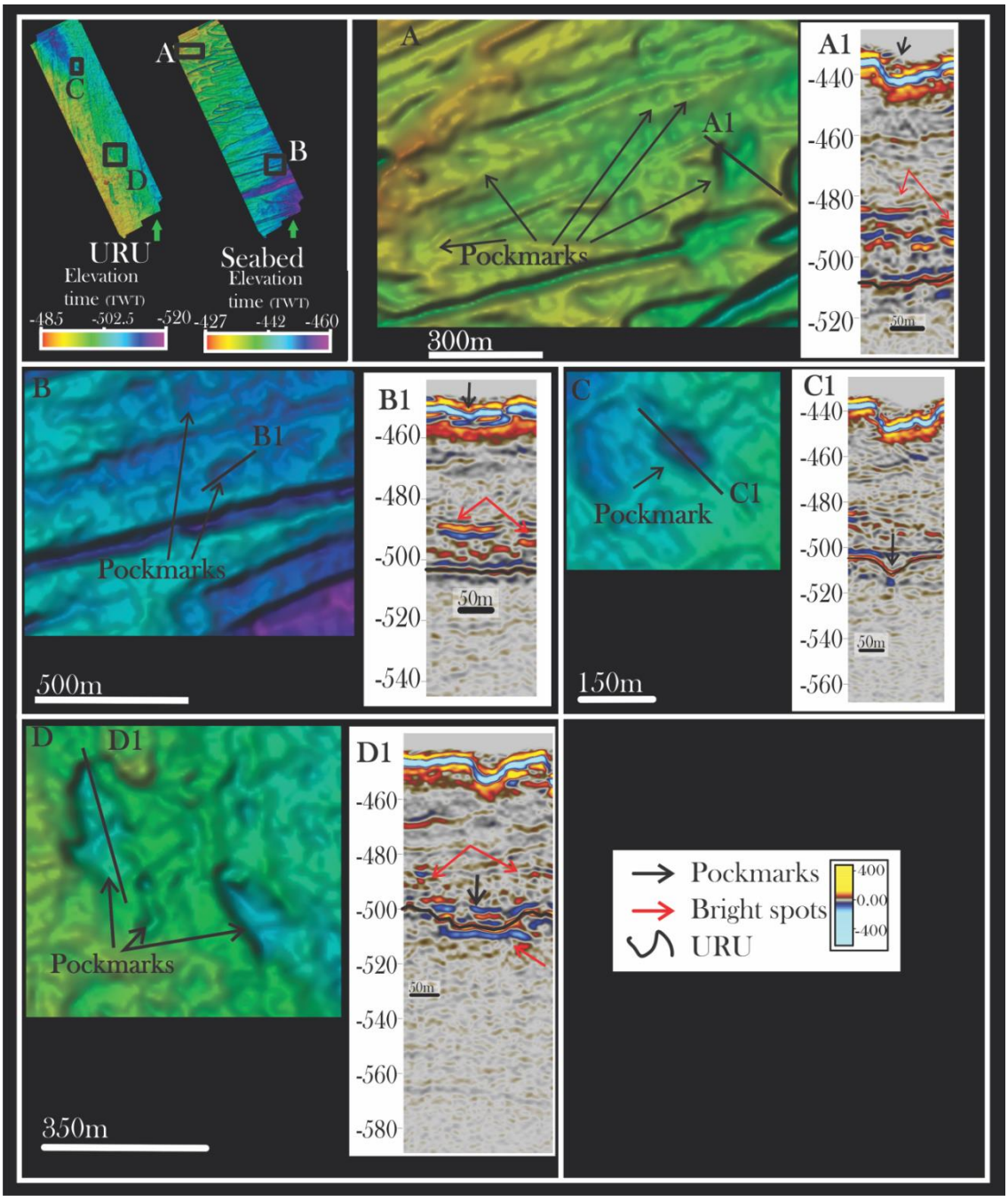

Figure 4.9: *A) pockmarks located on the northern areas of the seabed. A1) A seabed pockmark is displayed with the underlying bright spots and narrow pipes. B) Seabed Pockmark found located between iceberg ploughmarks. B1) Cross section of a seabed pockmark is placed just above a high amplitude anomaly and a pipe crossing the bright spots. C) A buried pockmark is situated on the northern part of the interpreted URU horizon. C1) Vertical seismic section is showing the cross section view of a pockmark. High amplitude anomalies and pipes are visible on top of the pockmark and chaotic reflections underlying the pockmark with an inclined pipe leading towards the pockmark. D) Elongated buried pockmarks located on southern side of the interpreted base of the glacial deposit Horizon. D1) A buried pockmark is located under scattered bright spot and chaotic reflections dominate the area underneath.*

Pockmarks are also present on the URU horizons. The buried pockmarks has circular to elliptical planar shape and range in diameter from 50 m to 300 m in diameters (figure 4.9 C&D). The pockmark pockmarks on the URU horizon are found just on top of chaotic reflection zones, and are surrounded by High amplitude anomalies with narrow pipes cutting across the bright areas.

4.4 Shallow gas related anomalies:

Enhanced reflections:

Shallow zones of enhanced reflections are predominantly constrained to the glacial unit and the URU reflector, i.e. the base of the glacial unit in the study area. Most of high amplitude anomalies encountered at the base of the glacial unit in study area show phase reversal compared to the seafloor reflection. The distributions of the shallow enhanced reflectors are presented below.

Snøhvit 2

The majority of the high amplitude reflections in the Snøhvit 2 dataset are limited to the glacial deposits, but there is a reflector -680ms below sea-surface with polarity reversal compared the seabed reflector. This reflector overlies a chaotic reflection zone, while the reflections just above are discontinuous with recognizable bedding pattern. The reflector with reversed polarity is often cut by locally diming zones. This reflector crossed the data set from east to west and covers around 4km^2 in the study area. This reflection is interpreted as top of gas chimney by Ostanin et al. (2013).

The URU reflection in the Snøhvit 2 dataset is the most pronounced reflector following the seabed. The URU reflector exhibits polarity reversal across the Snøhvit 2 dataset. The RMS

amplitude maps of the URU reflector show high amplitude anomalies oriented in the N-S direction, and the time structural maps of the URU in Snøhvit 2 show linear irregular furrow like structures in the same directions (figure 4.10). In addition to the N-S oriented high RMS amplitude vales, there is some random distributed linear high RMS amplitude values (Figure 4.10B).

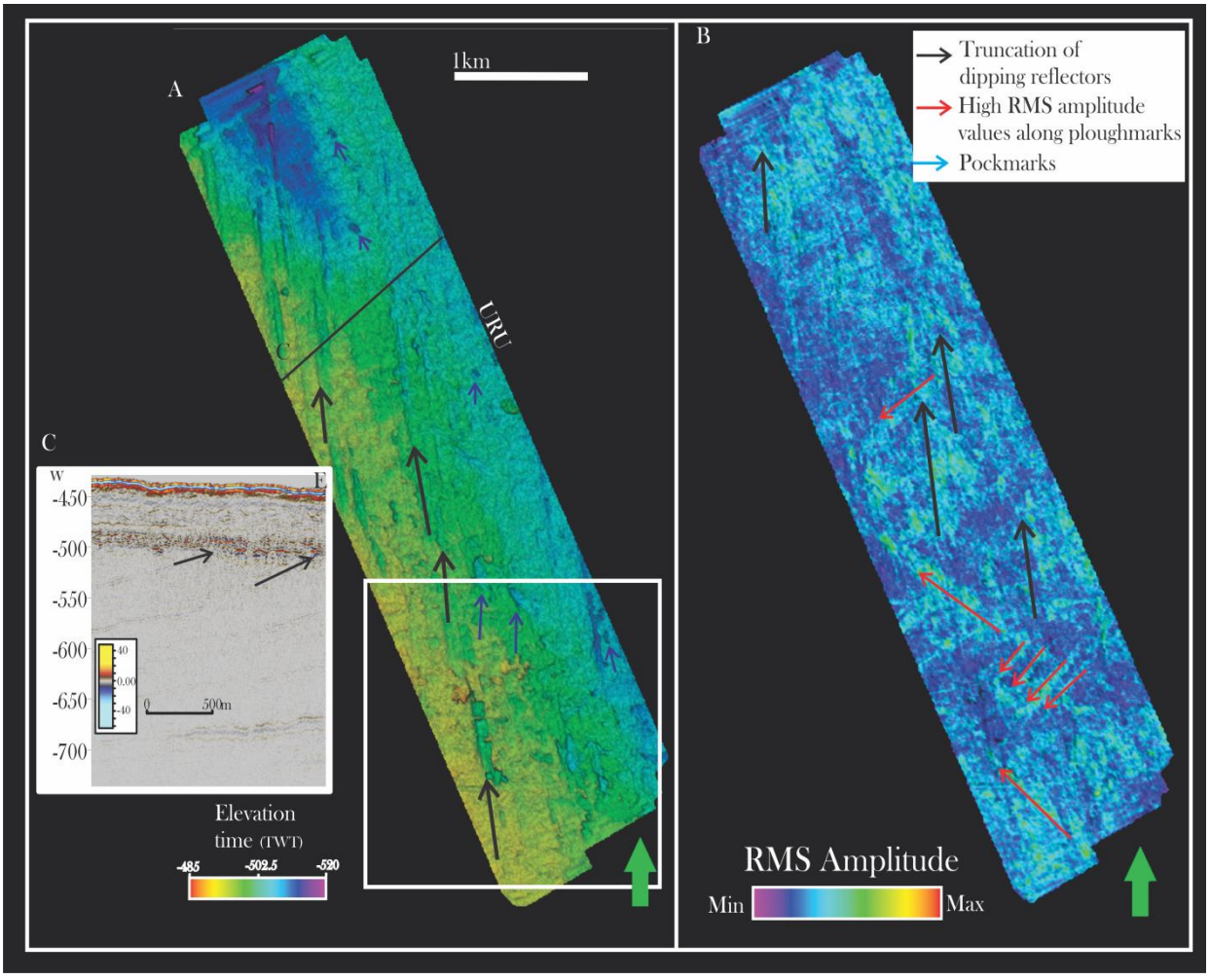

Figure 4.10: *A) Time structural map of the URU horizon in Snøhvit 1 seismic cube with N-S oriented linear truncation of the dipping reflectors of Torsk fm and randomly scattered pockmarks. (Vertical scale 5x exaggerated). B) RMS amplitude map computed around a 20ms window with the URU horizon in the middle of the interval. C) Vertical seismic section shows the dipping reflectors merge in to some of the high amplitude reflection below the glacial sediments.*

There are several discrete high amplitude areas just over the URU horizon. The high amplitude values that gave rise to the randomly oriented linear features were located about 10ms above the URU reflector of the Snøhvit 2 dataset. These amplitude anomalies are more than 1 km long and between 50 and 200 meters wide. A time slice across RMS amplitude volume attribute located -488ms below sea level of the dataset shows linear high amplitude features. These features correspond well with the features shown on a time slice across the variance volume attribute located -488ms. These high amplitudes are randomly oriented and distributed linear features are interpreted as iceberg scour marks (fig4.11).

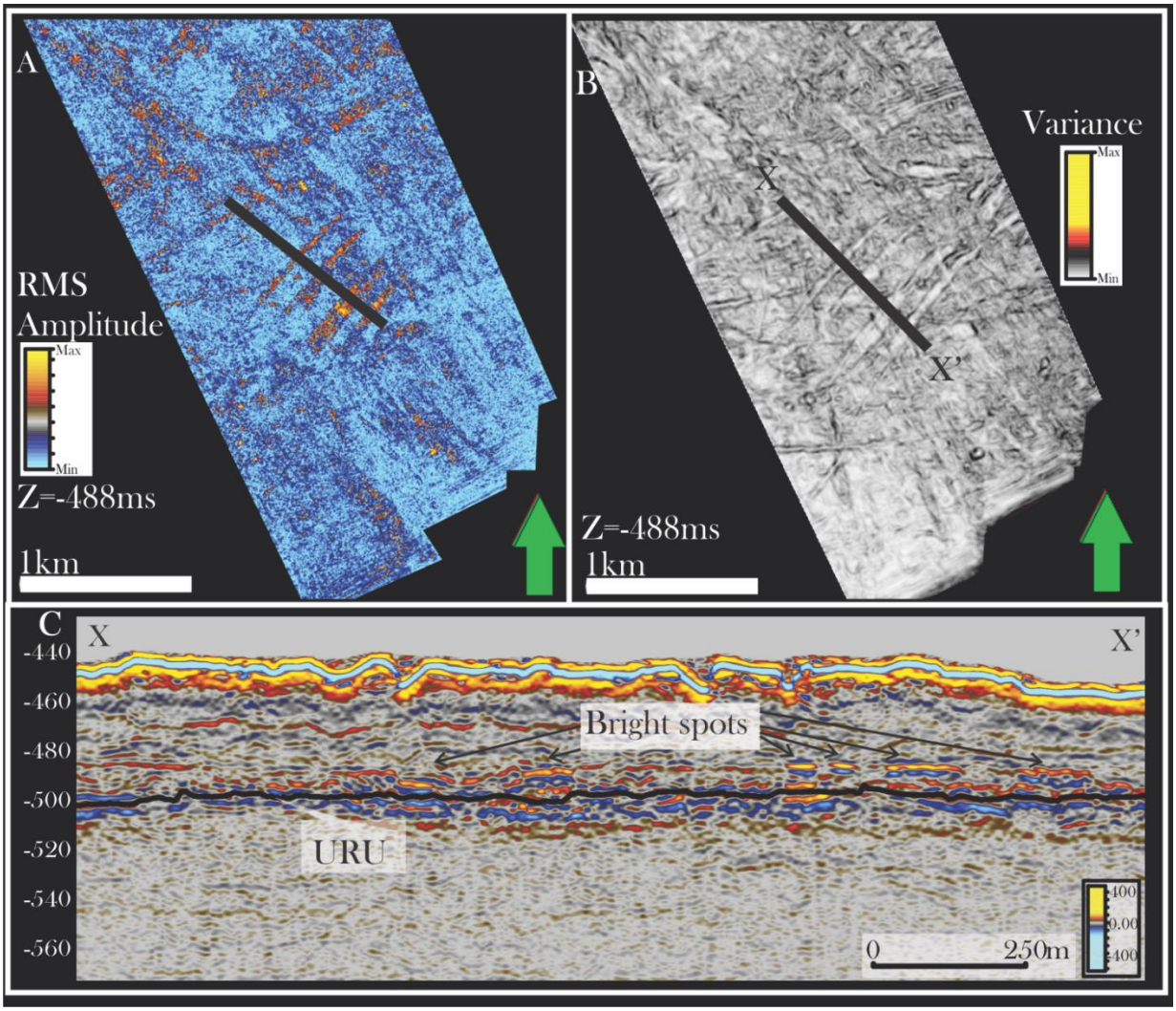

Figure 4.11: *A) time slice of RMS attribute cube generated using 9ms window located at -488ms below the sea-surface. B) Time slice of Variance Attribute cube located -488ms blow the sea-surface. Location of A&B is indicated by the white rectangle at figure 4.9. C) Vertical seismic section shows bright spots that gave rise to the high RMS value visible in figure 4.10A.*

Area 1

The deepest reflection in the Area 1 cube shows polarity reversal compared to the seabed reflection and cuts the dipping reflectors above (figure 4.1 & 4.12). Rajan et al. (2013) has interpreted the reflection as a Bottom Simulating Reflection (BSR) due to the presence of gas blow a Gas Hydrate Stability Zone (GHSZ), and the tilting of the BSR is caused by local variation in the geothermal gradient due to upward migrations of warm fluids. This change in the geothermal gradient moved the base of GHSZ vertically by about 120 meters towards the areas bordering high fluid flux areas.

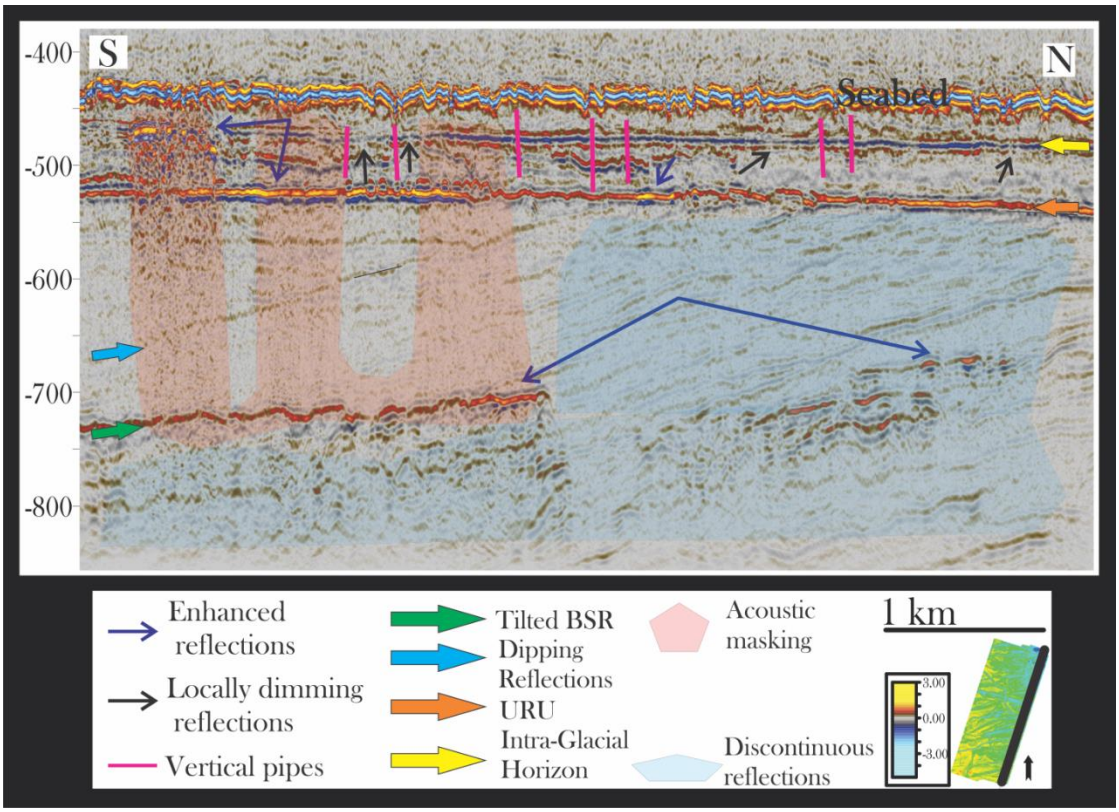

Figure 4.12 *a vertical seismic section across the Area 1 cube displays the vertical distribution of the high amplitudes.*

Apart from the tilted BSR, the majority of high amplitude reflections are positioned within the glacial deposits. The URU reflection exhibits phase reversal through the data coverage, with patches of higher amplitude reflections (Figure 4.12). The high amplitude RMS amplitude map was computed from a window enclosing the URU reflection to show the spatial distribution of the high amplitude zones. The high RMS amplitude values on the URU reflections are oriented N-S direction (figure 4.13B). The configurations of the high RMS amplitude values mimic the distribution of linear depressions on the URU time structure map (figure 4.13 A).

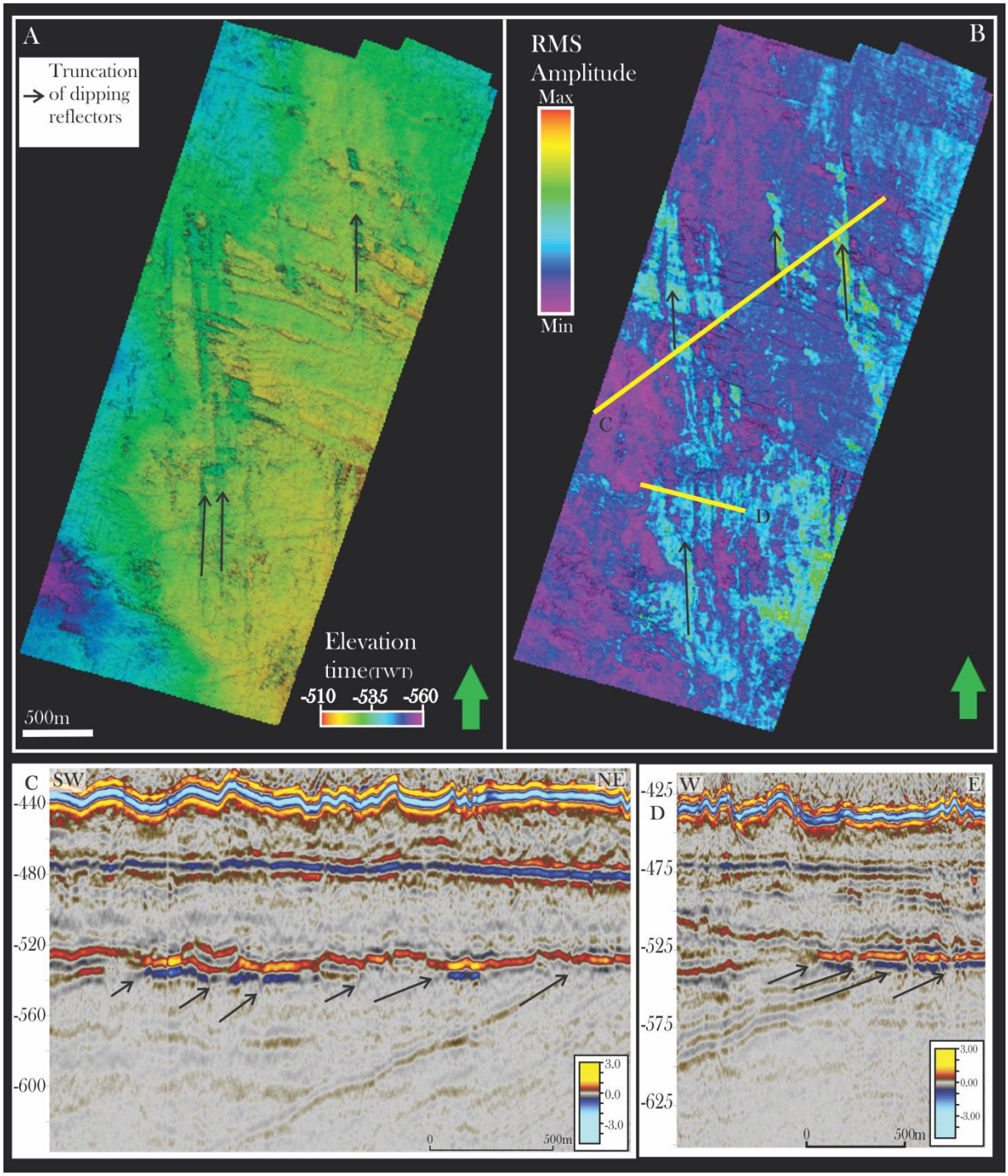

Figure 4.13: *A) time structure map of the URU horizon shows the distribution of N-S trending furrows (Vertical scale is 5x exaggerated) B) RMS amplitude map is generated using 10ms window with the URU horizon centered in the middle. The high RMS amplitude values correspond to the N-S trending furrows. C) Enhanced reflections on the vertical seismic section is underlain by dipping reflections. The dipping reflections are not easy to mark in the chaotic reflection zone but just under the enhanced reflections their terminations are visible and marked by the arrows D) westwards dipping reflections underneath the high amplitude reflections are marked by the arrows.*

The intra-glacial horizon in the Area 1 cube comprises high amplitude reflections spots with polarity reversal in the southern parts of the dataset (Figure 4.12 & 4.14 C, D & E). These patches of enhanced reflection are underlain by a vertical wipe-out zone that appear to continue all the way to the tilted BSR. Time slice from an RMS attribute cube located -470 ms below sea-surface shows the spatial distribution of the high amplitude patches (Figure 4.14). The large areas covered by the shallow enhanced reflections are about 0.3km^2 on the intra-glacial horizon. There is a circular high amplitude area at the southern edge of the dataset between the URU and intra-glacial horizon about -520 ms below sea-surface (figure 4.14 B&D). This bright reflection is overlain by a series of vertical lines of discontinuity, and acoustic pull down effect is visible on the reflections below.

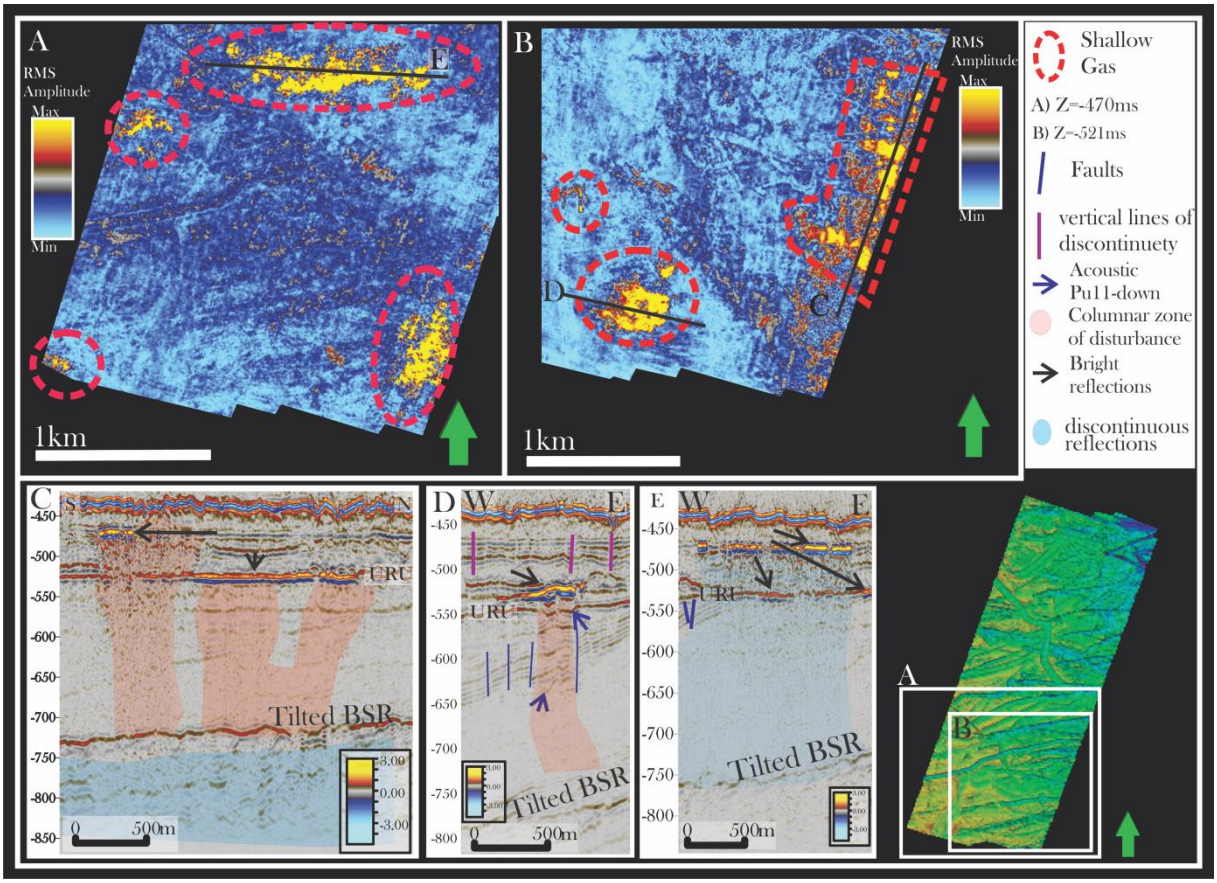

Figure 4.14: *A) shallow enhanced reflection spatial distribution shown on a time surface from RMS attribute cube (9ms window) located at -470ms below sea-sirface. B) High RMS values distributed on the southern part Area 1 shown in a time slice located -501ms below sea-surface (RMS window 9ms). C) Vertical seismic section displaying shallow high amplitude zone on the URU and intra-glacial reflection. D) High amplitude anomaly enclosed between the URU and intra-glacial reflection. E) High amplitude reflection along the URU and intra-glacial reflections highlighted.*

Snøhvit 1

Vertical seismic sections across the large pockmarks in the Snøhvit 1 dataset show stacked high amplitude anomalies just beneath the large pockmarks (figure 4.5D&E). These amplitude anomalies are circular in the planar view and decrease in diameter with depth away from the pockmarks. RMS amplitude map computed around the URU show increase in amplitude strength westwards (figure 4.15). There are NW-SE trending high RMS amplitude values on the URU horizon (figure 4.15). These values on the vertical seismic section correspond to where the dipping reflections terminate beneath the glacial unit.

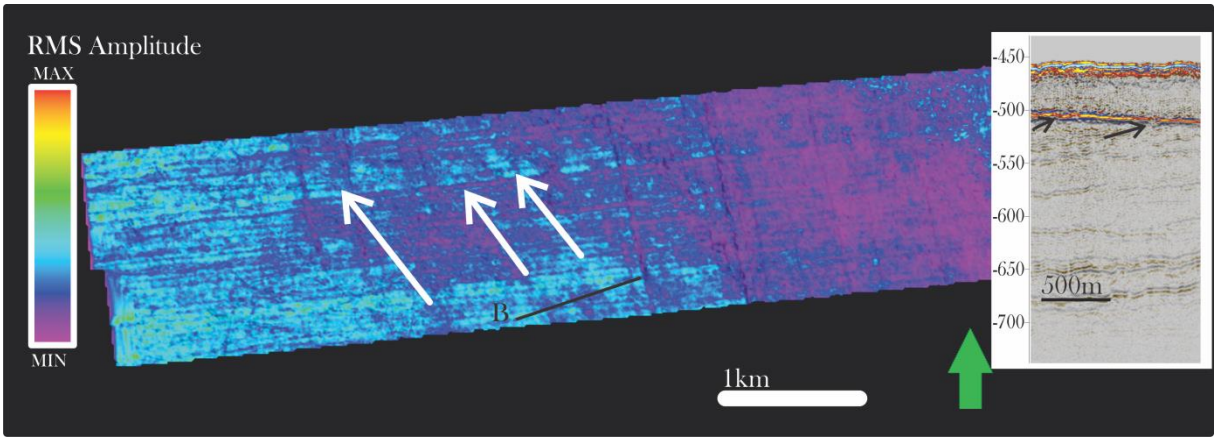

Figure 4.15: *RMS amplitude attribute map shows NW-SE trending high RMS amplitude values. On the vertical seismic section the high amplitudes are situated where the clinoforms meet the URU (RMS values extracted from RMS attribute cube (5ms window) using the URU horizon)*

Chimneys & Vertical lines of discontinuity (Narrow pipes):

Vertical zones of chaotic reflections interpreted as chimneys are observed in the study area. These chimneys in most cases terminate below enhanced reflections (figure 4.16). Such features appear frequently in the area 1 dataset emanating from BSR and often terminating below the URU and intra-glacial horizon high amplitude reflections (figure 4.14(B, C & D) & 4.16(A)). The overlying enhanced reflections and the neighboring reflections are vertically cut by narrow vertical lines of discontinuity. These vertical lines often extend from the areas of high amplitude to the seafloor. In the areas affected by the chimneys, the reflection patterns around are wiped-out and have similar plan view as the enhanced reflections (figure 4.14).

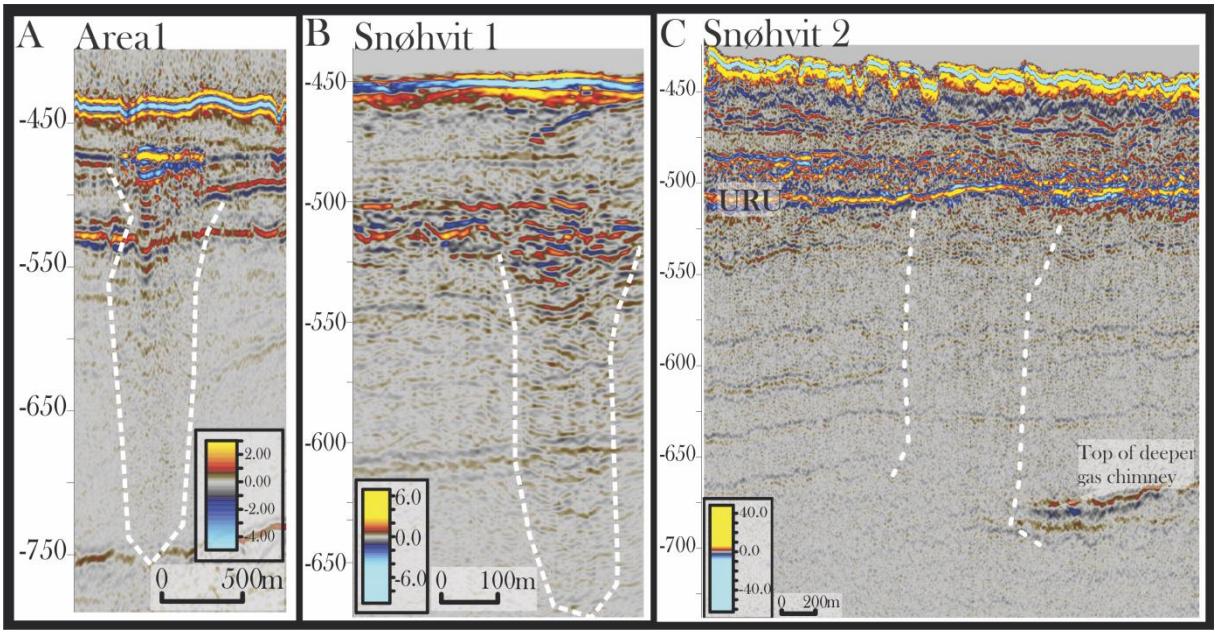

Figure 4.16: *A) cross section view of 200 m wide chimney underlying an enhanced reflection in the center of the Area 1 survey. B) A chimney on the eastern part of the Snøhvit 2 survey. C) A chimney emanating from a deeper gas chimney and cutting through the dipping reflection in the Snøhvit 2 area. White dotted lines marking the outline of the chimneys.*

The reflections beneath the URU in the Snøhvit 1 vertical sections are less continuous than those of the Area 1. Due to the discontinuous nature of the reflections the chimneys are not as clear as the ones observed in the Area 1 dataset. However, a chimney was observed at the western area of the seismic cube (figure 4.16(B)). The chimney terminates just below zone of high amplitude located on the URU horizon and vertical lines of discontinuities connect the enhanced reflections with the seabed and pockmarks. The dipping reflectors above the top of the gas chimney are barely recognizable, but in a vertical zone which extends from the URU and joins the chaotic reflections besides and under the top of the gas chimney the dipping reflectors are not recognizable in the Snøhvit 2(Figure4.16). This could be a gas chimney connected with the deeper gas chimney. As with the other datasets, the units between the URU and seabed contain vertical lines of discontinuities.

Enhanced reflections with phase reversal can be set up by gas charged porous sediment layers since the presence of gas changes the acoustic properties of the host sediment by lowering the speed of the acoustic signal relative to the surrounding (Løseth et al. 2009; Judd and Hovland, 2007). The enhanced reflections observed in the study area often appear in the vicinity of pockmarks, dim amplitude zones and vertical lines of discontinuity. A vertical region of unevenly distributed gas related to vertical migration of gas leads often to the generation of

vertical zones of distorted seismic reflections (Arntsen et al, 2007, Heggland, 1997, 1998). These reflections are often referred to as gas chimneys. Vertical lines of discontinuity/narrow pipes are observed predominantly in the glacial unit between the URU and seabed. However, these features are also observes within the dipping reflections of the Torsk Formation. Thin vertical low amplitude and/or discontinuous lines are present in shallow high resolution seismic data and may represent occurrence of fluids (Judd and Hovland, 2007). Dimming of amplitudes along stratigraphic reflections in seismic sections are associated with a minor dip in p-wave velocity due to the presence of gas in muddy sediments (Løseth et al, 2009; Judd and Hovland, 2007). The enhanced amplitude anomalies observed in the study area are interpreted as shallow gas accumulations and the interpretation is further supported by the presence of close relationship between the features mentioned above.

4.4 Faults

Snøhvit 1

Closely spaced networks of normal faults are identified crossing the dipping Torsk fm in Snøhvit 1 3D survey (Figure 4.17). Primarily N-S trending and curved faults dominate the variance attribute cube time slice in figure 4.17. The N-S faults extend over 2 km and continue beyond the data coverage. Throws between 4 and 10ms are common for the N-S oriented faults. The N-S trending faults are intersected by SW-NE trending minor faults with similar throws as the N-S trending once. The SW-NE trending faults extend over predominantly 300- 600 m lengths. All the identified faults are sealed below the URU.

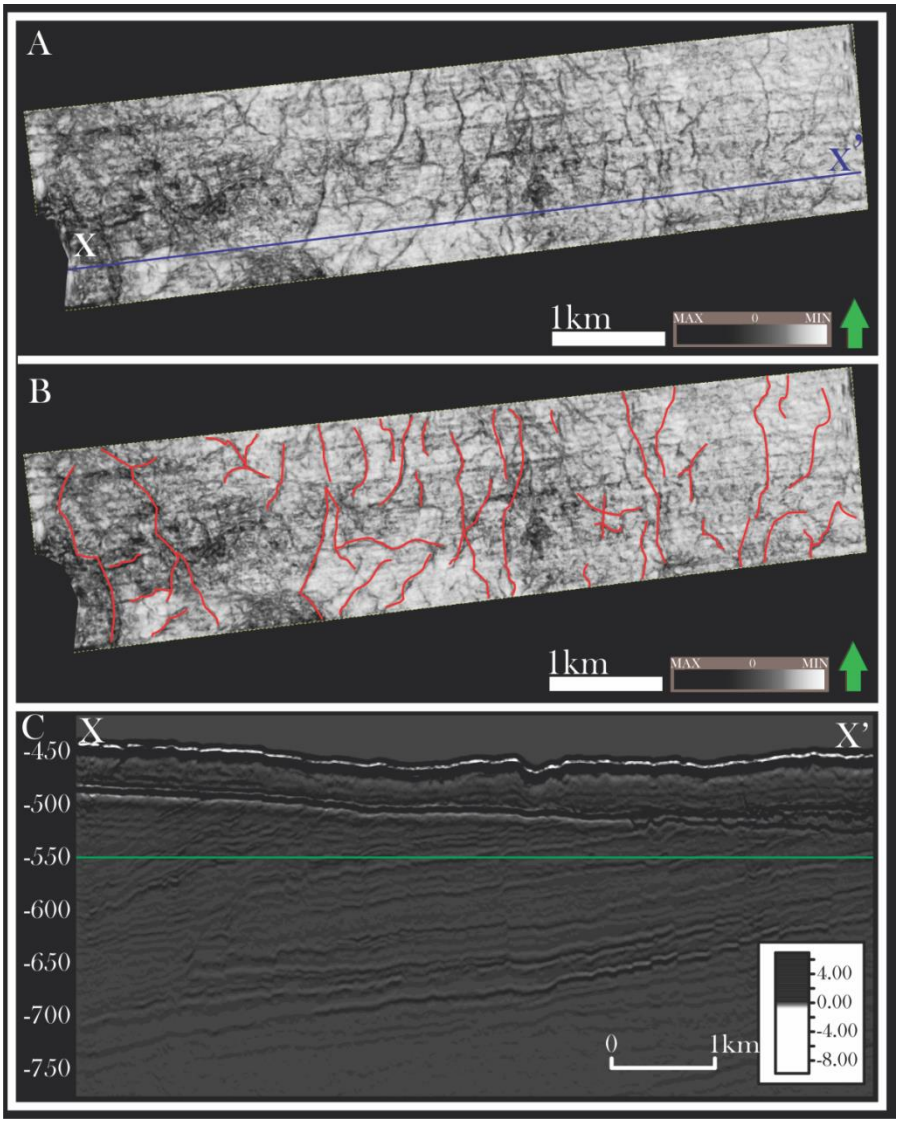

Figure 4.17: *A) time slice of Variance cube showing discontinuities on the seismic data at -550ms depth below the sea surface. B) The same time slice as A, with manually interpreted faults marked with red lines. C) vertical seismic section showing the cross section view of the faults.*

All of the faults as mentioned earlier terminate at the URU reflection which has high amplitude with reversed polarity. These closely spaced faults are often accompanied by vertically dimming reflections. Figure 4.18 shows vertical discontinuity in the reflection along the fault planes. The dimming of the reflection along fault planes is very common feature associated with the faults in the study area.

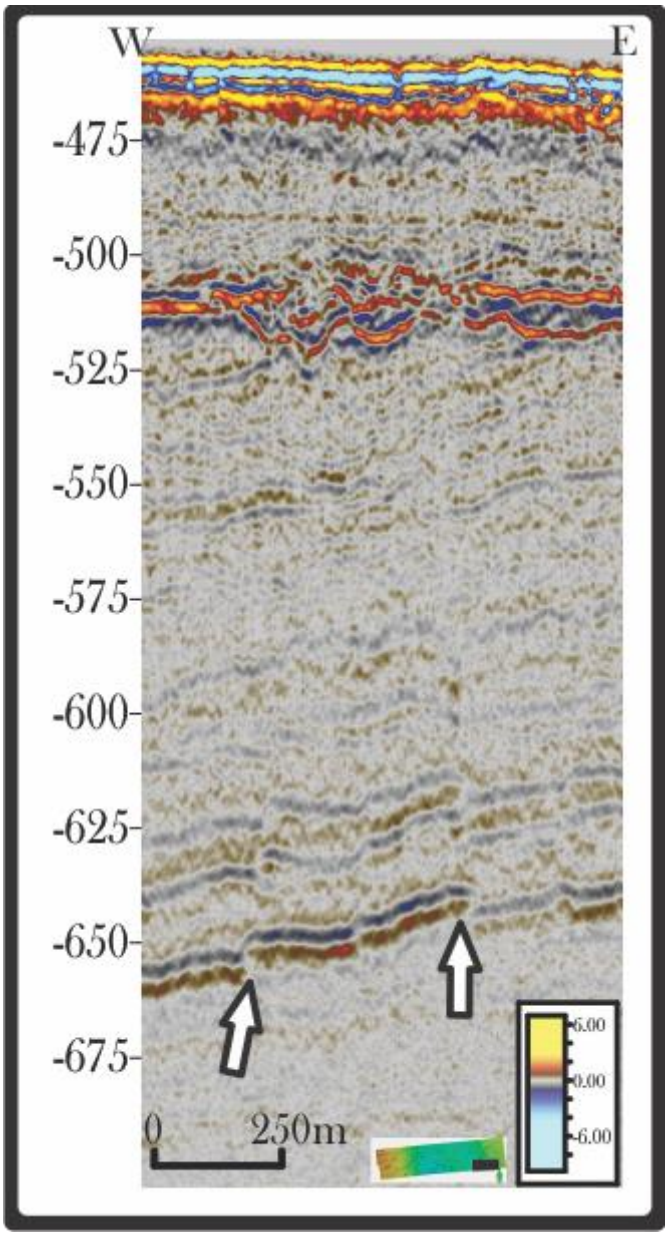

Figure 4.18: *Faults with decrease in amplitude along their fault plane. The arrows are pointing towards the vertically dimming reflections.*

Snøhvit 2

The dipping reflectors in the Snøhvit 2 dataset exhibit faulting at a lesser extent than the Snøhvit 1. This could be due to the more discontinuous nature of the reflections in the survey. The time slice of variance attribute cube located -580ms below sea-surface shows some E-W trending faults cross cut by N-S trending normal faults (Figure 4.19 A). The E-W trending faults extend up to 1.5 km in length and the throws are generally less than 10ms. The N-S oriented faults are similar size to the E-W oriented ones. These faults are all sealed below the URU. The reflector located -680ms below sea-surface was described in the section above. This reflector is affected by small network of faults (figure 4.19 B&C). Some of the faults go all the way up to the URU, while others are difficult to track above the top of the gas chimney reflection due to the constraints to the reflection continuity.

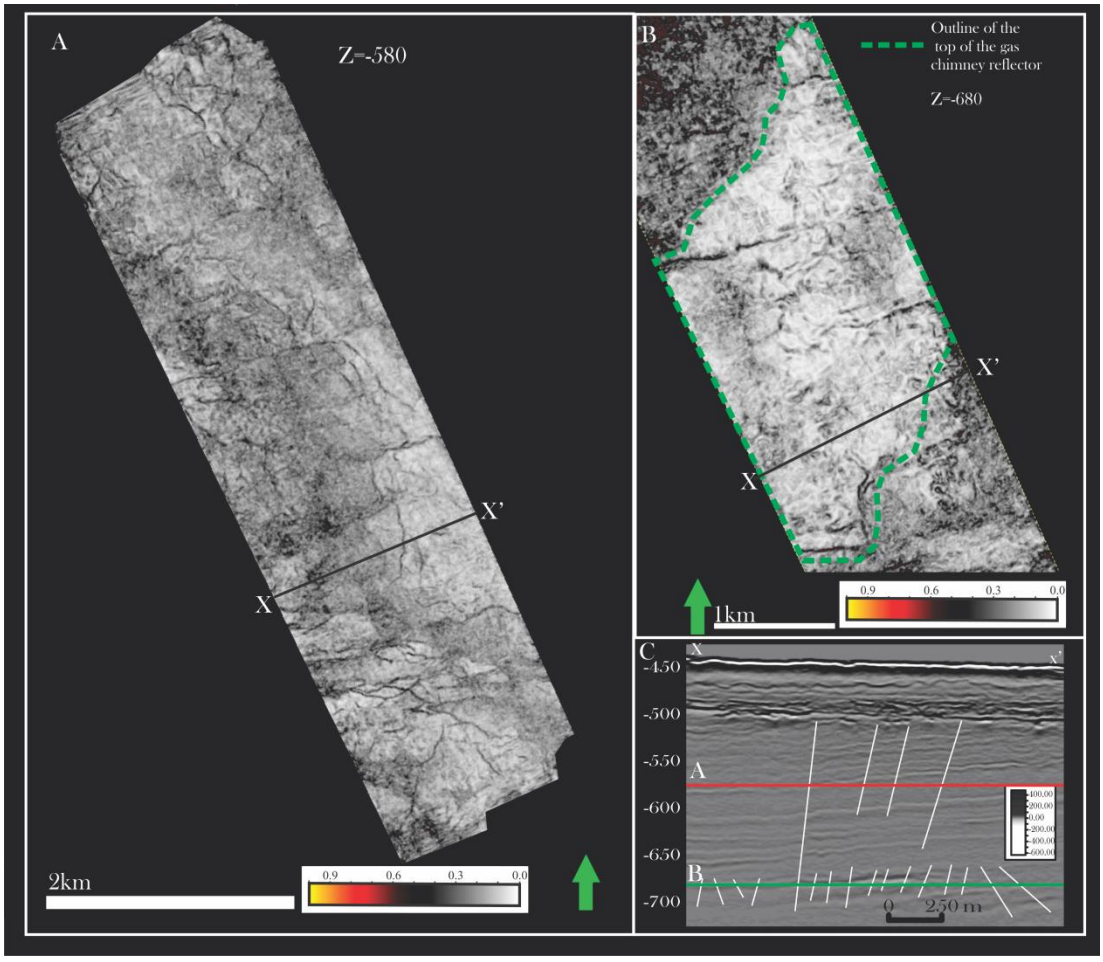

Figure 4.19: *A) N-S & E-W trending faults cross cutting each other. (Time slice of the Variance attribute cube located at -580ms below sea-surface) B) time slice obtained from a variance cube located at -680ms below sea-surface, indicating faults cutting the reflector located -680ms below sea surface. C) Vertical seismic section showing the cross section of the faults and location of the time slices.*

The dipping reflectors in the Snøhvit 2 survey are discontinuous over most of the survey area. This makes the identification of the faults, the area affected by faulting and their relationship with the gas related anomalies. The identified faults are often associated with vertically dimming reflections and enhanced reflections as displayed in figure 4.20. However, the RMS amplitude map computed around the URU does not show any correlation with the fault affected areas. This is also the case for the Faults in the Snøhvit 1 survey.

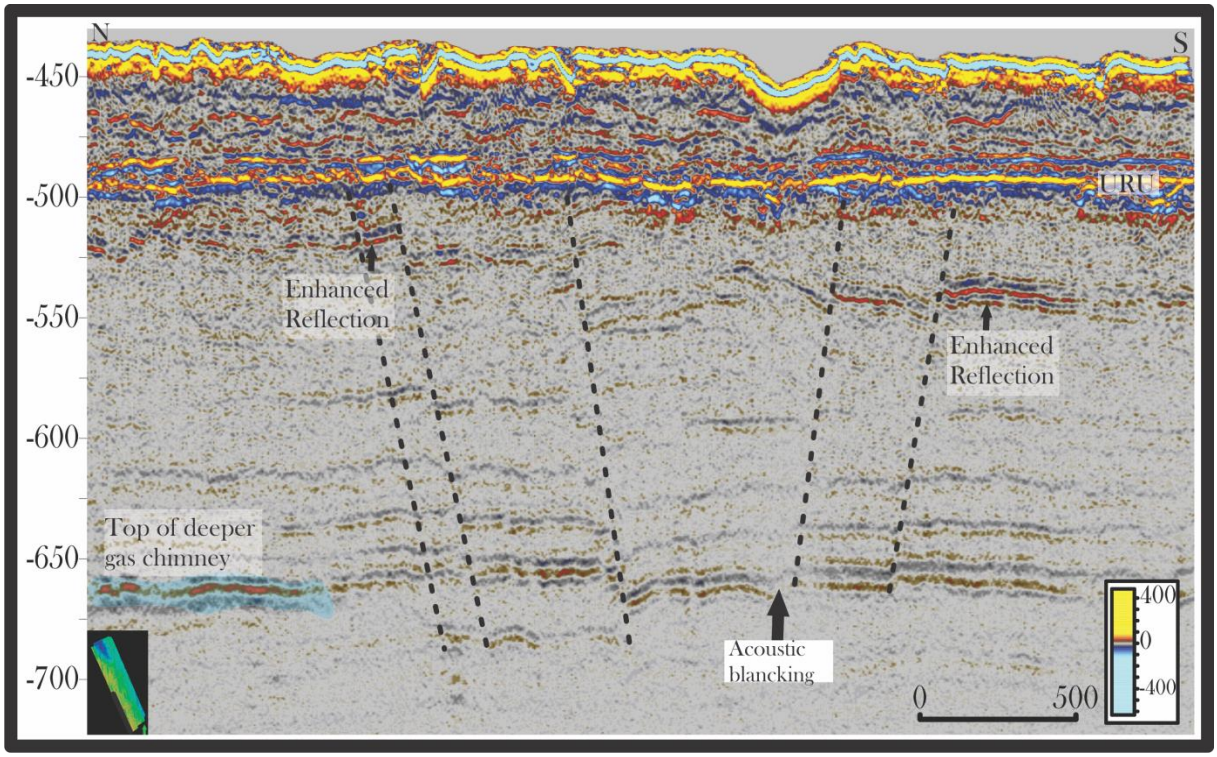

Figure 4.20: *A vertical seismic section shows the relationship between the faults and vertical dimming reflections and Enhanced reflections.*

Area 1

The faults in the Area 1 survey are located mainly on the southwestern corner. These faults are SE-NW oriented. They make closely spaced and arching fault network. The longest chain of faults in 2km long, and the faults continue outwards from the data coverage area. The throws are mainly between 4 and 5ms. The dipping reflections in other areas of the dataset don't appear to be faulted.

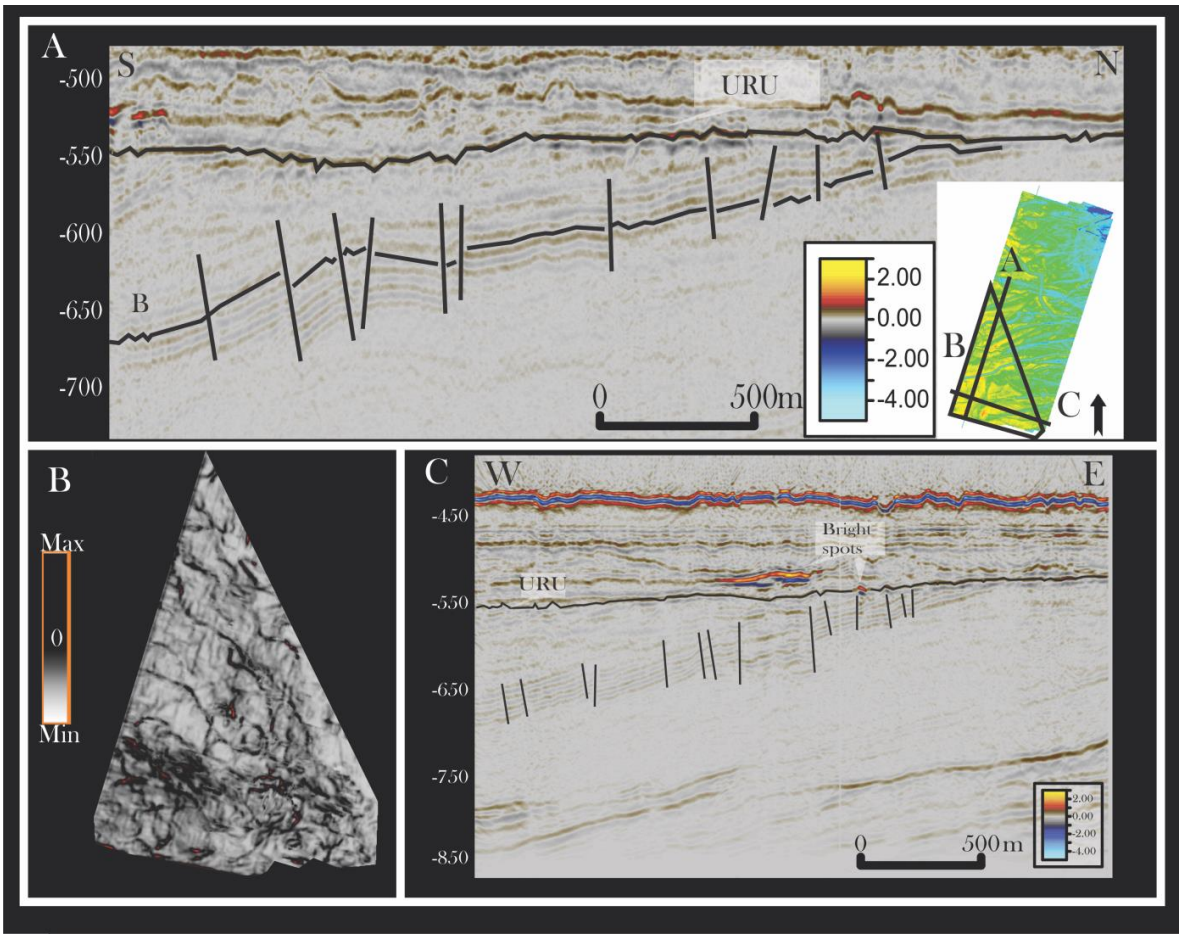

Figure 4.21) *A) vertical seismic section showing the cross section of the faults located on the south western corner of the Area 1 survey. B) Extracted variance values using a horizon indicated as B in figure 4.16A. C) Seismic line shows the relations ship between the faulted area and the bright reflection just above the URU reflector.*

A chaotic reflection zone is situated in the southwestern edge of survey just above the faults and under the URU reflection. This chaotic reflection zone overlain by patches of enhanced reflections located on the URU horizon and the intra-glacial horizon. Closely spaced fault networks are found underlying the chaotic reflection zone. Figure 4.21 shows the fault networks and the overlaying enhanced reflection with some patches of enhanced reflections scattered within the glacial unit.

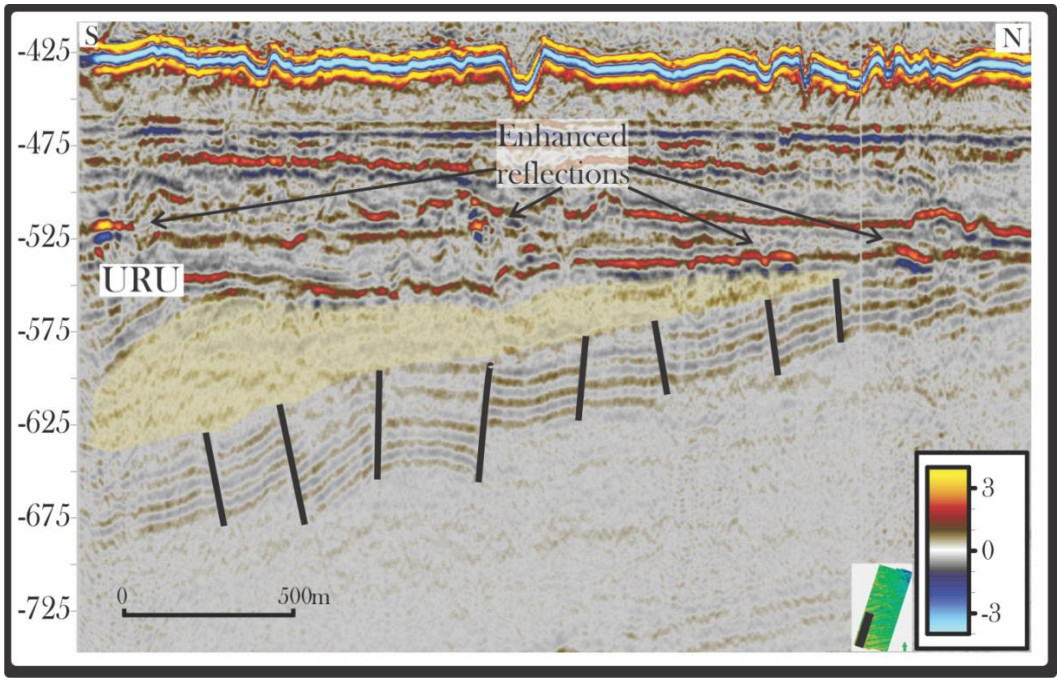

Figure 4.22: *A seismic section displays Faults overlain by chaotic reflections and patches of enhanced reflections.*

Chapter 5: Discussion

Evidence that support the presence of shallow gas and related pathways were presented from the data sets available in the previous chapter. These fluid related features will further be discussed in this chapter. Due to the limited penetration depth of the high resolution P-cable data, the presence of possible deeper gas sources and migration pathways cannot be obtained using the data available for the study. Nevertheless, there are several published studies that cover investigations of deeper gas sources and potential migration pathways and will be discussed in this chapter. Further, the factors that control the potential fluid migrations in the study area will be presented. This chapter will be concluded by a summary of the interpreted fluid migration pathways and their relations to the possible forcing mechanisms.

5.1: Pockmarks:

5.1.1 Seabed pockmarks

Snøhvit 1:

Numerous pockmarks are found scattered around the interpreted seabed horizon of the Snøhvit 1 cube (figure 4.2C). The average density of the pockmarks on the seabed is 120 pockmarks / km^2 and varies spatially on the surface (figure 4.4). There appears to be no correlation between the pockmark density on the surface and deeper features. An inverse relationship between pockmark density and the quaternary glacial unit thickness was found in a larger area in the Hammerfest Basin (Ostanin et al, 2013). However, this does not seem to be the case for the Snøhvit 1 area. With that being said, the relationship between the thickness of the glacial unit and the pockmark density could still exist in a larger area.

The western flank and a wide zone in the middle of the seabed exhibit lower pockmark densities than most of the rest of the seabed (figure 4.4). The morphology of western areas is dominated by iceberg ploughmarks. In the western area the sparsely distributed pockmarks are predominantly confined within the iceberg ploughmarks.

In addition to the small and densely populated pockmarks, some large pockmarks are seen spread around on the seabed structural map of Snøhvit 1 (figure 4.2C). These large pockmarks enclose some small pockmarks within them (figure 4.5 A & C). This could possibly be due to temporally separate episodes of fluid escape through the seabed in the study area.

Snøhvit 2:

Few pockmarks are found on the interpreted seabed Horizon of the Snøhvit 2 dataset (figure 4.9 A& B). The seabed is dominated by closely spaced iceberg ploughmarks and the identified pockmarks have been found mainly in areas unaffected by the iceberg plough marks. Due to the scarcity of the pockmarks on the seabed, any correlation with the deeper features is very difficult. Since the thickness of the glacial unit in the Snøhvit 1 and Snøhvit 2 is similar, the differences in the pockmark density between the two areas cannot be attributed to the inverse relationship established by Ostanin et al. (2013).

Area 1:

Densely populated iceberg ploughmarks are present on the seabed horizon of the Area 1 dataset as in the Snøhvit 2 area. As with the Snøhvit 2 dataset, there are very few pockmarks on the Area 1 seabed horizon (figure 4.7). These pockmarks are mainly situated above the shallow enhanced reflection zones in the quaternary glacial sediments units interpreted as shallow gas accumulations.

The formation of pockmarks depends on two conditions, the presence of fluid seepage through the seabed and the presence of soft sediments as recording medium (Chand et al, 2008, 2012; Judd and Hovland, 2007). Several gas flares has been detected at the RLFC in an area dominated by iceberg ploughmarks and devoid of pockmarks due to the lack of soft sediment (Chand et al, 2008). This shows that absence of pockmarks does not exclude the presence of past and present fluid seepage through the seabed. There appears to be an inverse proportionality between the pockmark density and the density of the iceberg ploughmarks based on the three datasets in the study area. This is likely to be due to the presence of pockmarks only within the ploughmarks with sufficient soft sediment cover, since there are pockmarks in the area confined within the ploughmarks. In the seabed structural map of Snøhvit 1 dataset, there are arrays of pockmarks that are aligned along a configuration of iceberg ploughmarks, even though there is no evidence of the presence of ploughmarks on the surface. The ploughmarks on which the pockmarks are aligned after could have been buried under thick layer of soft sediment. The scouring of icebergs can sometimes lead to the generation of a migration pathway for upwards moving fluid (Judd and Hovland, 2007, Hovland, 2002). The presence of shallow gas within features that resemble iceberg ploughmarks is shown in figure 4.11. Deep ice berg plough marks can enhance the permeability of the host sediments by creating small fractures (Judd and Hovland, 2007). This can explain the presence of arrays of pockmarks aligned along and enclosed completely within the iceberg ploughmarks.

The seabed in the study area is estimated to have been ice free 15-16 ka BP following the Last Glacial Maximum (LMG) (Rüther et al, 2011). The large pockmarks on the seabed of the Snøhvit 1 survey are likely to originate from the time directly after the ice sheet collapse. Large depressions with up to 300 m diameter were found in the Loppa High with small pockmarks encircled within (Chand et al, 2012). Chand et al. (2012) interpreted them as iceberg prodmarks since they in some cases appear where the iceberg ploughmarks start and the backscatter values of the features were similar to the values observed outside the pockmark areas. However, these

large pockmarks on the seabed of Snøhvit datasets have no association with the seabed iceberg ploughmarks and there are stacked enhanced reflections starting at the bottom of the pockmarks, and vertical discontinuity zones are found beneath the high amplitude reflections indicate that the larger pockmarks could also be related to fluid escape from the seabed. Two mega-pockmarks with diameters up to 1.9 km crisscrossed by iceberg ploughmarks were found on the seabed of the Hammerfest Basin (Ostanin et al, 2013). This indicates that the area has exhibited high fluid flux prior to the iceberg calving that can produce large pockmarks. This does not however exclude that some of the large depressions can be a result of iceberg plunging the seabed.

None of the identified small pockmarks in the study area are crossed by the iceberg ploughmarks. The pockmarks in the vicinity of the ploughmarks are fully enclosed by the ploughmarks. This is likely due to their absence during the collapse of ice sheets. They were probably generated in an ice free condition.

5.1.2 Buried Pockmarks

Pockmarks on the intra-glacial Horizon

The intra-glacial reflection is not present on the datasets acquired over the Snøhvit field. The URU horizon in the study area is thought to represent an ice free condition and is estimated to be younger than 0.7Ma (Ostanin et al, 2013). The intra-glacial horizon probably represents an ice free period in one of many glacial/inter-glacial cycles between 0.7ma and LGM. The survey over the RLFC has several small pockmarks on the intra-glacial horizon surrounded by patches of enhanced reflections. These pockmarks are likely generated as a result of vertical fluid migration as a response to a glacial retreat at the time when the horizon served as a seabed. The enhanced reflections on the intra-glacial reflection are interpreted as shallow gas accumulation. The migration of the fluid into the pore space on the intra-glacial is likely to have taken place after the formation of the pockmarks and the deposition of the overlying sediments.

URU Pockmarks:

Pockmarks on the URU horizon were only identified on the Snøhvit field surveys. The presence of the pockmarks indicates fluid escape through the surface following a deglaciation, since the URU is thought to represent the end of a glacial period (Ostanin et al, 2013).

5.2 Shallow gas accumulation and possible migration pathways:

Area 1:

Enhanced reflections in the RLFC dataset are abundant, and they are found at various stratigraphic levels (Figure 5,1). The shallowest high anomaly reflection is situated around 35ms twt below the seabed and the deepest between 700- 800 ms below the sea surface. The deepest reflection is interpreted as BSR (out of the scope of this study) that has been tilted as a result of the upwards flow of warmer fluid (Rajan et al, 2013). The BSR is continuous reflection over most of the data coverage. However, in some areas there is discontinuity in the BSR. This occurs predominantly below shallower gas accumulations, where a vertical zone of acoustic turbidity connects the BSR vertically to the enhanced reflections. Such zones are known as gas chimneys and they are caused by gas bubbles most commonly in fine grained sediments scattering acoustic energy leading to the generation of chaotic reflections (Judd and Hovland, 2007). These could be a vertical migration pathway for the gas trapped beneath the BSR. The upward flowing fluids from deeper strata can destabilize gas hydrates and lead to piercing of GHSZ creating vertical migration route (Chand et al, 2012).

There are patches of enhanced reflections on beneath the late Cenozoic glacial unit. The RMS amplitude map computed on a window enclosing the high amplitude reflections displays N-S trending high RMS amplitude values. The vertical seismic sections display that the high amplitude reflection often emanate from the termination of the westwards dipping reflections under the quaternary glacial units. Gas flares are observed towards the western parts of the Loppa High where the glacial sediments are absent, allowing fluid to migrate upslope (Chand et al, 2012), while large pockmarks are situated directly above the termination of the dipping reflections in the Hammerfest basin (Ostanin et al, 2013). This suggests that fluids are likely to flow up-dip along permeable areas of the dipping beds of the Torsk formation, while the glacial unit hinders the upslope migration of the fluids. This is further strengthened by the presence of high amplitude values along the strikes of the dipping reflections.

There are faults below the URU at the southwestern edges of the survey that are overlain by a zone of acoustic turbidity which itself is overlain by shallow gas accumulations. There are parts of the faulted reflections that exhibit pull-down effect due to the presence of shallow gas above. Fault related leakage is observed on most of the Barents Sea shelf (Vadakkepuliyambatta et al, 2013). The presence of enhanced reflections, acoustic masking, and a series of pockmarks in

the vicinity of the faults area suggests some of the ascending fluid might have used the faults planes as vertical migration pathways.

Vertical lines of discontinuity often emerging from enhanced reflectors dominate the glacial unit. Such features are usual in high-resolution shallow seismic data, and they can be set up due to the current or past presence of gas in the zone (Judd and Hovland, 2007). These features are likely to be associated with the vertical fluid flow in the upper most sediment in the study area.

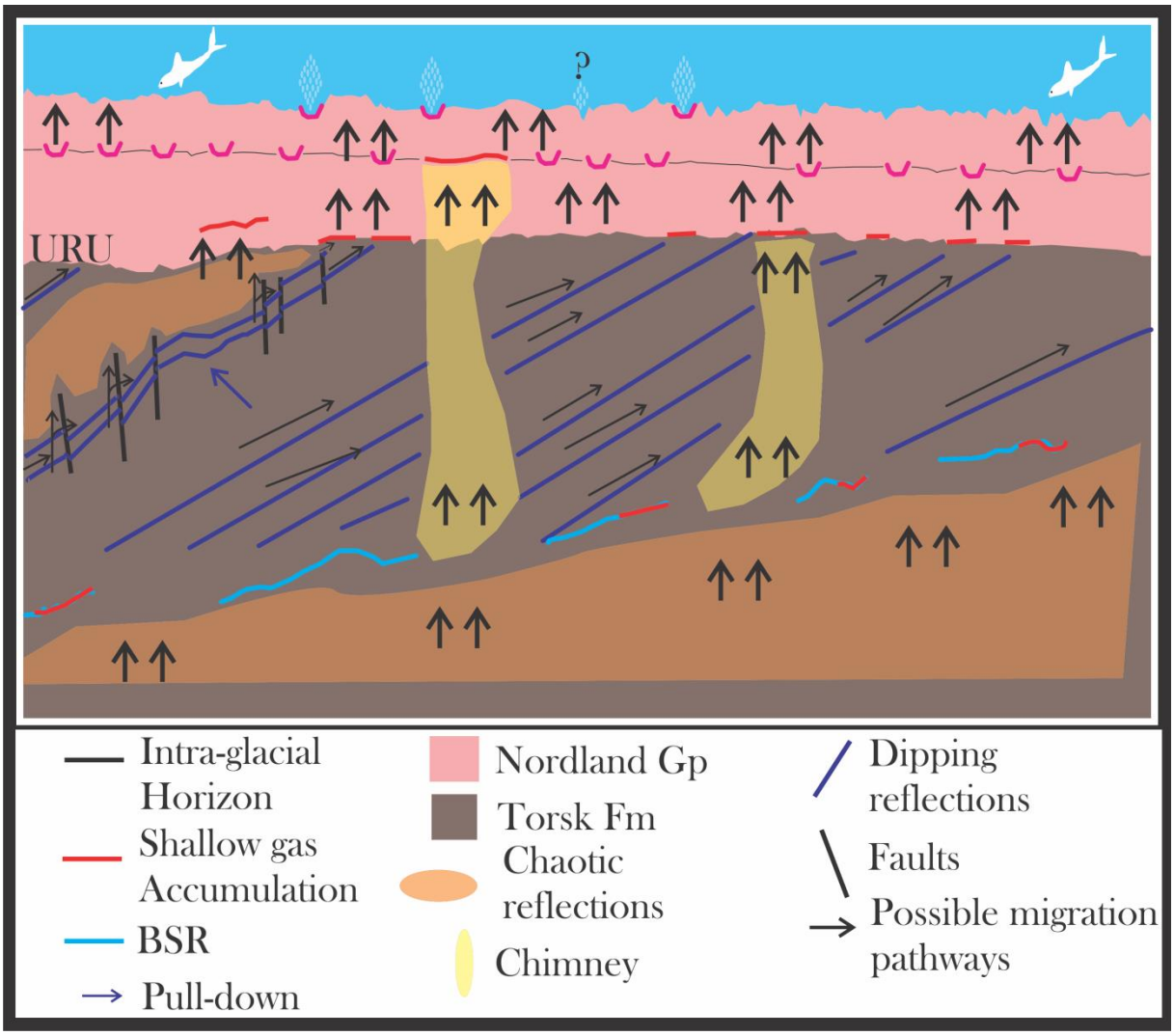

Figure 5.1: A m*odel illustrates the possible fluid migration pathways in the area 1 survey. A question mark is added to the bubbles seeping through the ploughmark.*

Snøhvit datasets:

The enhanced reflections in the datasets acquired over the Snøhvit field are not as wide spread as the ones on the RLFC. The base of the glacial unit is appears to be a major permeability barrier on both areas limiting the most of enhanced reflections just under the glacial units. RMS amplitudes generated around the URU horizon has high values along the strikes of the dipping reflectors. The clinoform of the Torsk formation dip towards the west in the Snøhvit 1 area, while the dipping reflection in the Snøhvit 2 has a southern component. As with the dipping reflection of the RLFC rising fluid are likely to pass through permeable bedding planes of the clinoforms as illustrated in figure 5.2 and 5.3.

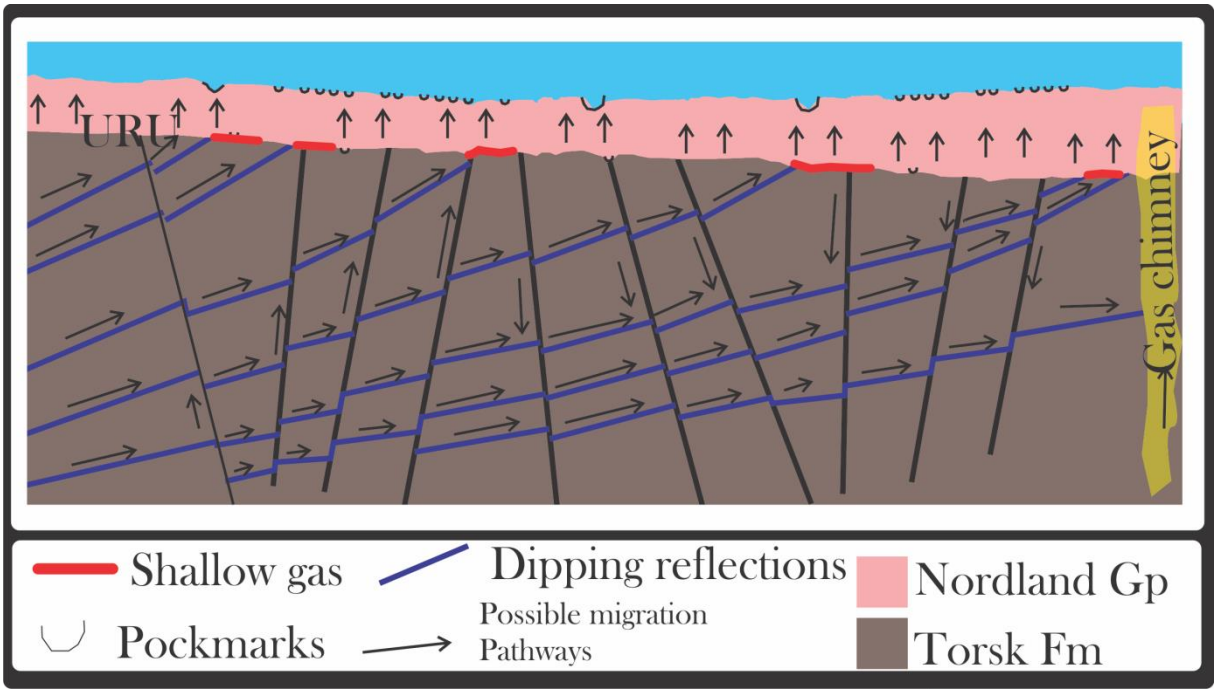

Figure 5.2: *A model illustrating possible fluid flow pattern in the Snøhvit 1 dataset.*

Acoustic masking and vertical lines of discontinuity are often found around in the vicinity of the faults. The deeper gas chimney in the Snøhvit 2 region is cross cut by faults that are sealed beneath the glacial unit. These faults may have acted or still acts as fluid conduit from the deeper areas. The clinoforms in the Snøhvit areas are barely recognizable in some areas. This could be due to the presence of gas sourced from the deeper chimney. Leakage along Paleocene-Eocene faults is thought to enhance the vertical migration along the bedding plane in the Hammerfest Basin (Ostanin et al, 2012). This fits well with the observations made in the study area.

The abundance of seabed pockmarks differentiates Snøhvit area from the Snøhvit 2 area. However, vertical lines of discontinuity are equally distributed on both areas. Hence, the lack of pockmarks could be due to the absence of soft material on the seabed.

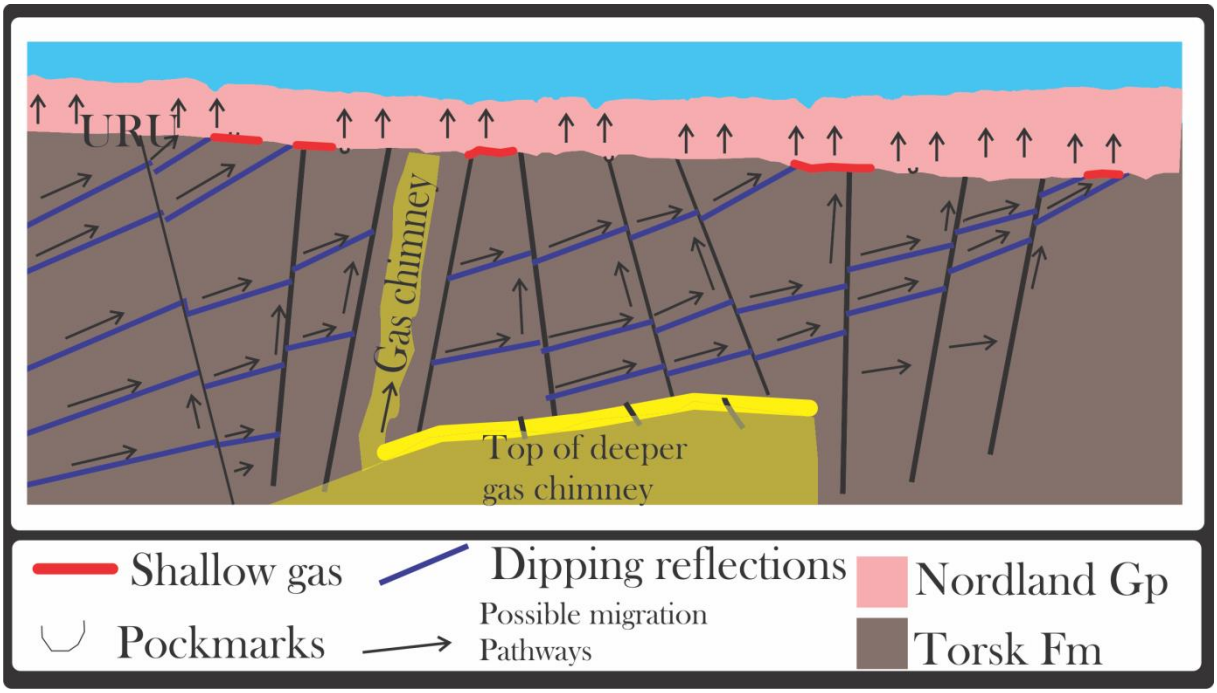

Figure 5.3: *simplified model of potential fluid flow in the Snøhvit 2 area*.

5.3: Deep source of fluids:

The enhanced reflections and pockmarks observed at various levels in the study area are likely due to the presence of gas in the pore spaces of sediments. The source of these shallow gas accumulations are likely to be locally produced biogenic gas, thermogenic gas from deeper source or a combination of both. The organic carbon content in the quaternary glacial unit is low and unlikely to be responsible for the shallow gas in the sediments and generation of pockmarks (Chand et al, 2008; Solheim & Elverhøi, 1993). Explorations for hydrocarbon have been ongoing in the Barents Sea area since the first seismic data was acquired in 1970 and the first drilling in the south Western Barents Sea took place in 1980 (Linjordet and Olsen, 1992). Several potential source rocks have been identified in the area as a result of the explorations and academic work (Linjordet and Olsen, 1992; Dore, 1995; Ohm et al, 2008; Rodrigues Duran et al, 2013a).

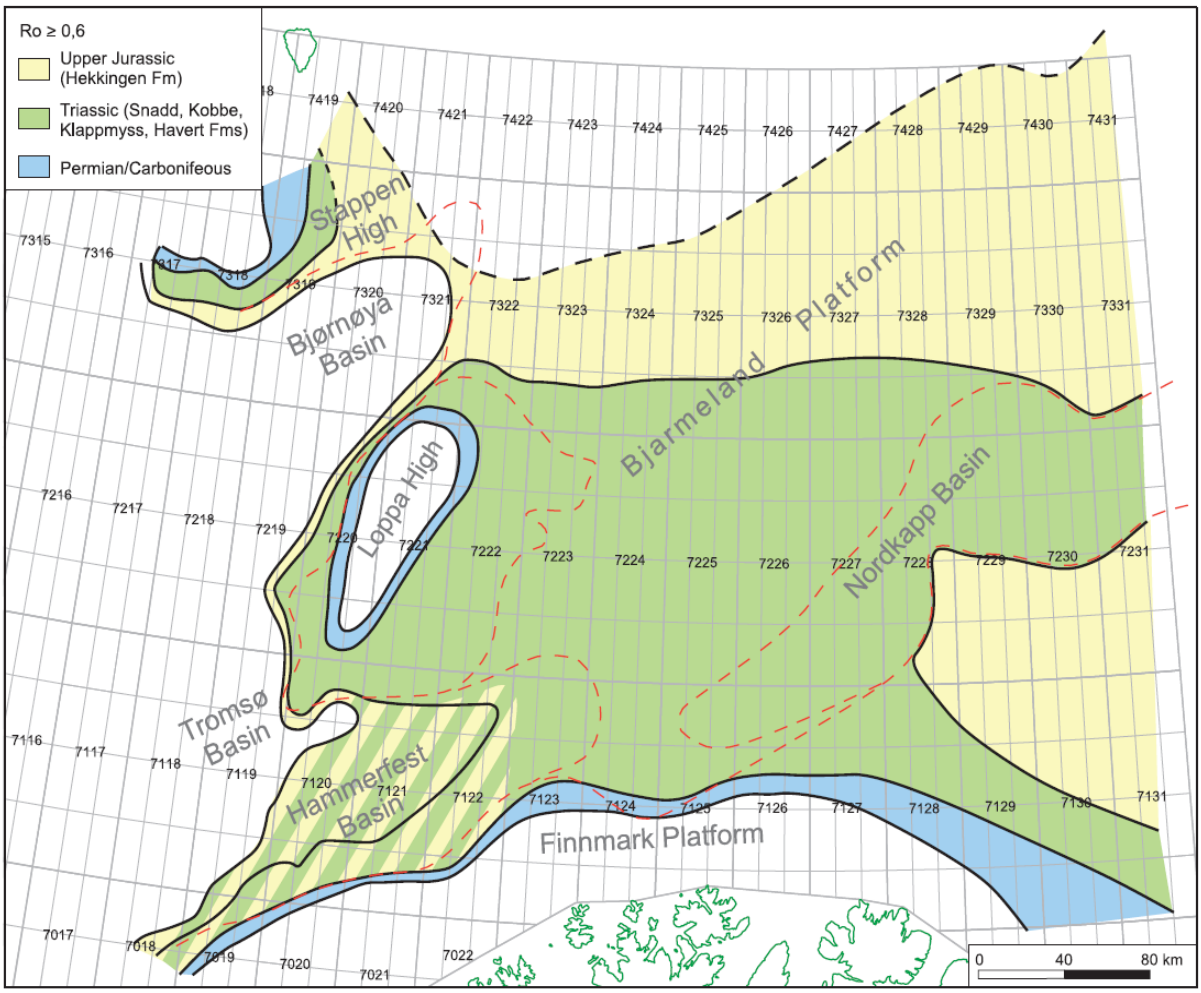

Figure 5.4: *Oil mature source rocks in the Barents Sea.(Figure from Ohm et al, 2008)*

There is hydrocarbon generation potential in all the stratigraphic units ranging from the carboniferous to the cretaceous in the Barents Sea (Ohm et al, 2008). The upper Jurassic Hekkingen, the Triassic shales of Kobbe and Snadd formations are the main source rocks in the Hammerfest Basin (Figure 2.5, Figure 5.4) (Linjordet and Olsen, 1992; Dore, 1995; Rodrigues Duran et al, 2013a, 2013b). The dark, organic rich shales of Hekkingen formation are present in most of the southern Barents Sea, but oil and gas maturity of this unit is restricted to the western parts of the Hammerfest Basin and western Loppa High (Dore, 1995). The Triassic shales are mature over the entire basin, and are estimated to have started hydrocarbon generation during the late Triassic-early Cretaceous, while the hydrocarbon generation started in the late Cretaceous in the Hekkingen formation (Rodrigues Duran et al, 2013a, 2013b). According to a 3D basin modeling implemented for the Hammerfest Basin 140 billion standard m^3oil and 300 billion m^3 gas have been generated by the main source rocks in the area (Rodrigues Duran et al, 2013a). Hydrocarbon generation in the source rocks ceased due to cooling of the source rock as a result of the Oligocene uplift in the Barents Sea (Rodrigues Duran, 2013b).

Some of the hydrocarbons generated in the Triassic shales and the Hekkingen formation migrated to the lower middle Jurassic sandstones (Linjordet & Olsen, 1992; Dore 1995). The migration of the hydrocarbons is thought to have taken place during the late Cretaceous-early tertiary through the overlying strata and fault planes into the reservoirs. The sandstones with interbeds of shales and mudstones of the Jurassic Stø Formation are the main reservoir in the Snøhvit field with up to 90% of the hydrocarbons in place. The Stø formation has the best reservoir quality with 17% average porosity and permeability ranging from 150 to 500 mD. The rest of the hydrocarbons are found in the Normela formation (Linjordet & Olsen, 1992). Minor gas accumulations are also found in the Triassic shales (Dore, 1995). An estimated 160 billion sm^3 gas and 73 million sm^3 oil in the Jurassic sandstones is found sealed the shaly Fuglen and Hekkingen Formations. However, Geochemical and petrophysical analyses along with the mismatch between the estimated generated (migrated to the reservoir) hydrocarbons and the hydrocarbons present in the reservoir suggest leakage from the reservoir. The leakage is assumed to have taken place through SE-NW oriented faults that penetrate through the seal (Linjordet & Olsen, 1992).

.

5.4 Triggering mechanisms:

In the time span from the estimated onset of the expulsion of hydrocarbons from the source rock to the present several critical geological events related to fluid migration have taken place in the Barents Sea. The Barents Sea has under gone multiple phases of uplifts (Vorren et al, 1991; Henriksen et al, 2011b) and glacial and interglacial cycles (Andreassen et al, 2008; Kneis et al, 2009) within this time frame. These geological activities play significant role in the upward migration of fluids (Lerche et al, 1997; Dore and Jensen, 1996) in the study area.

Erosion and uplift are often closely linked processes (Dore and Jensen, 1996). Figure 5.2 illustrates the uplift in the Barents Sea. The reservoir in the Snøhvit field is believed to have been subjected to substantial amount of uplift estimated to be around 900m (Figure 5.5) (Linjordet and Olsen, 1992). Uplift and erosion of basins affect the fluid migration and generation in various ways (Dore and Jensen, 1992; Henriksen et al, 2011b).

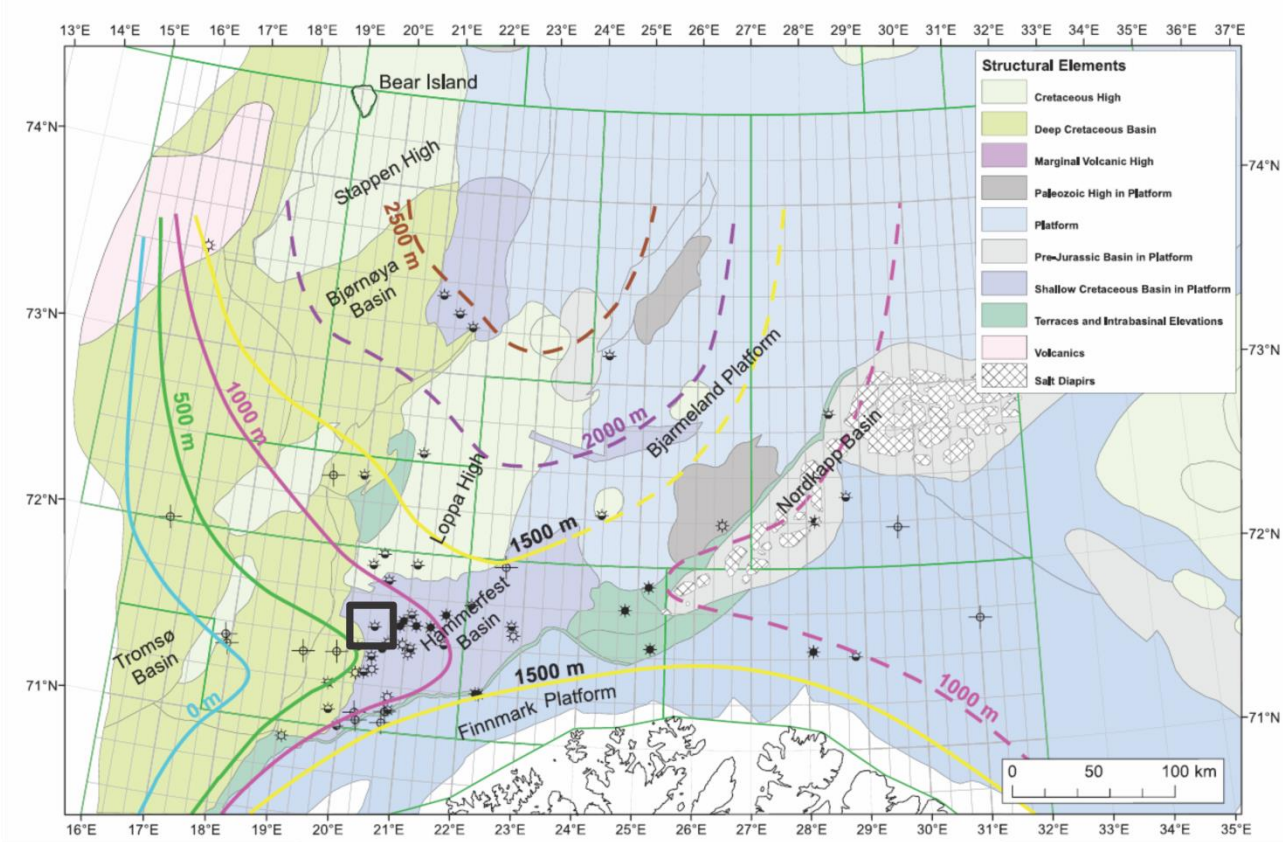

Figure 5.5: *An estimate of Cenozoic uplift in the Barents Sea region derived from vitrinite reflectance (R_o), black rectangle shows the approximate position of the study area. (Figure from Ohm et al (2008))*

The differential nature of the uplift exhibited in the Barents Sea has led to tilting of the structures (Dore and Jensen, 1996). Tilting of the reservoir structures is thought to be one of the reasons behind loss of oil out of the spillpoint (Ohm et al, 2008). The differential uplift may have caused reactivation of some of the faults that aid the vertical migration of fluids (Ostanin et al, 2012). Uplift induced tilting

Removal of the overburden along with uplift causes loss of pressure which results in expansion of the gas in the pore space and exsolusion of dissolved gas (in oil and formation water) (Chand et al, 2008; Dore and Jensen, 1996). A significant amount of oil has been lost from the reservoirs in the Snøhvit field because of the expanding gas following the uplift and erosion. In addition to gas expansion, uplift and erosion can alter physical properties of shales. Erosion of the overburden removes some of the confining pressure exhibited by shales, and this leads to lowering of the strain needed to brittle fracturing of the shaly overburden (Dore and Jensen, 1996).

The glacial and inter-glacial cycles in the late Cenozoic evolution of the Barents Sea may have influenced various aspects of the vertical migration of fluids in the study area. The chain reaction that takes place as a result of glaciation affects the subsurface fluids directly and indirectly. Reduction in permeability can be caused by the presence of impermeable ice that prohibits upwards ascending fluids. In addition the presence of glaciers lowers the governing geothermal gradient and increases the pressures, which in turn leads to the formations of impermeable clatherate (Lerche et al, 1997). The increase in pressure and decrease in permeability simultaneously can raise the pore pressure above the hydrostatic pressure (Rodrigues Duran et al, 2013a). The cyclic loading and subsequent unloading of large ice masses on the lithosphere has caused an oscillation in hydrostatic pressure (Lerche et al, 1997). The fluctuation of hydrostatic pressure was estimated to be about 5 MPa in the Barents Sea during the glacial and interglacial cycles in the late Cenozoic time assuming 750m thick glaciers (Cavanagh et al, 2006). A slight increase of overpressure is estimated as the cumulative effect of pore pressure (increase in pore pressure can be offset by subglacial melt water flow carrying some of the weight of the overlying glacier) and hydrostatic pressure increase leading to compaction of the compressible gas during the glaciation periods (Rodrigues Duran et al, 2013). Glacial erosion that removed up to 3000m of sediments (Henriksen et al, 2011b) accompanied by retreat of the ice sheet (unloading of mass) leads to reduction of the hydrostatic and pore pressure driving the expansion of gas(Rodrigues Duran et al, 2013a). The collapse of ice sheets is thought to destabilize the gas hydrates as the favorable conditions (Pressure and temperature)

are altered (Lerche et al, 1996). The removal of ice sheets following deglaciation is thought to decrease the GHSZ releasing free from the hydrates (Chand et al, 2008) and enhance the release of dissolved gas from formation water and liquid hydrocarbons (Dore and Jensen, 1996). This expansion of gas (plus the additional gas supply from gas hydrates and dissolved gas) and removal of the overburden because of glacial erosion can cause capillary failure of the seal and vertical migration of the fluids (Rodrigues Duran et al, 2013a). Fracturing and fault reactivation is likely to take place due to differential loading of the ice sheets (Lerche et al, 1996) lowering the capillary pressure needed to compromise the seal integrity. The presence of pockmarks on most of the surfaces that represent an ice free period is supports the close correlation between deglaciation and fluid migration. The observed leakage across the Barents Sea is often coincides with the presence of deep seated faults likely to be due to the glacial cycles, post-glacial isostatic uplift and erosion of the shelf. The areas exhibiting most leakage related features are extensional fault dominated areas and fault complexes such as the Hammerfest Basin and RLFC (Vadakkepuliyambatta et al, 2013). The Snøhvit 2 area is underlain by a gas chimney that is coupled with a reactivated fault (Ostanin et al, 2013). The study area in the RLFC is underlain by chimneys associated with faults that are likely utilized as fluid migration pathways (Vadakkepuliyambatta et al, 2013). The source of the shallow gas observed in the seismic data is likely to be deep and thermogenic in origin.

5.5 Summary:

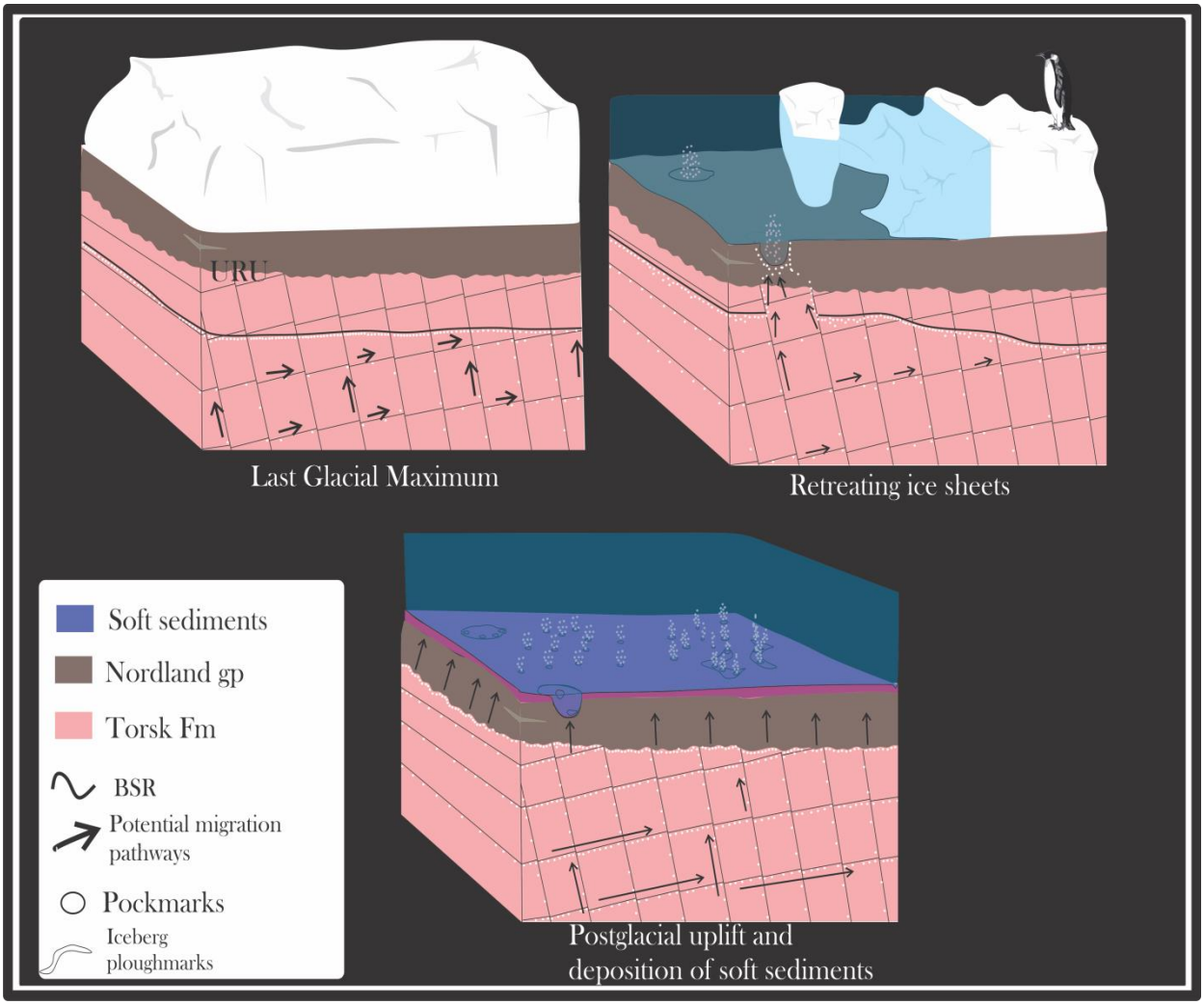

Figure 5.5: *Model shows the potential relationship between a glacial cycle and possible fluid seepage episodes in the pockmark dominated area and the formation of different sets of pockmarks.*

The load of large ice masses during the LMG ca. 19ka BP on Hammerfest basin has probably led to increase in pore pressure of the reservoirs, while prohibiting their vertical ascension by the formation of GHSZ (figure 5.5) and the ice sheets themselves acting as permeability barriers. The increase in the pore pressure is likely to have been balanced by the increase in hydrostatic pressure and melt water seasonally supporting parts of the ice masses. However, some degree of over pressure is likely to have developed, leading to reduction in volume of the compressible gas.

The retreat of the glaciers along with removal of some of the overburden due to erosion could have led to the expansion of compressed gas, and upwards surge of hot fluids along zones of high permeability (reactivated faults due to differential glaciation)(figure 5.5). This has the potential to intensify the dissociation of the gas hydrates in localized areas (further increase in over pressure) and fluid flows out to the water column leaving pockmarks behind.

Deposition of soft glaciomarine/marine sediments and postglacial uplift follows the complete collapse of ice sheets. The uplift along with the upward shift and dissociation of the GHSZ has probably led to fluid seepage. The presence of soft sediments on the seafloor makes the preservation of the pockmarks possible as illustrated in figure 5.5 .

Chapter 6 Conclusion:

- The fluids trapped beneath the quaternary strata have used the bedding planes of the early Tertiary succession to migrate upslope. The upward migration of the fluids has been enhanced by the faults sealed below the URU. The glacial sediments act as permeability barrier in the study area.
- Vertical migration of fluids from the URU to the seabed is likely to have been through narrow vertical zones of fractures.
- Seabed and buried pockmarks are good evidences seepage of fluid through the seabed. The distribution of these pockmarks in the study area does not correspond to any structures underneath, and it is likely to be controlled by the presence of soft sediments on the seabed.
- There are pockmarks on surface that represented ice free conditions (current seabed, intra-glacial horizon and the current seabed). This is due to the chain reaction that follows the glaciation and deglaciation of a basin. There is a close relationship between glaciation cycles and fluid flow episodes in the study area.
- Multiple episodes of fluid flow are indicted by the presence of large pockmarks enclosing smaller once. The first stage is likely to be due to focused fluid flow following deglaciation area after the LMG and dissociation of gas hydrates as a result of the upward migration of hot fluid and glacial retreat. The second is probably represents a low flux fluid flow due to postglacial uplift and further destabilization of GHSZ.
- Many pockmarks are found within iceberg ploughmarks. This could be due to the presence of fracture network near the base of the pockmarks leading to upward migration of fluids. Pockmarks are then generated where there is sufficient amount of soft sediment cover inside the iceberg ploughmarks.

References

Andreassen, K., Nilssen, E. and Ødegaard, C., 2007. Analysis of shallow gas and fluid migration within the Plio-Pleistocene sedimentary succession of the SW Barents Sea continental margin using 3D seismic data. Geo-Marine Letters, 27(2): 155-171.

Andreassen, K., Laberg, J.S. and Vorren, T.O., 2008. Seafloor geomorphology of the SW Barents Sea and its glaci-dynamic implications. Geomorphology, 97(1-2): 157-177.

Arntsen, B., L. Wensaas, H. Loseth og C. Hermanrud. 2007. "Seismic modeling of gas chimneys." Geophysics 72(5): SM251-SM259.

Badley, M. E. (1985). Practical Seismic Interpretation. International Human Resources Development Corporation. Boston.

Berndt, C., 2005. Focused fluid flow in passive continental margins. Phil. Trans. R. Soc. A, 363: 2855-2871.

Bjørlykke, K. (2001). "Sedimentologi og petroleumsgeologi."

Breivik, A.J., Faleide, J.I. & Gudlaugsson, S.T. 1998. Southwestern Barents Sea margin: late Mesozoic sedimentary basins and crustal extension. Tectonophysics nr 293,p 21 - 44.

Cartwright, J., & Husse, M., 2005. 3D seismic technology: the geological 'Hubble'. Basin Research 25, pp. 1-20.

Cartwright, J., Huuse, M., Aplin, A., 2007. Seal bypass systems. AAPG Bulletin 91 (8),p. 1141-1166.

Cavanagh Andrew, J., Di Primio, R., Scheck Wenderoth, M. and Horsfield, B., 2006. Severity and timing of Cenozoic exhumation in the southwestern Barents Sea. Journal of the Geological Society, 163(5): 761.

Chand, S., Mienert, J., Andreassen, K., Knies, J., Plassen, L. and Fotland, B. 2008. Gas hydrate stability zone modelling in areas of salt tectonics and pockmarks of the Barents Sea suggests an active hydrocarbon venting system. Marine and Petroleum Geology, 25(7): 625-636.

Chand, S., Rise, L., Ottesen, D., Dolan, M.F.J., Bellec, V. & Bøe, R., 2009. Pockmark-like depressions near the Goliat hydrocarbon field, Barents Sea:Morphology and genesis. Marine and petroleum geology v. 26, pp 1035-1042

Chand, S., Thorsnes, T., Rise, L., Brunstad, H., Stoddart, D., Bøe, R., Lågstad, P., Svolsbru, T., 2012. Multiple episodes of fluid flow in the SW Barents Sea (Loppa High) evidenced by gas flares, pockmarks and gas hydrate accumulation. Earth and Planetary Science Letters 331-332, 305-314.

Cathles, L.M., Su, Z., Chen, D., 2010. The physics of gas chimney and pockmark formation, with implications for assessment of seafloor hazards and gas sequestration. Marine and Petroleum Geology 27 (1), 82-91

Dalland, A., Worsley, D., Ofstad, K., 1988. A lithostratigraphic scheme for the Mesozoic and Cenozoic succession offshore mid- and northern Norway. Norw. Pet. Dir. Bull. 4: 65 p.

Dore A.G. 1991. The structural foundation and evolution of Mesozoic seaways between Europe and the Arctic. Palaeogeography, Palaeoclimatology, Palaeoecology, 87 p 441-492

Doré, A.G., 1995. Barents Sea Geology, Petroleum Resources and Commercial Potential. Arctic, 48(3): 207–221.

Doré, A.G., Jensen, L.N., 1996. The impact of late Cenozoic uplift and erosion on hydrocarbon exploration: offshore Norway and some other uplifted basins. Global and Planetary Change 12 (1-4), p. 415-436.

Dowdeswell, J.A. and Ottesen, D., 2013. Buried iceberg ploughmarks in the early Quaternary sediments of the central North Sea: a two-million year record of glacial influence from 3D seismic data. Mar. Geol. 344,p. 1-9.

Eriksen, F.N., Assad, M.,Eriksen, O.K., Stokke, H.H., Planke, S. 2014. HiRes P-Cable Data from Shallow Reservoir Mapping and Geohazard Predictions Case Examples from the Barents Sea. presentation in First Applied Shallow Marine Geophysics Conference, Athens

Faleide, J.I. Gudlaugsson, S.T Jacquart, G. 1984. Evolution of the Western Barents Sea. Marine and Petroleum Geology vol. 1, P. 123- 150

Faleide, J.I. Vågnes, E. Gudlaugsson, S.T. 1993. Late Mesozoic-Cenozoic evolution of the south-western Barents Sea in a regional rift-shear tectonic setting. Marine and Petroleum Geology, vol 10 p 186-214Faleide, J.I. et al., 2008. Structure and evolution of the continental margin off Norway and the Barents Sea. Episodes, 31: 82-91.

Faleide, J.I., Solheim, A, Fiedler, A, Hjelstuen, B.O. , Andersen, E.S., Vanneste, k. 1996. Late Cenozoic evolution of the western Barents Sea-Svalbard continental margin. Global and Planetary Change 12,p. 53-47

Faleide, J.I. Tsikalas, F. Breivik, A.J. Mjelde, R. Ritzmann, O. Engen, Ø. Wilson, J. and Eldholm, O. 2008. Structure and evolution of the continental margin off Norway and the Barents Sea. Episodes, vol. 31, nr.1, s. 82-91

Gabrielsen, R.H., Færseth, R.B., Jensen, L.N., Kalheim, J.E. and Riis, F., 1990. Structural elements of the Norwegian continental shelf, Part I. The Barents Sea Region. Norwegian Petroleum Directorate Bulletin, 6: 33 pp.

Gay, A., Lopez, M., Cochonat, P., Séranne, M., Levaché, D., Sermondadaz, G., 2006. Isolated seafloor pockmarks linked to BSRs, fluid chimneys, polygonal faults and stacked Oligocene-Miocene turbiditic palaeochannels in the Lower Congo Basin. Marine Geology 226 (1-2), 25-40.

Gay, A., Lopez, M., Brendt, C. & Seranne, m., 2007 Geological controls on focused fluid flow associated with seafloor seeps in the Lower Congo Basin. Marine Geology v. 244(1-4). Pp. 68-92

Gudlaugsson, S.T., Faleide, J.I., Johansen, S.E. and Breivik, A.J., 1998. Late Palaeozoic structural development of the South-western Barents Sea. Marine and Petroleum Geology, 15(1): 73-102.

Haavik, K.E., and Landrø, M. 2014. Iceberg ploughmarks illuminated by shallow gas in the central North Sea. Quaternary Science Review 103, pp. 34-50.

Heggland, R., 1997. Detection of gas migration from a deep source by the use of exploration 3D seismic data. Marine Geology, 137(1-2): 41-47.

Heggland, R., 1998. Gas seepage as an indicator of deeper prospective reservoirs; a study based on exploration 3D seismic data. Marine and Petroleum Geology, 15(1): 1-9.

Henriksen, E., Ryseth, A.E., Larssen, G.B., Heide, T., Ronning, K. & Sollid, K. 2011a. Tectonostratigraphy of the greater Barents Sea: implications for petroleum systems. Memoirs of the Geological Society of London. 35:pp. 163-195

Henriksen, E., Bjørnseth, H.M., Hals, T.K., Heide, T., Kiryukhina, T., Kløvjan, O.S., Larssen, G.B., Ryseth, A.E., Rønning, K., Sollid, K., Stoupakova, A., 2011b. Uplift and erosion of the greater Barents Sea: impact on prospectivity and petroleum systems. Society, London, Memoirs, vol. 35, pp. 271-281.

Hurst, A. Cartwright, J.A., Huuse, M., Jonke, R., Schwab, A., Duranti, D., & Coronin, B.T. 2004. Significance of large scale sand injectites as longterm fluid conduits: evidence from seismic data. geofluids v. 3, p. 263-247

Hovland, M., 1981. Characteristics of pockmarks in the Norwegian Trench. Marine Geology, 39: 103-117.

Hovland, M. 2012. The Geomorphology and Nature of Seabed Seepages processes. In Blondel, P. (ed) Bathymetry and its applications. InTech, pp, 79-101.

Judd, A.G., Hovland, M., Dimitrov, L.,I., Garcia Gil, S., and Jukes, V. 2002. The geological methane budget at Continental Margins and its influence on climate change. Geofluids 2, pp. 109-126

Judd, A.G., Hovland, M., 2007. Seabed Fluid Flow: The Impact on Geology, Biology and the Marine Environment. Cambridge University Press, 475 p.

Knies, J., Matthiessen, J., Vogt, C., Laberg, J. S., Hjelstuen, B. O., Smelror, M., and Larsen, E., 2009, The Plio-Pleistocene glaciation of the Barents Sea-Svalbard region: a new model based on revised chronostratigraphy: Quaternary Science Reviews, v. 28, no. 9-10, p. 812-829.

Knutsen, S.-M. and Vorren, T.O., 1991. Early Cenozoic sedimentation in the Hammerfest Basin. Marine Geology, 101(1-4): 31-48.

Lerche, I., Yu, Z., Tørudbakken, B., Thomsen, R.O., 1997. Ice loading effects in sedimentary basins with reference to the Barents sea. Marine and Petroleum Geology 14 (3), 277-338.

Ligtenberg, J.H., 2005. Detection of fluid migration pathways in seismic data; implications for fault seal analysis. Basin Research, 17(1): 141-153.

Linjordet, A. and Olsen, R.G., 1992. The Jurassic Snohvit gas field, Hammerfest Basin, offshore northern Norway. AAPG Memoir, 54: 349-370.

Løseth, H., Gading, M., Wensaas, L., 2009. Hydrocarbon leakage interpreted on seismic data. Marine and Petroleum Geology 26 (7), 1304e1319.

Ohm, S.E., Karlsen, D.A., Austin, T.J.F., 2008. Geochemically driven exploration models in uplifted areas: examples from the Norwegian Barents Sea. American Association of Petroleum Geologists Bulletin 92, 1191-1223.

Ostanin, I., Anka, Z., di Primio, R. and Bernal, A. 2012. Identification of a large Upper Cretaceous polygonal fault network in the Hammerfest basin: Implications on the reactivation of regional faulting and gas leakage dynamics, SW Barents Sea. Marine and Petroleum Geology. V332-334, p 109-125

Ostanin, I., Anka, Z., di Primio, R. and Bernal, A. 2013. Hydrocarbon plumbing systems above the Snøhvit gas field: Structural control and implications for thermogenic methane leakage in the Hammerfest Basin, SW Barents Sea. Marine and Petroleum Geology, V 43, p. 127-146

Pau, M., Hammer, Ø., and Chand, S. 2014. Constraints on the dynamics of pockmarks in the SW Barents Sea: Evidence from gravity coring and high-resolution, shallow seismic profiles. Marine Geology V. 355, pp. 330-345

Parnell, J. & Schwab, AM. 2003. 'Seismic evidence for the distribution and migration of fluids in sedimentary basins'. GeoFluids, vol 3, no. 4, pp. 213-217.

Planke, S., Eriksen F.N., Berndt, C., Meinert, J., Bünz, S., and Lippus, C. 2013. P-Cable High-Resolution seismic site survey Technology. Presentation in CHIKYU+10, Tokyo

Petrel, 2013. Petrel E&P Software Platform.

Plaza-Faverola, A., Bünz, S., Mienert, J., 2011. Repeated fluid expulsion through subseabed chimneys offshore Norway in response to glacial cycles. Earth and Planetary Science Letters 305 (3-4), pp. 297-308.

Rafaelsen, B., Andreassen, K., Kuilman, L.W., Lebesbye, E., Hogstad, K., and Midtbø, M. 2002.Geomorphology of buried glacigenic horizons in the Barents Sea from three-dimensional seismic data. Geol. Soc. London, Spec. Publ., vol. 203, pp. 259–276

Rajan, A., Bünz, S., Mienert, J. and Smith, A. 2013. Gas hydrate systems in petroleum provinces of the SW-Barents Sea. Marine and Petroleum Geology V 16. P 91-106

Reemst, P. and Cloetingh. S. 1994. Tectonostratigraphic modelling of Cenozoicuplift and erosion in the south-western Barents Sea. Marine and Petroleum Geology 1994 V. 11(4) .P. 478- 490

Rodrigues Duran, E., di Primio, R., Anka, Z., Stoddart, D., Horsfield, B., 2013a. 3D-basin modelling of the Hammerfest Basin (southwestern Barents Sea): a quantitative assessment of petroleum generation, migration and leakage. Marine and Petroleum Geology 45, 281–303.

Rodrigues Duran, E., di Primio, R., Anka, Z., Stoddart, D., Horsfield, B., 2013b. Petroleum system analysis of the Hammerfest Basin (southwestern Barents Sea): Comparison of basin modelling and geochemical data. Organic Chemistry 63, pp. 105-121

Rüther, D.C., Mattingsdal, R., Andreassen, K., Forwick, M., Husum, K., 2011. Seismic architecture and sedimentology of a major grounding zone system deposited by the Bjørnøyrenna Ice Stream during Late Weichselian deglaciation. Quaternary Science Reviews 30 (19-20), 2776-2792.

Schlumberger. 2011. Interpreters guide to seismic attribute.

Selley, R. C. (1998). Elements of Petroleum Geology (2. ed.).

Smelror, M. Petrov, O.V. Larssen, G.B. Warner, S.C. (Eds). 2009. Atlas: Geological History of the Barents Sea. Geological Survey Of Norwey. Norges Geologisk Undersøkelse, Trondheim.

Solheim, A., Elverhøi, A., 1985. A pockmark field in the Central Barents Sea; gas from a petrogenic source? Polar Research 3, 11–19.

Solheim, A., and Elverhøi, A., 1993, Gas-related sea floor craters in the Barents Sea: Geo-Marine Letters, v. 13, no. 4, p. 235-243.

Vadakkepuliyambatta, S., Bunz, S., Mienert, J., and Chand, S. 2013. Distribution of subsurface fluid-flow systems in the SW Barents Sea. Marine and petroleum geology. V. 43. pp. 208-221.

Veeken, P. 2007. Seismic Stratigraphy, basin analysis and reservoir characterization. .Handbook in Seismic Exploration

Vorren, T.O., Hald, M., & Lebesbye, E. 1988. Late Cenozoic Environments in the Barents Sea. Paleoceanography, vol 3, n. 5, pp. 601-612

Vorren, T.O. Richardsen, G. Knutsen, S.M. and Henriksen, E. 1991. Cenozoic erosion and sedimentation in the western Barents Sea. Marine and Petroleum Geology vol 8, P 317- 340

Vorren, T.O., & Laberg, J.S. 1997. Trough mouth Fans - Paleoclimate and Ice-sheet Monitors. Quaternary Science Reviews, Vol. 16, pp. 865-881

Vorren, T.O. 2005. Subaquatic landsystems: continental margin. In Evans, D. & Gooster, L. eds. GLACIAL LANDSYSTEMS. New York: Arnold, pp 289-312.

Vågnes, E. 1997: Uplift at thermo-mechanically coupled ocean-continent transforms: Modeled at the Senja Fracture Zone, southwestern Barents Sea. Geo-Marine Letters 17, 100 – 109

Woodworth-lynas, C.M.T., Josenhans, H.W., Barrie, J.V., Lewis, C.F.M., and Porrott, D.R., 1991. The physical processes of seabed disturbance during iceberg grounding and scouring. Continental Shelf Research, Vol. 11, Nos 8-10, pp. 939-961